



Norwegian University of
Science and Technology

New type of energy exchanger for ventilation air

Martin Fogh Lundekvam

Master of Energy and Environmental Engineering

Submission date: June 2016

Supervisor: Hans Martin Mathisen, EPT

Norwegian University of Science and Technology
Department of Energy and Process Engineering

EPT-M-2016-82

MASTER THESIS

for

Student

Martin Fogh Lundekvam

Spring 2016

New type of energy recovery exchanger for ventilation air*En ny type varmegjenvinner for ventilasjonsluft***Background and objective**

Heat recovery from exhaust ventilation air is required in almost every kind of building. For most applications, the heat wheel is the preferred solution. In applications where several flats are supplied from the same air handling unit, transfer of smell from exhaust air to fresh supply might be a problem with the heat wheel. Flat plate exchangers do not have this problem, but their efficiency is reduced due to frost problems at low outdoor temperatures. By using a membrane that transfers moisture, frost can be avoided and the efficiency increased. A PhD work within this field is now approaching its end. This master thesis will be a continuation of some parts of this work.

The objective of the master work will be to make measurements on the membrane exchangers with regard to indoor air quality and efficiency and to evaluate the membrane exchanger's performance

The work is a continuation of the student's specialisation project.

The following tasks are to be considered:

1. Continue the literature survey on membrane heat exchangers
2. Summing up the theory for membrane heat exchangers
3. Plan the laboratory experiments in accordance with previous experiments of Liu Peng
4. Perform experiments and analyse the results
5. Evaluate the applicability of the membrane energy exchanger

-- ” --

Within 14 days of receiving the written text on the master thesis, the candidate shall submit a research plan for his project to the department.

When the thesis is evaluated, emphasis is put on processing of the results, and that they are presented in tabular and/or graphic form in a clear manner, and that they are analyzed carefully.

The thesis should be formulated as a research report with summary both in English and Norwegian, conclusion, literature references, table of contents etc. During the preparation of the text, the candidate should make an effort to produce a well-structured and easily readable report. In order to ease the evaluation of the thesis, it is important that the cross-references are correct. In the making of the report, strong emphasis should be placed on both a thorough discussion of the results and an orderly presentation.

The candidate is requested to initiate and keep close contact with his/her academic supervisor(s) throughout the working period. The candidate must follow the rules and regulations of NTNU as well as passive directions given by the Department of Energy and Process Engineering.

Risk assessment of the candidate's work shall be carried out according to the department's procedures. The risk assessment must be documented and included as part of the final report. Events related to the candidate's work adversely affecting the health, safety or security, must be documented and included as part of the final report. If the documentation on risk assessment represents a large number of pages, the full version is to be submitted electronically to the supervisor and an excerpt is included in the report.

Pursuant to "Regulations concerning the supplementary provisions to the technology study program/Master of Science" at NTNU §20, the Department reserves the permission to utilize all the results and data for teaching and research purposes as well as in future publications.

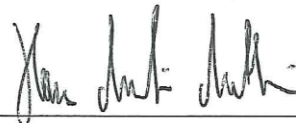
The final report is to be submitted digitally in DAIM. An executive summary of the thesis including title, student's name, supervisor's name, year, department name, and NTNU's logo and name, shall be submitted to the department as a separate pdf file. Based on an agreement with the supervisor, the final report and other material and documents may be given to the supervisor in digital format.

- Work to be done in lab (Water power lab, Fluids engineering lab, Thermal engineering lab)
 Field work

Department of Energy and Process Engineering, 13. January 2016



Olav Bolland
Department Head



Hans Martin Mathisen
Academic Supervisor

Research Advisor:
Liu Peng

Preface

This report was written at the Department of Energy and Process Engineering (EPT) at the Norwegian University of Science and Technology, Trondheim, Norway. This thesis is connected with a PhD within the field of membrane heat exchangers.

I would like to thank Hans Martin Mathisen, professor at EPT, for guidance and help as my supervisor.

I would also like to thank Peng Liu, PhD candidate at EPT, for good discussions and for helping me find relevant literature for this report.

Lastly I would like to thank Lars Konrad Sorensen for providing necessary equipment and help in making the flow pattern test rig.

Martin Fogh Lundekvam, Mc. Student
The Department of Energy and Process Engineering, the Norwegian University of Science and Technology, Trondheim, 16. June 2016

Sammendrag

Energieffektive varmevekslere er viktige for å minimalisere energien som kreves for oppvarming og ventilasjon. I bygninger med sentralisert luftbehandlingsaggregat er det viktig å unngå lekkasjer mellom avkast og tilluft. På grunn av dette, er flate platevarmevekslere, som er kompakte og lette å forsegle, valgt. I kaldt klima har platevarmevekslere et problem med kondensering og isdannelse i varmevekslerens kjerne. Dette gir en avtagende generell ytelse. For å maksimere ytelsen forskes det på membranvarmevekslere som både overfører fuktighet og følbare varme. Denne avhandlingen er en videreføring av enkelte deler av et tidligere arbeid med en membranvarmeveksler bygget i laboratoriet ved Institutt for energi- og prosesssteknikk ved NTNU.

I et tidligere arbeid ble membranvarmeveksleren testet under vinterforhold. Denne avhandlingen fokuserer på membranvarmevekslerens ytelse i løpet av våren og høsten basert på gjennomsnittstemperatur og gjennomsnittlig relativ luftfuktighet for byene Oslo, Bergen og Trondheim. For å oppnå den nødvendige relative fuktigheten er en kokeplate med kolbe blitt koblet til testtrikken nær kjernen ved tilluftssiden. Det ble funnet ut at i milde og fuktige klima som man har i Bergen, ville det ikke være ideelt med bruk av en membranvarmeveksler med hensyn til menneskers helse og det totale energiforbruket. Den enkle implementeringen av kokeplaten og kolben viste seg å føre til en høy grad av usikkerhet med hensyn til temperatur og relativ fuktighet. Det ble derfor anbefalt at ved fremtidige eksperimenter med membranvarmeveksleren burde tilførselen av damp flyttes lenger bort fra membranvarmevekslerens sin kjerne eller erstattes med en mer pålitelig kilde for damp.

Ytelsen til membranvarmeveksleren ble vurdert, og en liten strømningsmodell ble laget. Denne skulle vise om strømningsmønsteret ble påvirket av en aluminium-mesh plassert mellom membransjiktet som støtte til membranen. Forsøkene viste at meshen ikke påvirket strømningsmønsteret sammenlignet med en åpen kanal uten mesh.

Abstract

Energy efficient heat exchangers are important to minimise energy needed for heating and ventilation. In buildings with centralised air handling units it is important to avoid leakages between the exhaust and supply air. For this reason, flat plate heat exchangers, which are compact and easy to seal, are chosen. In cold climates flat plate heat exchangers have a problem with condensation and frost formation inside the exchanger core reducing overall performance. To maximise the performance, flat plate membrane energy exchangers transferring both sensible and latent heat are being investigated. This thesis is a continuation of some parts of a previous work with a membrane energy exchanger built in the laboratory at the Department of Energy and Process Engineering at NTNU.

In a previous work the MEE was tested during winter conditions. This thesis focussed on the MEE performance during spring and autumn conditions for the cities Oslo, Bergen and Trondheim. In order to achieve the needed relative humidity a simple boiling flask was connected to the MEE test rig close to the supply inlet. It was found that in mild and moist climates, such as that in Bergen, the MEE would not be ideal, with regards to energy consumption and human health. The simple boiling flask proved to cause a high level of uncertainty in regard of temperature and RH. It was therefore recommended that for future experiments on the MEE, the boiling flask should either be moved farther away from the MEE core or be replaced with a more reliable source for steam.

The MEE performance was reviewed, and a small flow pattern test rig was made. The test rig would reveal whether the flow pattern was affected by an aluminium mesh placed between the membrane layers for support. The experiments showed that the effect of the mesh was negligible compared to an open channel flow.

Table of contents

1	Introduction	1
1.1	Background.....	1
1.2	Objective.....	2
2	Literature review and state of the art.....	3
2.1	Introduction to frosting.....	3
2.2	Configurations	4
2.3	Flow patterns Quasi-counter flow MEE.....	5
2.4	Membrane properties	6
2.4.1	Dense membranes	6
2.4.2	Porous membranes	6
2.5	Test rig membrane	7
3	Theoretical modelling	9
3.1	Flow pattern test rig.....	9
3.1.1	Dimensioning entry and exit length	9
3.1.2	Volumetric flow rate	10
3.2	Membrane energy exchanger test rig	11
3.2.1	Pressure drop and airstream velocity	11
3.2.2	Moisture transfer resistance	12
3.2.3	Heat and mass transfer	14
3.2.3	Effectiveness	16
3.3	Uncertainty.....	17
4	Experimental setup.....	21
4.1	Flow pattern setup	21

4.2	Quasi-counter-flow setup	22
4.2.1	Relative humidity	23
4.2.2	HSE report.....	23
5	Results	25
5.1	Flow pattern test rig.....	25
5.1.1	Pressure drop	25
5.1.2	Flow pattern.....	25
5.2	Effectiveness.....	27
5.3	Moisture and condensation	30
5.4	Pressure drop	31
5.5	Temperature and RH fluctuation	32
5.6	Long run performance	34
5.7	Indoor RH.....	41
6	Discussion	43
6.1	Moisture supply air	43
6.2	Pressure drop and flow rate	43
6.3	Moisture transfer resistance.....	45
6.4	Evaluation of the flow pattern test rig	45
6.5	Evaluation of the MEE test rig	46
7	Conclusion.....	47
8	Further Work.....	49
	References	51
	Appendix	53

List of Figures:

2.1	Frosting inside channel of exhaust air	3
2.2	Quasi-counter- flow	4
2.3	Flow pattern open channel quasi-counter flow [12]	5
2.4	Aluminium mesh used in MEE	5
2.5	a) <i>Parallel cylindrical pores</i> b) <i>Voids between stacked spheres</i>	7
3.1	<i>Normal and actual flow</i>	10
3.2	<i>Deviation from Hyland-Wexler</i>	13
3.3	<i>Sensible and latent effectiveness fluctuations</i>	18
4.1	<i>Sensible and latent effectiveness fluctuations</i>	21
4.2	<i>Quasi-counter-flow test rig[5] with permission</i>	22
5.1	<i>Pressure drop over mesh for flow pattern rig</i>	25
5.2	<i>Flow pattern with aluminium mesh compared to open channel flow [4]</i>	27
5.3	<i>Unrealistic effectiveness results at 30-40% RH</i>	28
5.4	<i>Change in moisture transfer due to higher specific humidity for supply air at 10-12 °C at 30-40% RH</i>	28
5.5	<i>RH needed at 22 °C when supply inlet is at 15 °C, 70% RH</i>	29
5.6	<i>Sensible and latent effectiveness found experimentally and with NTU method</i>	30
5.7	<i>Water condensed per kg of air inside MEE at 60% RH for exhaust inlet</i>	31
5.8	<i>Water condensed per kg of air inside MEE at 30-40% RH for exhaust inlet</i>	31
5.9	<i>Boiling flask setup</i>	33
5.10	<i>Fluctuations in temperature for critical values</i>	34
5.11	<i>Fluctuations in RH for critical values</i>	34

5.12	<i>Boiling flask cap before and after experiments. Hole has expanded due to shrinking of material.</i>	35
5.13	<i>Effectiveness for 6,9 °C supply inlet long run test</i>	36
5.14	<i>Effectiveness for 10,3 °C supply inlet long run test</i>	36
5.15	<i>Effectiveness for 14,7 °C supply inlet long run test</i>	37
5.16	<i>Condensing water inside MEE for 6,9 °C supply inlet long run test</i>	37
5.17	<i>Condensing water inside MEE for 10,3 °C supply inlet long run test</i>	38
5.18	<i>Condensing water inside MEE for 14,7 °C supply inlet long run test</i>	38
5.19	<i>Pressure drop over MEE supply side at 6,9 °C supply inlet</i>	39
5.20	<i>Pressure drop over MEE supply side at 10,3 °C supply inlet</i>	40
5.21	<i>Pressure drop over MEE supply side at 14,7 °C supply inlet</i>	40
6.1	<i>Temperature difference over time between supply inlet and exhaust outlet for 5,3 °C.</i>	44
6.2	<i>Temperature difference over time between supply inlet and exhaust outlet for 12,6 °C.</i>	44
6.3	<i>Dräger air current tube</i>	46

List of Tables:

2.1	<i>Typical values for lower exhaust temperature depending on heat exchanger [11]</i>	4
3.1	<i>Total uncertainty with 60% RH exhaust inlet air and 70% RH supply inlet air</i>	19
3.2	<i>Total uncertainty for long running test with 53% RH exhaust inlet air and 70% RH supply inlet air</i>	19
5.1	<i>Preliminary calculations for the Reynolds number</i>	26
5.2	<i>Pressure drop over orifice plate at start and finish</i>	32
5.3	<i>Pressure drop over orifice plate at start and finish long run</i>	39
5.4	<i>Moisture loads in a building</i>	41
5.5	<i>Simulation results with different parameters</i>	42
6.1	<i>Average condensation rate inside MEE at the</i>	45

Definitions:

Frosting limit, T_{frost}	The lowest temperature allowed on the exhaust side of the heat exchanger. If the air is colder, frost may form inside the heat exchanger
Hydrophilic	Loves water
Hydrophobic	The opposite of hydrophilic
Membrane	Material that lets some substances penetrate and some not to penetrate.
MEE	Membrane Energy Exchanger
RH	Relative humidity. The percentage of moisture the air can hold. 100% means the air is saturated. 0 % means the air is completely dry.
Diffusion	Net movement of molecules from a high concentration area to a low concentration area.
Driving potential	An ion's ability to go through the membrane
ZEB	Zero emission building

Nomenclature

Parameter	Description	Unit
\dot{V}	Volumetric flow rate	m^3/s
\bar{x}	Arithmetic mean	
A	Usable area of exchanger	(m^2)
C	Discharge coefficient/Heat capacity	
C_p	Specific heat capacity of air	(kJ/kgK)
c_r	Capacity ratio	
D	Diffusivity/ Inner pipe diameter	$(\text{m}^2/\text{s})/(\text{m})$
d	Inner diameter orifice plate	(m)
D_h	Hydrodynamic diameter of an air channel	(m)
g	Gravitational force	(m/s^2)
H	Channel height/	(m)
h	Convective heat transfer coefficient	$(\text{W}/\text{m}^2\text{K})$
J	Water vapour flux	$(\text{m}^3/\text{m}^2\text{s})$
j	Colburn factor	
k	Convective moisture transfer	(kg/ms)
L_p	Permeability of porous membrane	(m^2/s)
\dot{m}	Mass flow	(kg/s)
n	Number of measurements/number of molecules	
P	Pressure	(Pa)
q	Total heat transfer rate	(W)
r	Pore size / moisture resistance	$(\text{m})/(\text{m}^2\text{s}/\text{kg})$
s	Standard deviation	
T	Temperature	(K)
t	Temperature / t-value	$(^\circ\text{C})$
tr	Transmissivity	
U	Total heat transfer coefficient/mass transfer coefficient	
u	Velocity through channel	(m/s)
V	Flow rate	(L/min)
v	Kinematic viscosity	(m^2/s)
W	Channel width	(m)
w	Moisture content	(kg/kg)
x	Entry length /	(m)

Acronyms

Le	Lewis number
NTU	Number of transfer units
Nu	Nusselt number
Pr	Prandtl number
Re	Reynolds number
RH	Relative humidity
Sc	Schmidt number
Sh	Sherwood number

Greek letters

δ	Membrane thickness	(m)
Δ	Change in chosen parameter	

ε	Effectiveness of membrane / pore porosity of membrane / expansibility factor	
β	Diameter ratio	
γ	Heat capacity ratio	
η	Viscosity	(Pa*s)
λ	Thermal conductivity	(W/mK)
μ	Dynamic viscosity	(Ns/m ²)
ρ	Density	(kg/m ³)
τ	Tortuosity	

Subscripts

c	Cross section
cou	Counter
cro	Cross
E	Exhaust
fd	Fully developed
frost	Frost formation conditions
h	Heat/hydraulic/hydrodynamic
in	Into the exchanger
l	Latent
m	Membrane,manometer or moisture
max	Maximum
min	Minimum
out	Out of the exchanger
p	Porous membrane
r	Random
S	Supply
s	Sensible / systematic
sat	Saturation
t	thermal
tot	Total
v	Vapour
w	Water

1 Introduction

1.1 Background

Heat recovery in ventilation systems is required in almost every building. Buildings account for 40 % of the total energy consumption worldwide [1]. Most of the energy required in cold climate goes towards heating and ventilation. Therefore, an efficient heat recovery system is essential to the energy performance and energy savings in buildings. It is estimated that heat recovery of ventilation air regains 60-95% of the heat from the exhaust air [2]. In Nordic countries, flat plate heat exchangers have been a common system implemented in flats with centralised air handling systems. When temperatures go below the frosting limit, certain prevention mechanisms, such as bypassing and preheating of the supply air must be implemented in order to prevent blockages caused by built-up ice [3]. The use of these frost prevention techniques lowers the overall performance of the heat exchanger. In order to increase frosting free operating time and efficiency in the Nordic climate in an energy efficient way, new methods are being investigated.

This thesis is connected to a previous master thesis [4] and a PhD [5] within the field of membrane energy exchangers. It is argued that membrane energy exchangers can provide the solution for frosting problems in Nordic environments. Moisture transfer through membranes from the exhaust air to supply air prevents frosting from occurring. With a lower moisture content in the exhaust air, more heat can be transferred before any condensation and frost appears. This in turn leads to a higher total efficiency and indoor air quality [1]. In addition to being more efficient it will also prevent irritation of the eyes and airways by increasing indoor RH during winter months [6] increasing indoor air quality. The author did not find any research on the flow pattern of this type of spacer filled Membrane Energy Exchanger. The research into spring and autumn conditions, when temperature and moisture content of the outside air are higher, was also not found.

The experiments in this thesis will be a continuation of the work Peng Liu started [5]. The same experimental energy exchanger will be used. Liu tested the exchanger under cold operating conditions in order to check the frosting limits and the performance during normal frosting conditions. In this thesis, the emphasis will be on spring and autumn conditions linked to weather data from Oslo, Bergen and Trondheim.

This report will give a brief introduction to the theory used for both the flow pattern test rig and the MEE test rig. Furthermore, the experimental results will be presented and evaluated. They will be further discussed and recommendations for further work and improvements, as well as concluding remarks, are presented.

1.2 Objective

Membrane energy exchanges may have great potential as an energy savers compared to conventional flat plate heat exchangers because of their ability to transfer moisture from one airstream to the other. Since it has been tested in winter conditions in previous works [5, 7], the author wanted to test the MEE during spring and autumn conditions. The author was interested to investigate the MEEs performance at higher outdoor moisture levels and to see how this affected the performance and indoor air. The temperature and RH was chosen on a basis of the mean temperatures and RH of the cities stated above. The objectives of this thesis are:

- Building a flow pattern rig of the quasi-counter-flow membrane energy exchanger to examine the influence of the corrugated screen spacer on the airstream within the MEE.
- Testing the MEE for spring and autumn conditions in regards to sensible- and latent effectiveness and condensation.
- Evaluating the MEE performance and discussing its relevance for cold climates during spring and autumn conditions.

2 Literature review and state of the art

The literature used in this thesis have been found using Scopus, Science Direct, books and through ISO/NS standards.

2.1 Introduction to frosting

In order to fully understand why this type of MEE is being investigated a short explanation about its positive capabilities during winter conditions in a Nordic climate is required.

Conventional flat plate heat exchangers are commonly used in Nordic countries for energy efficient ventilation [8]. The two airstreams are separated, which diminishes the risk of cross contamination. The absence of moving parts also makes it reliable. Conventional flat plate heat exchangers are made up of many thin plates in parallel alignment. The plates separate the exhaust and supply air and sensible heat is transferred due to forced convection. The conventional flat plate heat exchanger only transfers sensible heat, which can lead to frosting problems in cold climates due to condensation and eventually frost formation of the moist air. Frost occurs when the outside temperature drops below the frosting limit, which is determined by operating conditions and exchanger type [9]. As a result of the low temperature of the outside air and a high relative humidity of indoor air, frost will start to build up inside the heat exchanger. This leads to a decrease in efficiency and increase in pressure drop on the exhaust side of the exchanger. If no defrosting measures are considered, ice will block the heat exchanger and may at worst case damage the heat exchanger [10].

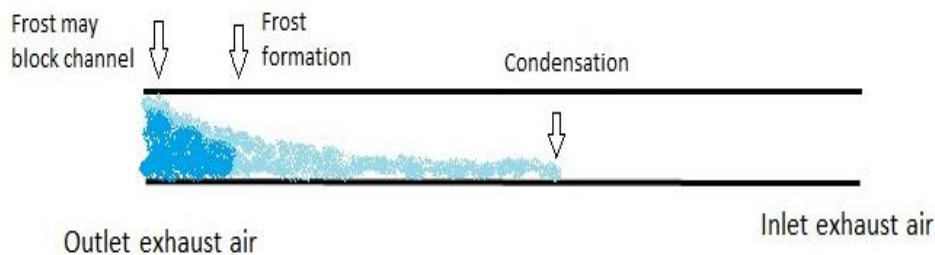


Figure 2.1 *Frosting inside channel of exhaust air*

In Figure 2.1, a simple explanation of how frosting occurs inside the heat exchanger is explained. As the hot and humid exhaust air cools down due to the heat transfer from exhaust air to supply air, the amount of water the air can hold decreases. As the airstream gets closer to its dew point temperature, the relative humidity increases. When the air reaches 100% relative humidity, water will start to condense inside the channel. If the flat plate keeps a lower temperature than 0°C , frost may start to form.

For flat plate heat exchangers there are different frosting limits, determined by type of building and frost prevention techniques in place. The table below is from NS3031, showing typical values for the lowest exhaust outlet air temperature permitted.

Heat exchanger and frost prevention	T_{frost}
Recuperative (flat plate exchanger) in other buildings (lower humidity than residence)	+0 °C
Recuperative (flat plate exchanger) in residence, with optimum (economic) frost prevention	+5 °C
Recuperative (flat plate exchanger) in residence, with normal (conservative) frost prevention	+9 °C

Table 2.1 Typical values for lower exhaust temperature depending on heat exchanger [11]

2.2 Configurations

There are two basic configurations for flat plate heat exchangers that are relevant for this thesis: Counter-flow, with efficiencies varying from 50 – 80 % and cross-flow, with about 10% less efficiency [10]. The cross-flow has been the most used arrangement due to its simplicity in sealing, cleaning and its low pressure drop. Efficiency and easy sealing are combined in a quasi-flow configuration, which is utilised in this project.

The figure below shows the function of the quasi-counter-flow where it exploits the efficiency of the counter-flow with the simplicity of sealing in the cross-flow.

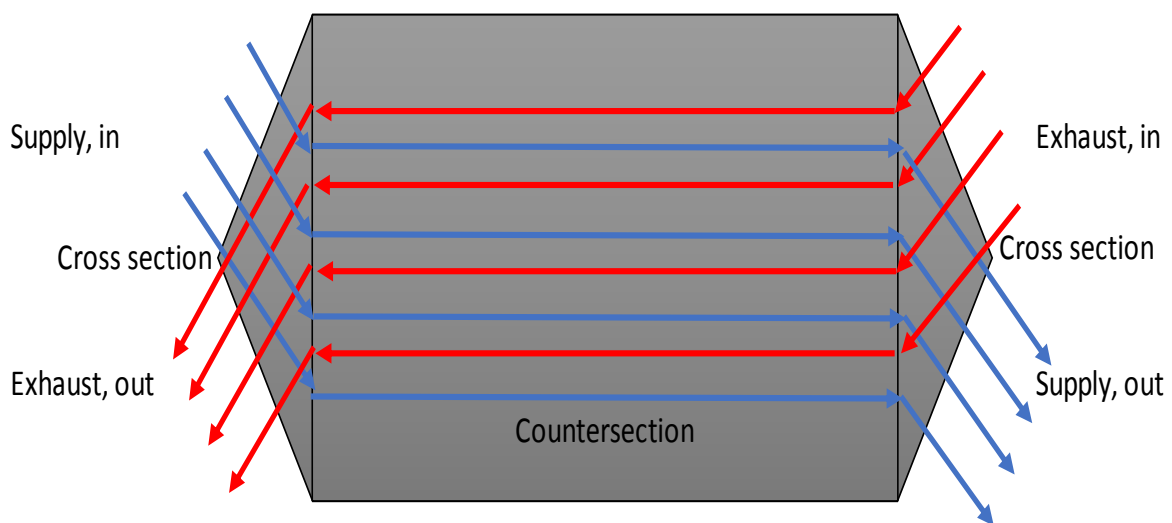


Figure 2.2 Quasi-counter-flow

2.3 Flow patterns Quasi-counter flow MEE

In [12] the flow pattern of an open channel quasi-counter flow MEE is described. Zhang uses CFD analysis to investigate the flow pattern, humidity and temperature distribution. The flow pattern can be seen in Figure 2.3 below.

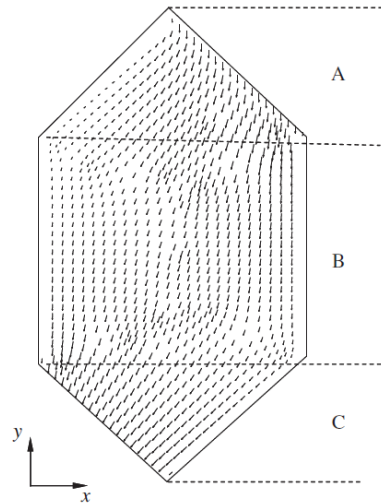


Figure 2.3 Flow pattern open channel quasi-counter flow [12]

The quasi-counter flow rig used in this thesis, however, is not an open channel MEE. Inside the channel there is an aluminium mesh designed to support the membrane when the membrane surface gets bloated [4]. In order to investigate the flow pattern of the quasi-counter-flow rig, a single channel test rig has been made. The results and the comparison to a test for open channel flow in [4] is reviewed in the results. This is the first time the flow pattern of this design has been investigated.

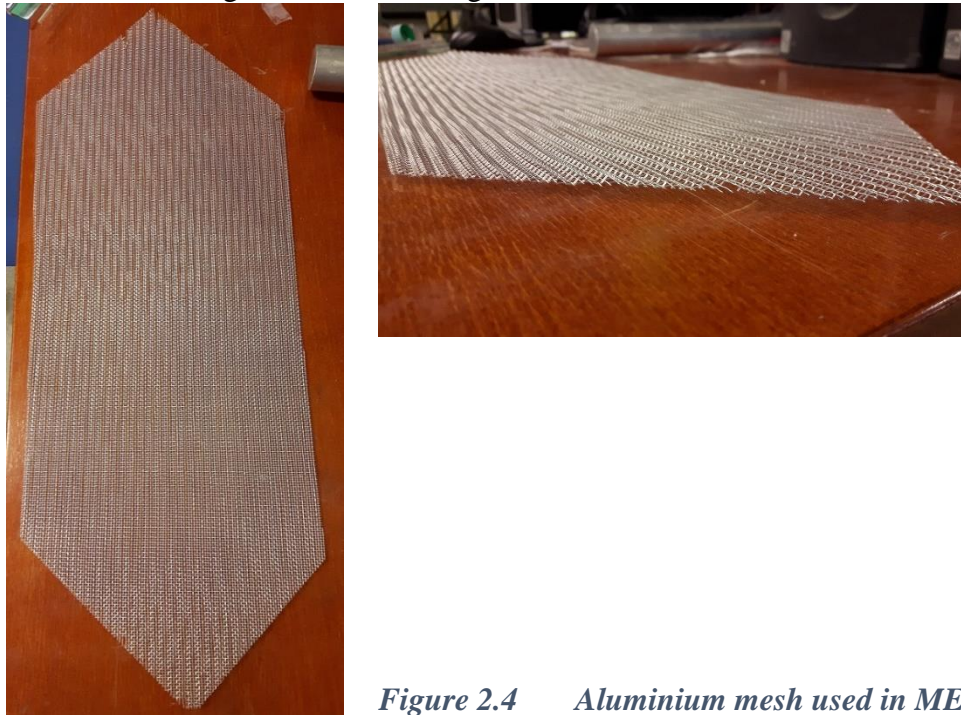


Figure 2.4 Aluminium mesh used in MEE

2.4 Membrane properties

Membranes can be made up of many different materials, but for cold climates, polymers are the preferred solution. Unlike paper membranes, which are used in hotter, more humid climates, polymer membranes don't get damaged that easily when the temperature drops below zero at the membrane surface [10]. An important feature of membranes is the permeability, which is the ability for water vapour to transfer through the membrane from one side to the other. We can distinguish membranes into two main types based on the pore geometry:

- Dense membranes
- Porous membranes

They can also be differentiated by their form: flat sheet or hollow fibre [13].

2.4.1 Dense membranes

Dense membranes typically have pores in the magnitude of 0.1 nm. The water vapour adsorbs onto the polymer and diffuses through the membrane on a molecular level. These membranes are used for gas separation processes, such as O₂ from N₂, CO₂ from combustion and water vapour from air. The membranes used in ventilation systems are hydrophilic and have a water/air selectivity of up to 10⁵. This means that for every molecule of N₂ that passes through the polymer, 10⁵ molecules of H₂O pass through, assuming equal driving potentials. Being hydrophilic, the membranes are highly permeable. With higher permeability, less area is needed for the process. Increasing permeability and selectivity have become an important area for research and development. Researchers have been looking at new polymer materials, ceramic materials, liquid membranes and composite membranes [13].

2.4.2 Porous membranes

Porous membranes typically have pores in the magnitude of 0,03 to 0,1 µm with porosities varying between 40 % and 70 %. In porous membranes, water vapour diffuses through the mixture within the pores. Unlike dense membranes, porous membranes are hydrophobic. This keeps the water molecules attracted to each other rather than solid material. Surface tension is created and the water is kept from entering the pores creating a liquid to gas interface. Unlike dense membranes, porous membranes are used to contact a liquid with gas [13]. Within porous membranes a subdivision into parallel cylindrical pores and voids between stacked spheres can be made. The figure 2.5 represents the simplified geometry of the porous membrane. If the pores differ in size, the vapour transfer across the membrane will change accordingly to a change in vapour pressure, where the smaller pores will become permeable at greater vapour pressure. This relation can be shown in figure 6 of [14], where the moisture transfer diffusive resistance decreases with an increase in relative humidity for all membranes tested. When the pore size is constant over the entire membrane the diffusivity is considered constant at different vapour pressure [5]

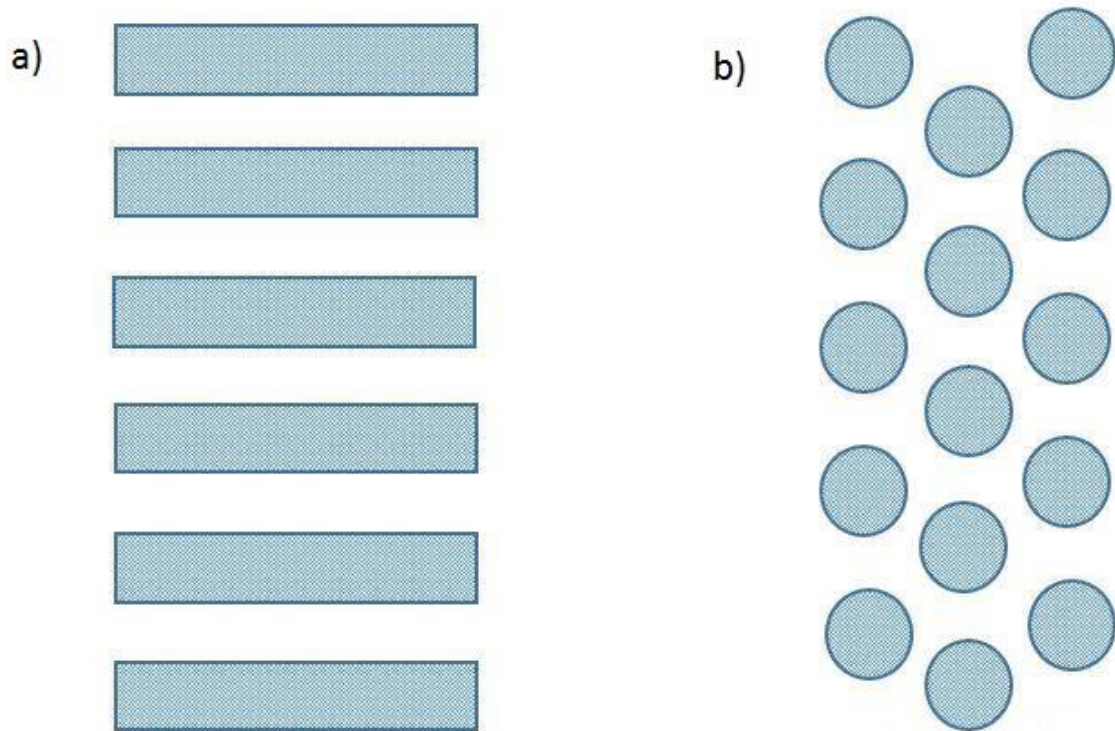


Figure 2.5 *a) Parallel cylindrical pores*
 b) Voids between stacked spheres

2.5 Test rig membrane

In the MEE test rig an isoporous hydrophobic membrane with parallel cylindrical pores perpendicular to the membrane is assumed. Since the pore size is considered constant over the entire membrane the permeability will remain the same at different vapour pressures. When the membrane is exposed to high levels of humidity, it gets bloated and expands. This would result in blockages and uneven flow through the exchanger, but has been solved by inserting the aluminium mesh mentioned earlier.

3 Theoretical modelling

The theory is divided into two main components. One concerning the specific theory needed for the flow pattern test rig and the second part for the remaining theory essential for the membrane energy exchanger.

3.1 Flow pattern test rig

3.1.1 Dimensioning entry and exit length

Reynold number [15]:

$$Re = \frac{\rho u D_h}{\mu} = \frac{u D_h}{\nu} \quad (1)$$

Where u equals the velocity, D_h the hydraulic diameter and ν the kinematic viscosity. The hydraulic diameter is used because the ducts are non-circular. The Reynolds number is a dimensionless quantity that shows the relationship between viscous and inertial forces. The Reynold number is used to determine whether the flow is laminar or turbulent. The Reynolds number determines which equation is to be used. With a relatively low velocity and hydraulic diameter compared to the kinematic viscosity, laminar flow equations are used.

Hydraulic diameter [15]:

$$D_h = \frac{4 * \text{crosssectional area}}{\text{wetted perimeter}} = \frac{4(H * W)}{2H + 2W} \quad (2)$$

The hydraulic diameter for non-circular ducts equals the cross-section area over the wetted area with H being the height and W, the width.

Prandtl number [15]:

$$Pr = \frac{C_p \mu}{\lambda} \quad (3)$$

The Prandtl number is a dimensionless quantity that shows the relationship between the viscous and thermal diffusion rate. The Prandtl number decides which formula to use in order to find the entry length of the duct. When the Prandtl number is $1 < Pr$, the hydrodynamic boundary layer develops faster than the thermal boundary layer. The opposite effect occurs when $1 > Pr$. Since $Pr \approx 0,71$ for air, the hydrodynamic entry length (5) is used to calculate the required entry length for the flow pattern test rig.

Thermal entry length [15]:

$$\left(\frac{x_{fd,t}}{D_h}\right)_{lam} = 0,05 Re Pr \quad (4)$$

Hydrodynamic entry length [15]:

$$\left(\frac{x_{fd,h}}{D_h}\right)_{lam} = 0,05 Re \quad (5)$$

With the calculated hydrodynamic entry length, the minimum required entry duct for the flow pattern test rig is known.

3.1.2 Volumetric flow rate

In order to obtain the same volumetric flow through the flow pattern test rig compared to the MEE, three rotameters have been utilized to measure the normal flow rate. The normal conditions are a set standard on the rotameter at predetermined conditions. The actual flow rate is found by converting the normal flow, using the pressure difference of a vacuum cleaner and the standardized pressure of the rotameter.

The air can be treated as an ideal gas, so the flow rate can be found through the ideal gas law:

$$PV = nRT \quad (6)$$

The amount of molecules is assumed to stay the same

$$V_1 = \frac{P_2 V_2 T_1}{P_1 T_2} \quad (7)$$

Where P_1 is pressure at normal conditions, P_2 pressure at actual conditions, T_1 is temperature at normal conditions, T_2 actual temperature of air, V_1 normal litre per minute and V_2 litre per minute. For a channel flow with a velocity lower than 1 m/s these conversion calculations can be neglected and normal flow used as one can see in figure 3.1. The channel flow rate for the exchanger test rig is chosen to be from 2-3 m/s and the conversion calculations mentioned above are therefore not neglected.

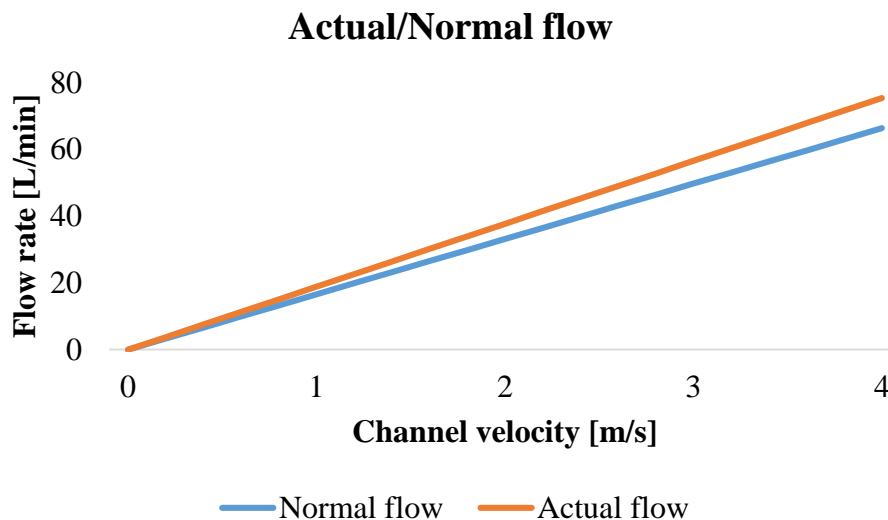


Figure 3.1 Normal and actual flow

3.2 Membrane energy exchanger test rig

3.2.1 Pressure drop and airstream velocity

In order to determine the velocity of the airstream in the MEE test rig, pressure drop is measured with a manometer over an orifice plate. The pressure drop is used to indicate the airflow rate, which in turn will give the velocity of the airstream

The general equation for the volumetric flow is [15]:

$$\dot{V} = A_c u \quad (8)$$

Where A_c is the cross sectional area and u the velocity.

The mass flow rate for the orifice plate can be determined as [16]:

$$\dot{m} = \frac{C}{\sqrt{1 - \beta^4}} \varepsilon \frac{\pi}{4} d^2 \sqrt{2\Delta P \rho} \quad (9)$$

Where C is the discharge coefficient, β the diameter ratio, ε the expansibility factor, d the inner diameter of the orifice plate, Δp the pressure drop over the orifice plate and ρ the density of air.

The diameter ratio can be expressed as [16]:

$$\beta = \frac{d}{D} \quad (10)$$

Where D is the inner diameter of the pipe.

The expansibility factor is found [16]

$$\varepsilon = 1 - (0,351 + 0,256\beta^4 - 0,93\beta^8) \left[1 - \left(\frac{p_2}{p_1}\right)^{1/\gamma}\right] \quad (11)$$

Where γ is the heat capacity ratio for air.

The simplified discharge coefficient is [16]

$$C = 0,5961 + 0,0261\beta^2 - 0,216\beta^8 + 0,000521 \left(\frac{10^6 \beta}{Re_D}\right)^{0,7} + \left(0,0188 + 0,0063 \left(\frac{19000\beta}{Re_D}\right)^{0,8}\right) \beta^{3,5} \left(\frac{10^6}{Re_D}\right)^{0,3} \quad (12)$$

The full discharge coefficient calculations are located in Appendix A

The pressure drop is defined as:

$$\Delta p = \rho_m g h_p \quad (13)$$

Where ρ_m is the manometer fluid density, g is gravitational constant and h_p is height difference in the manometer fluid on p_1 and p_2 side. The pressure drop can be read from the manometer at the test rig.

3.2.2 Moisture transfer resistance

To express the vapour transfer through the parallel cylinders in the membrane Hagen-Poiseuille equation is used [17]:

$$J = \frac{\varepsilon r^2 \Delta P_{wv}}{8\eta\tau \delta} \quad (14)$$

Where ε is the porosity, r the pore radius (m), η the liquid viscosity(Pa*s), τ the tortuosity, δ the membrane thickness (m). For the membrane installed the water vapour transfer has been tested by the manufacturer. It transfers 8.4 kg/(m²day) at 25 °C isothermal condition with one stream operating at 50% humidity and the other with dry air.

The water vapour pressure can be expressed as a function of relative humidity and saturation pressure:

$$P_{wv} = P_{sat}RH \quad (15)$$

The pressure for 100% humidity at a certain temperature is called the saturation pressure. The saturation pressure can be defined as [18] of the Magnus-Tetens formula:

$$P_{sat} = 6,112 * \exp\left(\frac{17,67 * t}{t + 243,5}\right) \quad (16)$$

Where t is the temperature in °C. It has an accuracy within 0,1% for the temperature interval -30 °C to 35 °C in comparison to the Hyland- Wexler equation:

$$\ln(P_{sat}) = \left[-\frac{5800.2206}{T} + 1.3914993 - 0.48640239 * 10^{-1}T + 0.41764768 * 10^{-4}T^2 - 0.14452093 * 10^{-7}T^3 + 6.545973 \ln(T) \right] \quad (17)$$

In order to calculate the pressure for any value of RH, we multiply P_{sat} by the factor $\frac{RH}{100}$:

$$P = 6,112 * \exp\left(\frac{17,67 * t}{t + 243,5}\right) * \frac{RH}{100} \quad (18)$$

The absolute humidity can be defined by using the ideal gas law (6) and the equation (18) and multiplying by 18.02, the molecular weight of water and adjusting units from g/m³ to kg/kg [19]:

$$w = \frac{6,112 * \exp\left(\frac{17,67*t}{t+243,5}\right) * RH * 2,1674}{(273,15 + t) * 1,204 * 10^3} \quad (19)$$

Where RH is the relative humidity in percent and t is the temperature in Celsius.

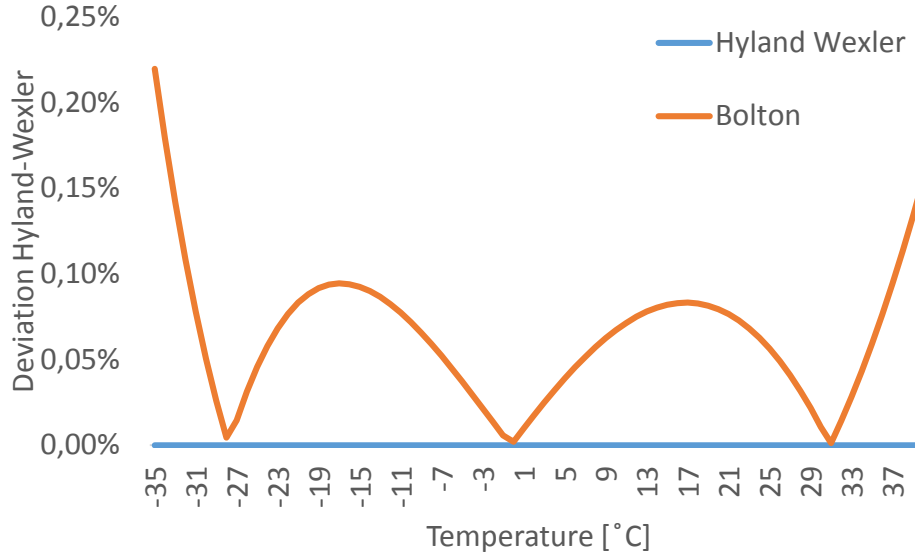


Figure 3.2 Deviation from Hyland-Wexler

$$P_{wv} = \frac{(273,15 + t) * w}{0,0018} \quad (20)$$

Inserting (20) into (14), the water vapour transfer can now be expressed as:

$$J = \frac{273,15 + t}{0,0018} \frac{\epsilon r^2}{8\eta\tau} \frac{w_{mE} - w_{mS}}{\delta} \quad (21)$$

The moisture transfer diffusive resistance for the membrane is defined as:

$$r_{mm,p} = \frac{w_{me} - w_{ms}}{J} \quad (22)$$

The moisture transfer diffusive resistance tells us how permeable the membrane is towards water vapour. A higher resistance gives a lower latent effectiveness.

Inserting equation (21) into (22) we get:

$$r_{mm,p} = \frac{0,0018\delta}{(273,15 + t) \frac{\varepsilon r^2}{8\eta\tau}} \quad (23)$$

The hydraulic permeability of the membrane can further be determined as $L_p = \frac{\varepsilon r^2}{\eta\tau}$ [17] giving:

$$r_{mm,p} = \frac{0,0018\delta}{(273,15 + t)L_p} \quad (24)$$

3.2.3 Heat and mass transfer

The Colburn j factor is a dimensionless heat transfer coefficient used to calculate the natural convective movement of heat to gases and liquids through a surface [15]. For the purpose of this thesis we have a gas in the form of air with the membrane acting as the surface. It is defined as:

$$j = \frac{Nu}{RePr^{\frac{1}{3}}} = \frac{h}{C_p\rho u} Pr^{2/3} \quad (25)$$

Where the Nusselt number, Nu , is the relationship between the total heat transfer and conductive heat transfer. The Colburn j factor used for the calculations in this thesis have been based on the experimental factor obtained in a previous work on the MEE presented[5]. It is defined as:

$$j = 0.23Re^{-0.45} \quad (26)$$

By rearranging equation (25) in order to get the heat transfer coefficient we get:

$$h = \frac{jC_p\rho u}{Pr^{2/3}} \quad (27)$$

Where C_p is the heat capacitance of air, ρ the density of air, u the velocity of the air.

The Schmidt number can be defined as:

$$Sc = \frac{\nu}{D_{wv}} \quad (28)$$

Where D_{wv} is the mass diffusivity of water vapour in air. The Schmidt number is a dimensionless quantity that defines the relationship between viscous and molecular diffusion rate.

The Lewis number can be written as:

$$Le = \frac{Sc}{Pr} \quad (29)$$

Where the Lewis number is a dimensionless relationship between the thermal diffusivity and mass diffusivity.

Using the Chilton-Colburn analogy and rearranging with (29) we find the convective moisture transfer [15]:

$$\frac{Sh}{ReSc^{\frac{1}{3}}} = \frac{Nu}{RePr^{\frac{1}{3}}} \quad (30)$$

The Sherwood number can be written as:

$$Sh = NuLe^{\frac{1}{3}} \quad (31)$$

Where the Sherwood number is the ratio between mass transfer rate and diffusion rate. The Lewis number is said to be 1.22 – 1.99 for ventilation air and water vapour mixture at atmospheric states. For conditions in this thesis however it will be about 0.83.

The convective moisture transfer can be defined as [5]:

$$k = \frac{ShD_v}{D_h} \quad (32)$$

Using the equations (28) (31), (29), (25) and (1) above it can be shown that the convective moisture transfer can be defined as:

$$k = \frac{j\rho u \left(\frac{v}{D_{wv}}\right)^{\frac{1}{3}}}{\mu} \quad (33)$$

The heat conduction resistance through the membrane is [5]:

$$r_{hm} = \frac{\delta}{\lambda_m} \quad (34)$$

The overall sensible heat transfer coefficient can be defined as [20]:

$$U_s = \left[\frac{1}{h_s} + \frac{\delta}{\lambda} + \frac{1}{h_E}\right]^{-1} \quad (35)$$

Where $h_{S/E}$ is the convective heat transfer for the supply and exhaust air respectively, δ the membrane thickness and λ thermal conductivity.

With membrane thickness being very thin $\delta \approx 0$, the equation can be shortened to:

$$U_s = \left[\frac{1}{h_s} + \frac{1}{h_E}\right]^{-1} \quad (36)$$

The overall latent heat transfer coefficient can be defined as [5]:

$$U_l = \left[\frac{1}{k_S} + \frac{\delta}{\lambda_m} + \frac{1}{k_E} \right]^{-1} \quad (37)$$

Where λ_m is the diffusive mass transfer coefficient. Unlike the convective heat transfer, the moisture diffusion cannot be neglected and usually accounts for 65-90% of the total moisture transfer resistance [21].

3.2.3 Effectiveness

The quasi-counter-flow MEE can be defined as a composite heat exchanger, with a true counter-flow core and cross-flow headers. The exchanger heat transfer total effectiveness for an air to air heat exchanger can be written as [20]:

$$\varepsilon = \frac{q}{q_{max}} = \frac{C_E(h_{E,in} - h_{E,out})}{C_{min}(h_{E,in} - h_{S,in})} = \frac{C_S(h_{S,in} - h_{S,out})}{C_{min}(h_{E,in} - h_{S,in})} \quad (38)$$

The number of heat transfer units can be defined as:

$$NTU = \frac{UA}{C_{min}} \quad (39)$$

The NTU method is used to predict the performance of a heat exchanger. It is used for exchanger analysis when only the inlet temperatures are known. It relates the total heat transfer rate to quantities such as inlet and outlet temperatures, surface area of heat exchanger and the overall heat transfer coefficient [15].

For sensible counter-flow the effectiveness can be defined as [15]:

$$\varepsilon_{s,counter} = \frac{NTU_s}{1 + NTU_s} \quad (40)$$

The number of heat transferring units is considered the same for crossflow.

$$NTU_s = \frac{U_s A}{(\dot{m}C_p)_{min}} \quad (41)$$

For latent counter-flow [20]:

$$\varepsilon_l = \frac{NTU_l}{1 + NTU_l} \quad (42)$$

$$NTU_l = \frac{U_l A}{\dot{m}_{min}} \quad (43)$$

For a cross-flow the sensible and latent effectiveness can be defined as [5]:

$$\varepsilon_{s/l} = 1 - \exp\left[\frac{\exp(-NTU_{s/l}^{0.78}) - 1}{NTU_{s/l}^{-0.22}}\right] \quad (44)$$

Capacity ratio [20]

$$c_r = \frac{C_{min}}{C_{max}} \quad (45)$$

In the MEE rig already in place, c_r is assumed to be 1 because Cp and mass flow are considered to be approximately the same for both flows.

To find the overall effectiveness of the MEE, the two expressions for cross and counter flow need to be added together according to their contribution to the overall effectiveness. This relation can be expressed by [22]:

$$\varepsilon_{quasi-counter} = \frac{A_{cou}}{A_{tot}} \varepsilon_{cou\ flow} + \frac{A_{cro}}{A_{tot}} \varepsilon_{cro\ flow} \quad (46)$$

The experimental sensible effectiveness for a balanced flow is:

$$\varepsilon_s = \frac{T_{S,out} - T_{S,in}}{T_{E,in} - T_{S,in}} \quad (47)$$

The experimental latent effectiveness for a balanced flow is:

$$\varepsilon_l = \frac{W_{S,out} - W_{S,in}}{W_{E,in} - W_{S,in}} \quad (48)$$

3.3 Uncertainty

The uncertainty describes the accuracy of the experimental results. The uncertainty can be divided into two parts:

1. Random uncertainty: instrument accuracy, influence from other sources etc.
2. Systematic uncertainty: measurement calibration and upset of instruments etc.

From the graph below, we can see periodically random fluctuations in sensible effectiveness. We can also, to some extent, see that the latent effectiveness follows these fluctuations. The author believes these fluctuations are most likely due to a release of built up pressurised steam from the boiling flask into the supply inlet air. A delay was observed for the different thermocouples, with a sudden change in temperature and moisture conditions. It is believed that this caused irregularities in both sensible and latent effectiveness, as can be seen in the figure below.

Effectiveness fluctuations at 7,4 °C

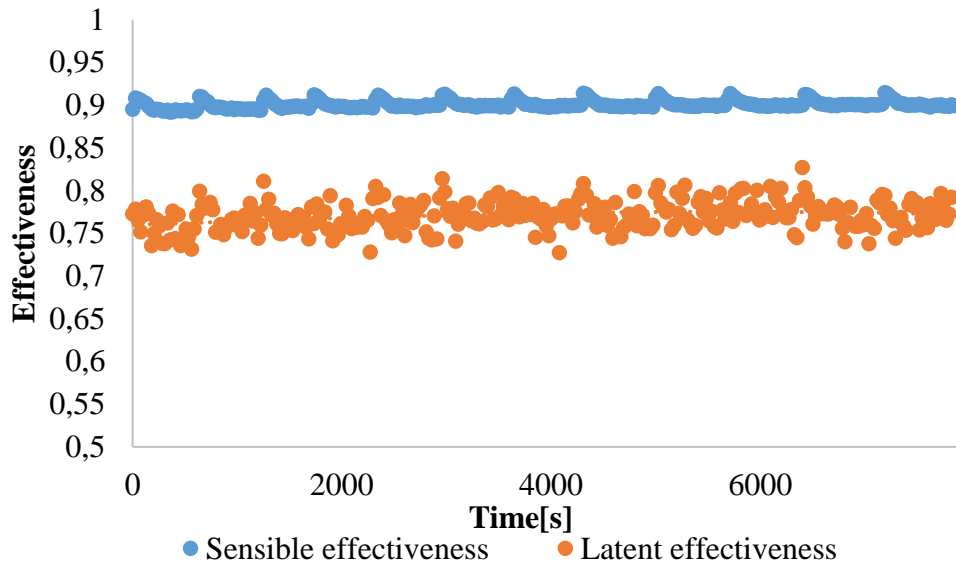


Figure 3.3 *Sensible and latent effectiveness fluctuations*

The random uncertainty is found by calculating the standard deviation. The standard deviation can be expressed as:

$$s = \sqrt{\frac{\sum_{i=1}^n (x_i - \bar{x})^2}{(n - 1)}} \quad (49)$$

Where \bar{x} is the arithmetic mean value and n is the number of measurements. Furthermore, using the standard deviation, the random uncertainty is found through the student t distribution. The number of degrees of freedom in this thesis is between 300-350 for most of the measurements. This gives a $t \approx 1,970$ for a confidence interval of 95% [23]

$$U_r = t * s \quad (50)$$

The systematic uncertainty is given by the manufacturers for the measurement devices. Calibration of the devices may also affect the systematic uncertainty.

The total uncertainty can be shown as:

$$U_t = \pm \sqrt{U_r^2 + U_s^2} \quad (51)$$

In table (3.1) the total uncertainties regarding the critical values are presented. In table (3.2) the total uncertainties for the long running tests are presented. The uncertainty calculations for the other temperatures can be found in appendix B

Parameter	5,3 °C	10,3 °C	15,1 °C
RHs,in [%]	±7,84	±4,83	±4,98
RHs,out [%]	±0,87	±0,90	±0,99
RHe,in [%]	±0,92	±0,66	±0,91
RHe,out [%]	±2,79	±2,96	±3,89
Ts,in [°C]	±0,81	±0,29	±0,40
Ts,out [°C]	±0,27	±0,10	±0,10
Te,in [°C]	±0,09	±0,08	±0,10
Te,out [°C]	±0,80	±0,26	±0,38
Sensible e [%]	±1,51	±0,04	±0,62
Latent e [%]	±3,82	±3,59	±6,38

Table 3.1 *Total uncertainty with 60% RH exhaust inlet air and 70% RH supply inlet air*

Parameter	6,9 °C	10,3 °C	14,7 °C
RHs,in [%]	±6,93	±3,88	±5,61
RHs,out [%]	±1,12	±0,93	±1,66
RHe,in [%]	±1,06	±0,91	±1,57
RHe,out [%]	±2,41	±1,77	±4,80
Ts,in [°C]	±0,95	±0,45	±0,42
Ts,out [°C]	±0,39	±0,26	±0,29
Te,in [°C]	±0,16	±0,16	±0,29
Te,out [°C]	±0,88	±0,51	±0,34
Sensible e [%]	±2,71	±2,34	±0,58
Latent e [%]	±4,89	±4,76	±16,83

Table 3.2 *Total uncertainty for long running test with 53% RH exhaust inlet air and 70% RH supply inlet air*

4 Experimental setup

The objective of the experimental part of this thesis was to investigate how the quasi-counter flow rig works during outdoor conditions ranging from 5-15 °C and 70% RH, with varying indoor humidity levels at 22 °C. In addition to these tests, an additional test rig was constructed with a single channel to view the flow pattern of the air inside the quasi-counter flow test rig.

4.1 Flow pattern setup

The flow pattern setup is a small-scale model of the MEE setup. The flow pattern setup has one operational duct with the same mesh as in the MEE. The setup does not have a membrane. The purpose of this experiment was to see how the mesh affected the flow of air inside the MEE. In order to visualise the dispersion of the air when it comes in contact with the mesh, smoke was implemented with a Dräger air current tube. The mesh was also coloured a matte black in order to see the smoke more clearly

A similar setup has been made in another work prior to this experiment [4]. This, however, only tested for open channel flow without the mesh.

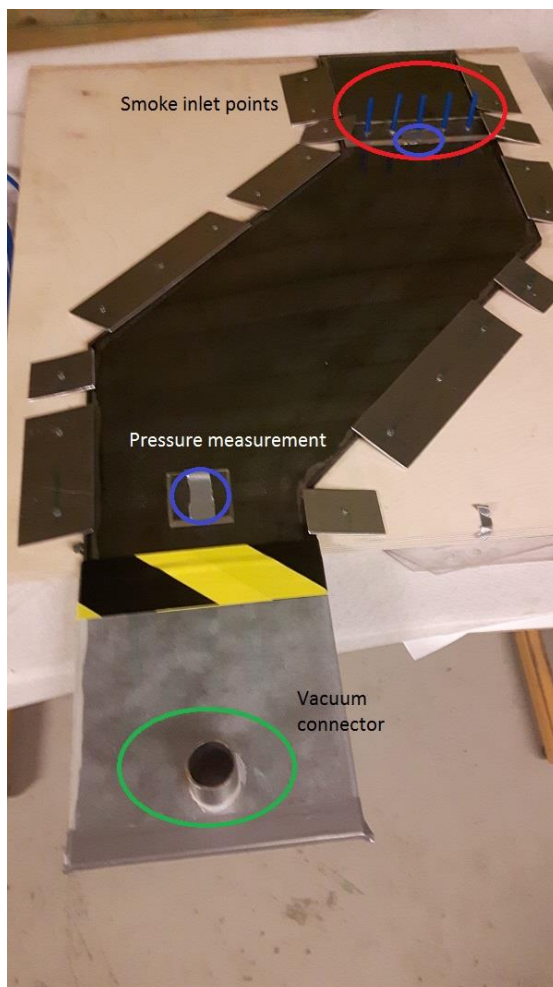


Figure 4.1 *Sensible and latent effectiveness fluctuations*

The supply air was taken from the lab room air and sucked through the exchanger channel by a vacuum cleaner. The air flow rate was measured using three rotameters. The negative pressure caused by the vacuum was considered substantial enough to take into account when calculating actual velocity from the normal conditions in the rotameters. Two holes were made before and after the mesh to measure the pressure drop over the exchanger. A manometer was used to measure the pressure drop. The top and bottom of the exchanger were pressed together with metal plates. To minimise leakages, a semi-viscous fluid was used as a sealant along the edges of the bottom. Five smoke-inlets in total were mounted on top of the inlet. They were spread evenly across the width, in order to look for differences in the airstream path direction.

4.2 Quasi-counter-flow setup

The quasi-counter-flow setup is made up of two environmental chambers, four fans, the MEE test section and connecting pipes. The MEE test section is made up of 18 air channels and 4 diffusors distributing the air.

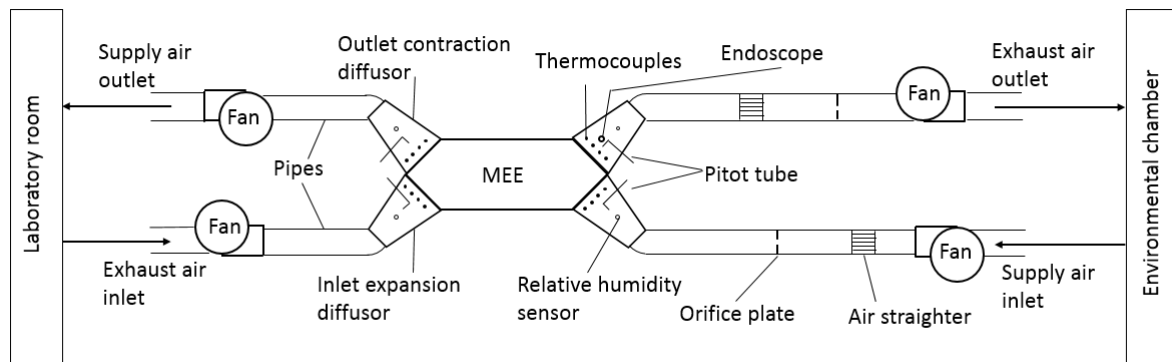


Figure 4.2 *Quasi-counter-flow test rig[5] with permission*

Temperature, pressure and RH is monitored through LabVIEW from a computer connected to the test rig. From the computer the humidifier can be switched on or off according to the experimental needs.

Pressure sensors are located before and after the MEE test section in both the exhaust and supply ventilation shaft in order to measure the pressure drop over the exchanger. To measure the airflow, two orifice plates are placed between the connecting pipes of the fan and MEE at the cold room side of the exchanger for both the supply and exhaust air. The temperature was monitored at the inlets and outlets of the MEE with four thermocouples at each location. They are spread evenly across the cross section. The use of more than one thermocouple is due to small differences in temperature at different positions. These differences are caused by the airstreams' exposure time inside the MEE, where the airstreams' closer to the edges of the MEE spend a longer time exchanging heat and moisture. This can be seen in figure 5.2 in the results of the airflow pattern test. In order to calculate the sensible and latent effectiveness, both the temperature and RH are essential to measure.

4.2.1 Relative humidity

In order to provide the needed RH for the airstreams a water spraying nozzle is installed within the air handling unit. The AHU provides the water for the exhaust inlet. In order to supply the RH needed for the supply inlet, a boiling flask providing steam is connected to the pipe near the inlet expansion diffusor.

4.2.2 HSE report

A HSE report was written for this experiment. It is listed in appendix F containing a detailed instrument list. The biggest risk with this experiment was being burned by the hot plate, boiling flask and its connecting tubes. The risks were found to be within acceptable limits to run the experiment.

5 Results

The experiments have been run at two different exhaust relative humidity levels. The humidity was set at 30-40% and 60% respectively. The exhaust inlet temperature was set at 22°C in both cases. The inlet supply temperature was set at 5-15°C with a RH at 70% according to weather data from three major cities: Oslo, Bergen and Trondheim during spring and autumn conditions. The mean temperature and RH of these cities are given in appendix C. In this section the main results will be presented. The remaining results can be seen in the appendix.

5.1 Flow pattern test rig

A test was performed for the flow pattern of an open channel quasi counter-flow MEE in 2012 [4]. This setup is similar, but has an aluminium mesh between the membrane layers. Therefore, a one-channel flow pattern test rig without membranes was developed in order to investigate whether the airflow would change substantially.

5.1.1 Pressure drop

The flow pattern rig was tested for velocities ranging from 0-2,8 m/s. With a pressure drop over the orifice plates of 28 Pa, the velocity within each channel in the MEE is 2,44 m/s. The pressure drop for the flow pattern test rig was 69 Pa. With 9 channels for both supply and exhaust air in the MEE this gave a total of 621 Pa loss over the exchanger, which correlates nicely with the pressure drop over the actual MEE.

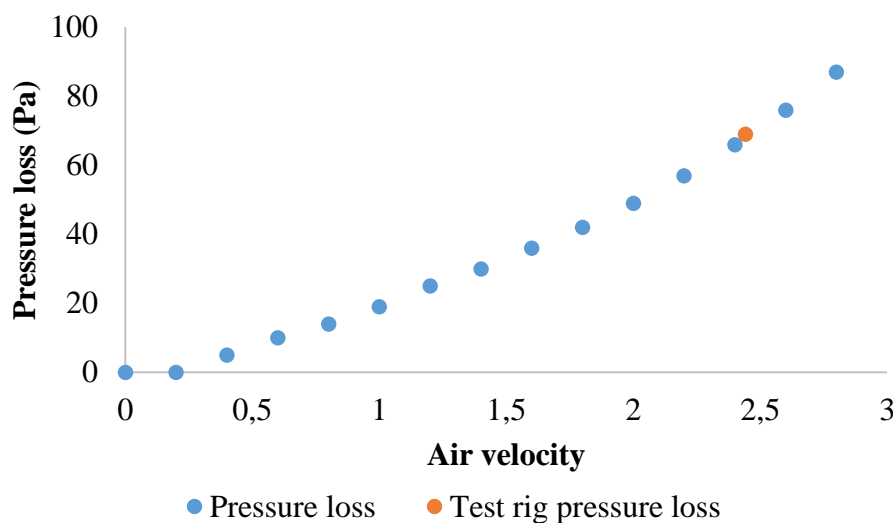


Figure 5.1 Pressure drop over mesh for flow pattern rig

5.1.2 Flow pattern

The flow pattern did not deviate much from the result received in [4]. The smoke followed the saw tooth grooves made in the aluminium mesh. It displayed a laminar flow as predicted according to the preliminary calculations for the Reynolds number. Since it is below the critical value of $2,3 \cdot 10^3$ for transitional flow it must be a laminar flow.

u	Re	u	Re
0	0,0	1,6	418,8
0,2	52,3	1,8	471,1
0,4	104,7	2	523,5
0,6	157,0	2,2	575,8
0,8	209,4	2,4	628,2
1	261,7	2,6	680,5
1,2	314,1	2,8	732,9
1,4	366,4		

Table 5.1 *Preliminary calculations for the Reynolds number*

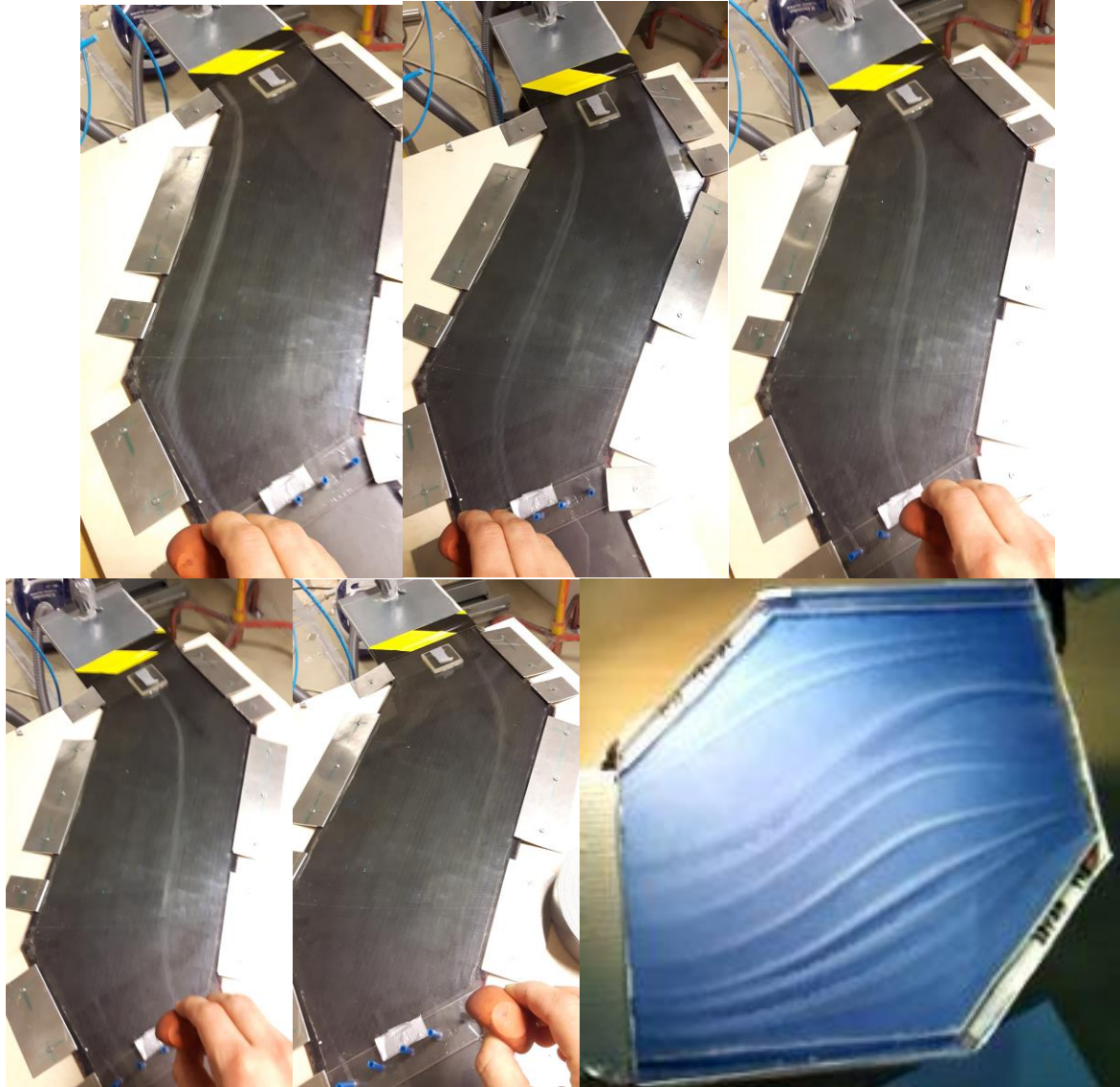


Figure 5.2 Flow pattern with aluminium mesh compared to open channel flow [4]

5.2 Effectiveness

The investigated temperatures and moisture levels gave a sensible effectiveness from 68-92% and inconsistent data for latent effectiveness for 30-40% RH. The inconsistency was due to higher moisture content at the supply inlet compared to the exhaust inlet. This resulted in a reversal of the moisture transfer and thereby a skewed and unrealistic result, because the equations used for the calculations no longer applied. The latent effectiveness gave consistent data for the lower temperature spectrum 5-10 °C. When looking at a Mollier Diagram (5.4) it was found that at around 10-12 °C, the moisture content in the supply inlet exceeds that of the exhaust inlet which results in the inconsistencies observed in figure (5.3).

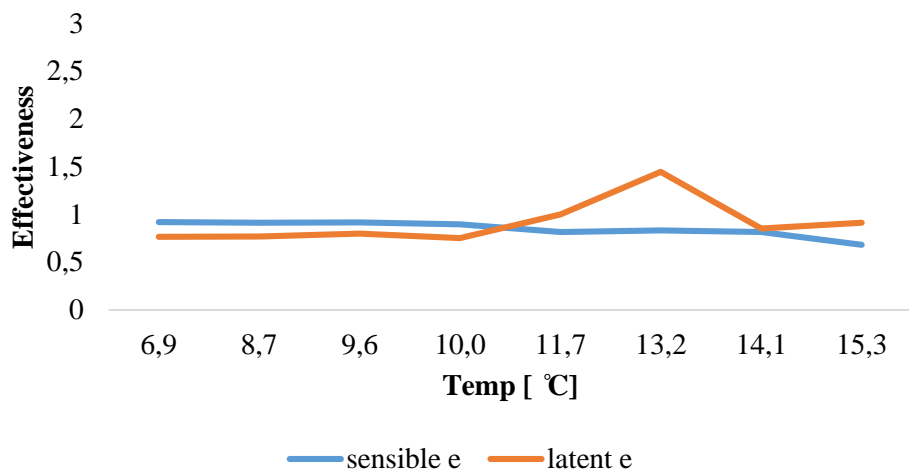


Figure 5.3 Unrealistic effectiveness results at 30-40% RH

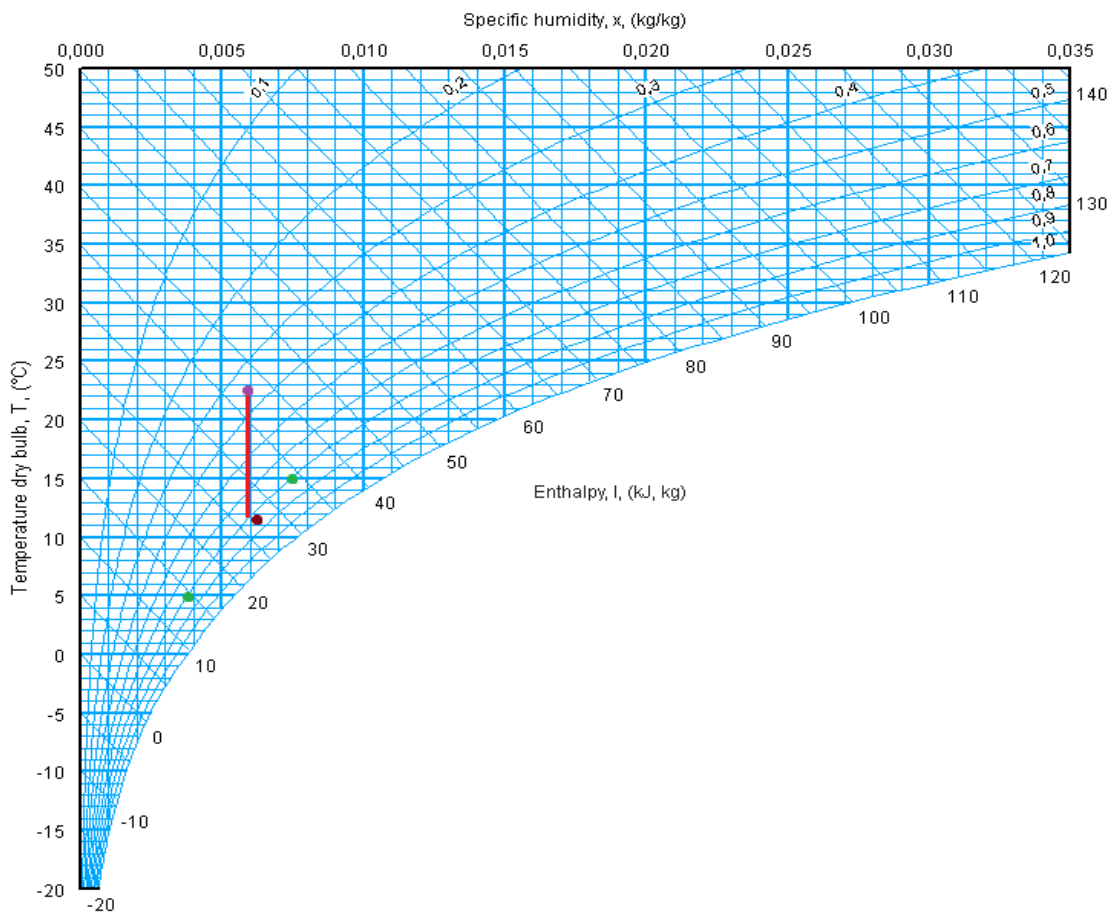


Figure 5.4 Change in moisture transfer due to higher specific humidity for supply air at 10-12 °C at 30-40% RH

In order to create a realistic result, a higher RH on the exhaust side had to be implemented. To be able to guarantee a higher moisture level than the outdoor air, the exhaust inlet required a RH of 46.5% minimum. As a safety measure 60 % RH was chosen for the exhaust in the experiments. This can be seen in figure below.

The sensible and latent effectiveness varied between 88,9 – 92,2 % and 73,6-79,8% respectively. The two effectiveness curves followed each other closely and, as expected, the latent effectiveness is lower than the sensible effectiveness. It is worth noting that the theoretical effectiveness is lower than the experimental effectiveness. It is the author's opinion that the uncertainties surrounding the boiling flask might have caused this effect. Further, the latent effectiveness found with the NTU-method is significantly lower than the experimental latent effectiveness compared to its sensible counterpart. This is due to a higher moisture transfer resistance compared to results in Peng Liu's calculations. In the author's calculation, the moisture transfer resistance is approximately 181 m²s/kg versus Liu's estimates of 100,8 m²s/kg. With his estimates for the moisture transfer resistant a latent effectiveness at approximately 78% is calculated, which is more in line with the results one would expect.

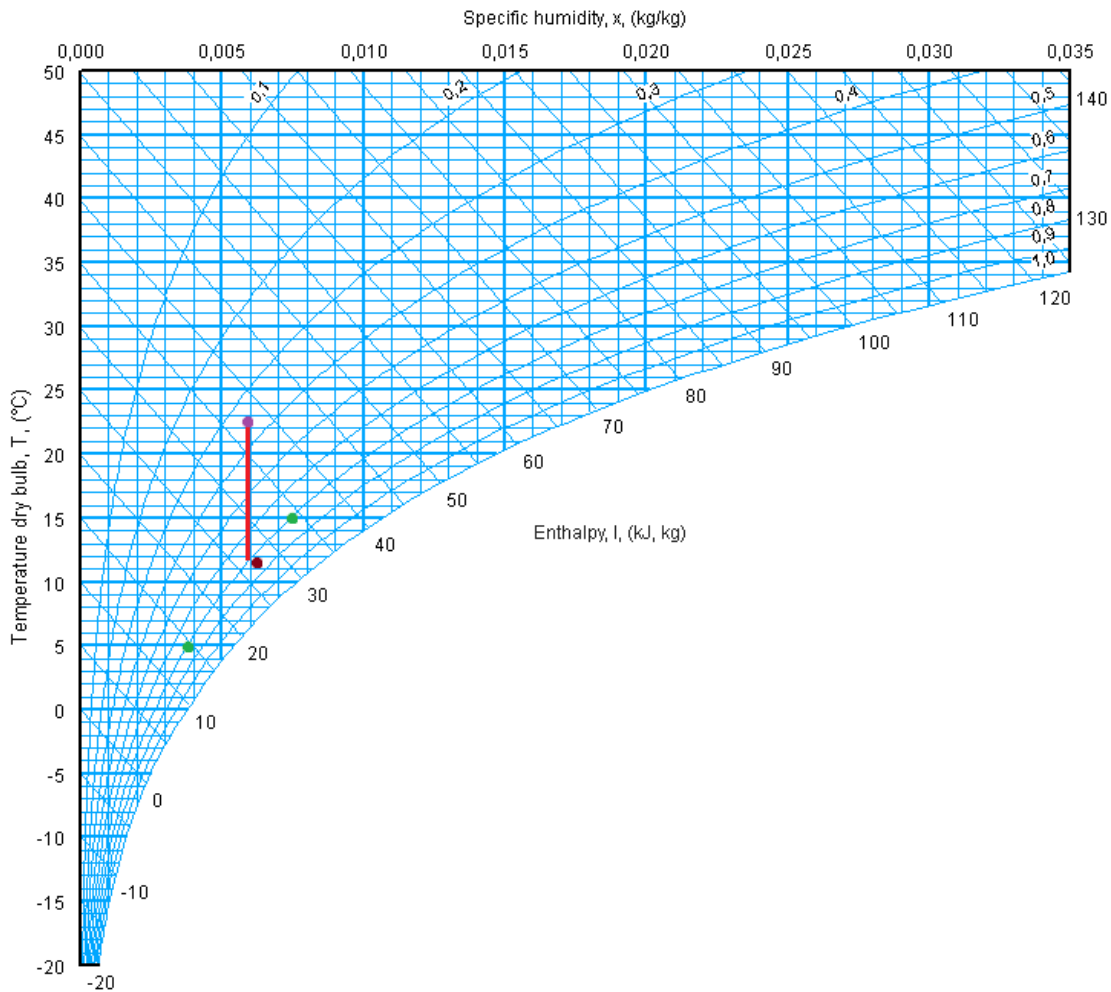


Figure 5.5 RH needed at 22 °C when supply inlet is at 15 °C, 70% RH

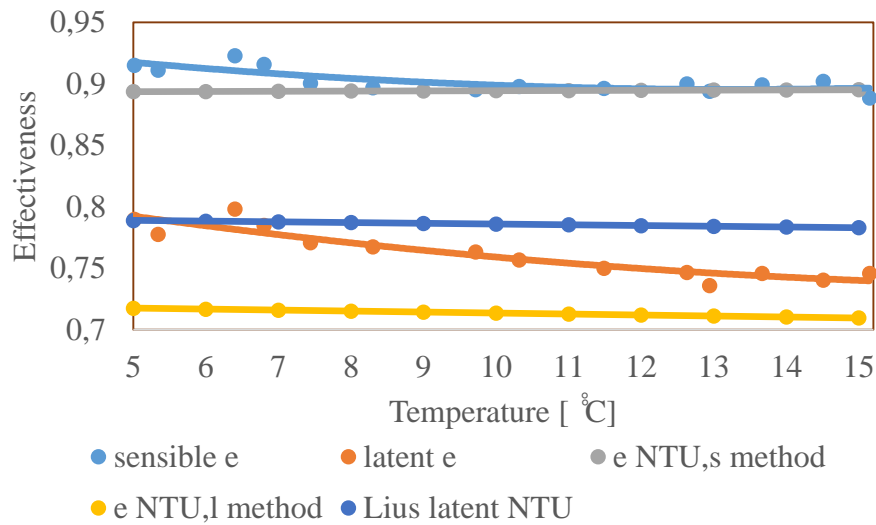


Figure 5.6 *Sensible and latent effectiveness found experimentally and with NTU method*

5.3 Moisture and condensation

When investigating the absolute moisture content into and out from the exchanger, it was uncovered that 1,8-5,2 % of the water condensed within the heat exchanger for the experiment using 60% RH. The amount drops with increasing outdoor temperature. This correlates with the theory for the moisture transfer resistance as seen in equation (24), which is reduced with increasing temperature. The same trend could be observed for the exhaust air at 30% for the interval that is consistent. Since the humidity level didn't rise up to 100% for any of the outlets and inlets, this should not have happened. One reason for the excess water could be excess steam from the boiling flask that had not mixed completely with the passing air. The author also observed that the temperature increased approximately 1-2 °C when the steam was added, which could be an indication of condensation.

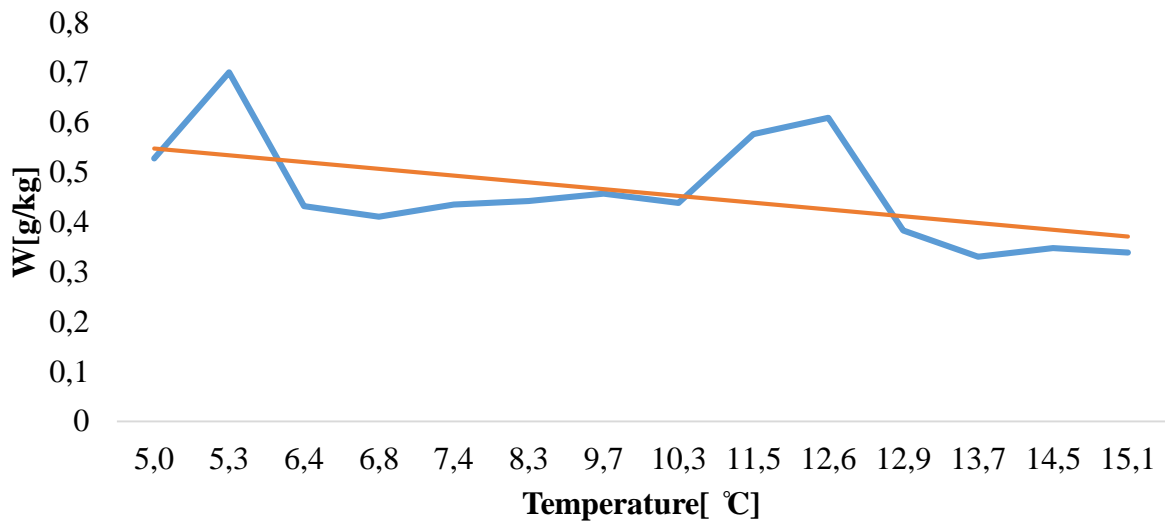


Figure 5.7 Water condensed per kg of air inside MEE at 60% RH for exhaust inlet

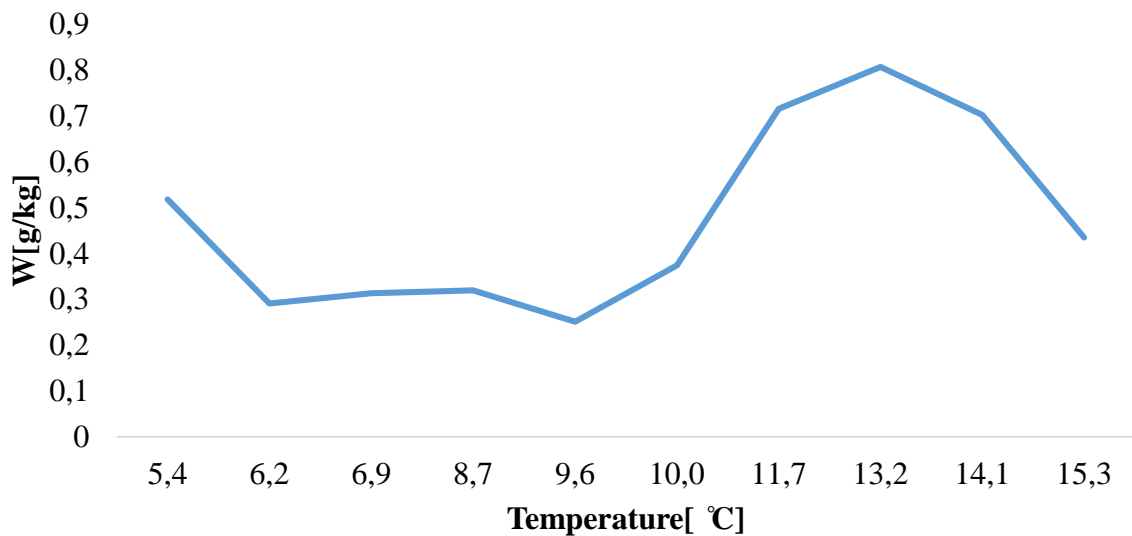


Figure 5.8 Water condensed per kg of air inside MEE at 30-40% RH for exhaust inlet

5.4 Pressure drop

In order to have the same flow rate for both the exhaust and supply air, the pressure drop over an orifice plate has been used to control the speed of the fans providing the air flow. The instruments at the test rig were not connected properly to LabVIEW due to technical

malfunction, so no consistent graphs could be produced for the pressure drop over the orifice plate or within the MEE. In the long-running tests, the pressure drop for the supply air was measured in LabVIEW. The pressure drop was controlled manually with four manometers. The pressure drop over the orifice plates was matched at 28 Pa for both supply and exhaust. The table(5.2) shows how the pressure drop over the orifice plates changed throughout the experiments, from start to finish. The overall pressure drop within the heat exchanger varied from approximately 550-650 on the supply side and 450-550 on the exhaust side. The pressure difference from finish to end of an experiment varied from 5-15 Pa for the exhaust side to 20-40 Pa for the supply side. The bigger difference in pressure drop for the supply is possibly due to the irregular feeding mechanism of the boiling flask crumpling the membrane as shown in [4]. In table (5.2) we can see that the pressure difference between the exhaust and supply air over the orifice plates is greater for lower temperatures. The pressure drop for the supply air could also be caused by the crumpling of the membrane. Since the pressure drop over the MEE is lower for the exhaust air it is possible that there is a higher flow for this section. This could explain the increase in pressure drop over the orifice plate.

Temperature	Pressure drop start		Pressure drop finish	
	Supply	Exhaust	Supply	Exhaust
15,2 °C	25	25	23	26
14,4 °C	28	28	26	28
13,8 °C	28	28	27	28
13 °C	28	28	28	28
12,6 °C	28	28	28	28
11,5 °C	28	28	28	29
10,3 °C	28	28	28	30
9,7 °C	28	28	28	28
8,3 °C	28	28	28	28
7,4 °C	28	28	27	29
6,8 °C	28	28	21	32
6,4 °C	28	28	20	30
5,3 °C	28	28	22	30

Table 5.2 *Pressure drop over orifice plate at start and finish*

5.5 Temperature and RH fluctuation

The moisture on the supply side is supplied by a boiling flask. Since this moisture is added at around 100 degrees this caused an effect on the temperature and RH. Since the feeding mechanism is controlled manually by a valve and depressurization in another flask limited to regularity, this caused fluctuations for both the temperature and RH. Beyond decreasing or increasing the effect of the hot plate, it was impossible to control the conditions within the boiling flask.

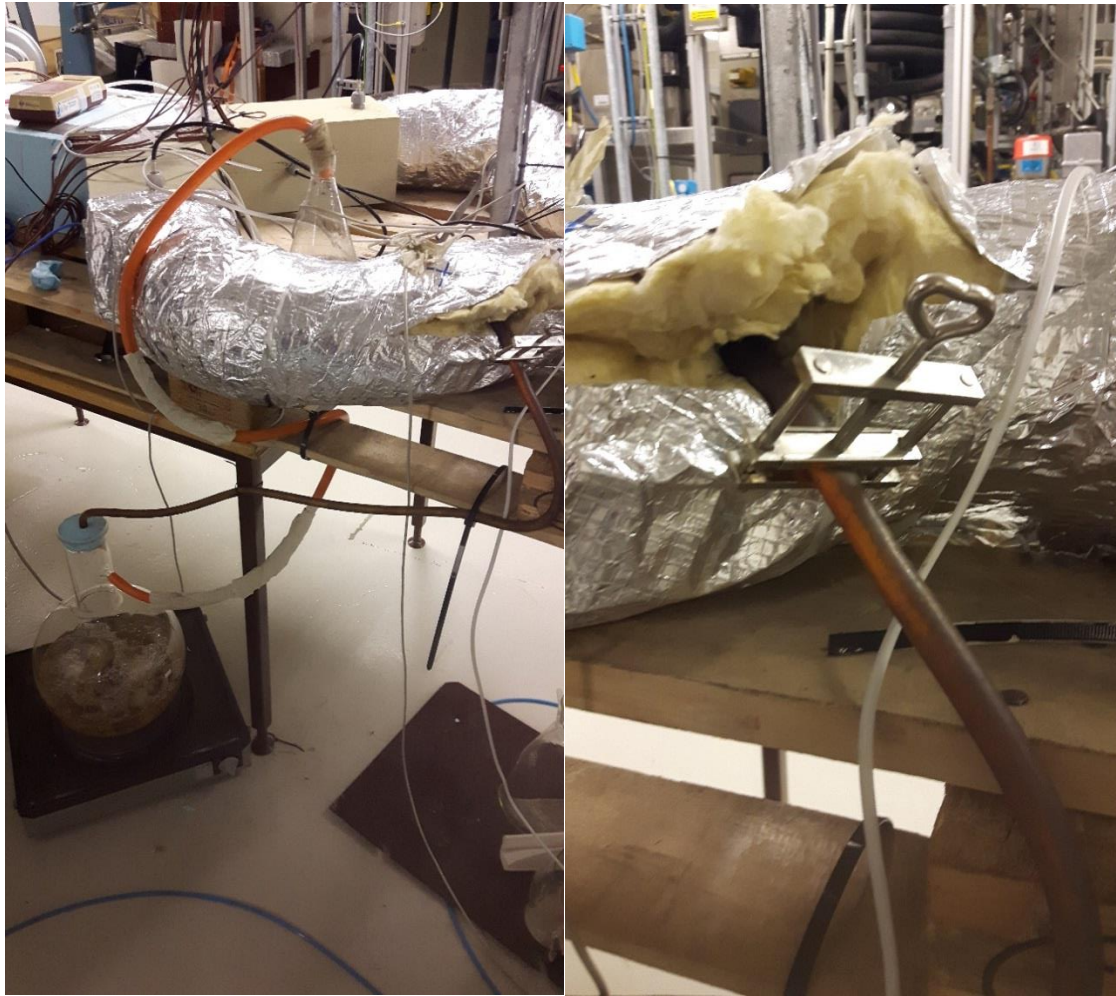


Figure 5.9 *Boiling flask setup*

This caused pressure build-up in the boiling flask until a pressure release occurred, causing higher temperatures and humidity levels for a short time, before normal operation resumed. As seen in table 3.1 the standard deviations for temperature and RH are listed for the lowest, middle and highest temperature range. As expected, the higher temperatures of 10,3 °C and 15.1 °C are the least affected. This is due to the greater capacity of higher temperatures to hold water without much change in RH and lower temperature difference between the air and steam. It is worth mentioning that the middle range temperature is actually more stable than the higher range temperature for RH and latent effectiveness. In figure (5.10) and (5.11) we can observe the temperature and RH fluctuations.

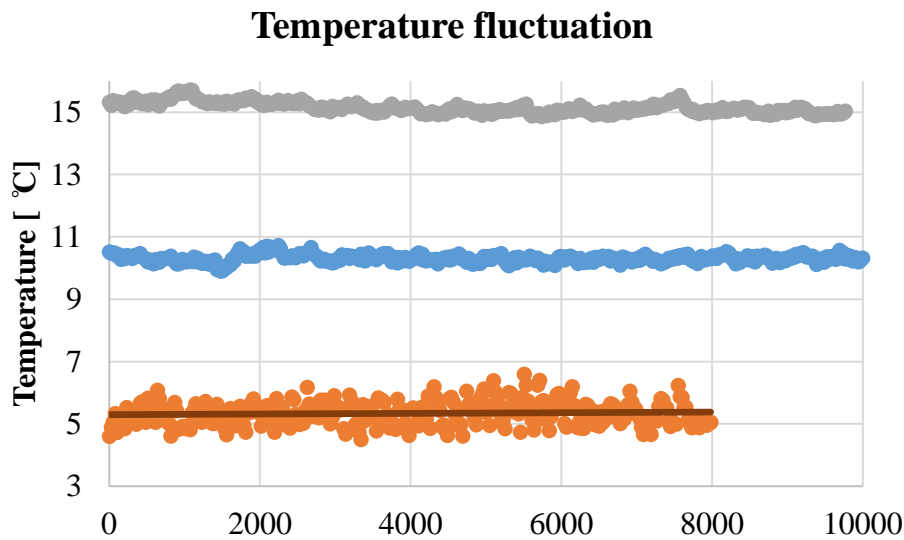


Figure 5.10 *Fluctuations in temperature for critical values*

We can clearly see the difference in fluctuations from both graphs. Especially the fluctuations for 5 °C are significant.

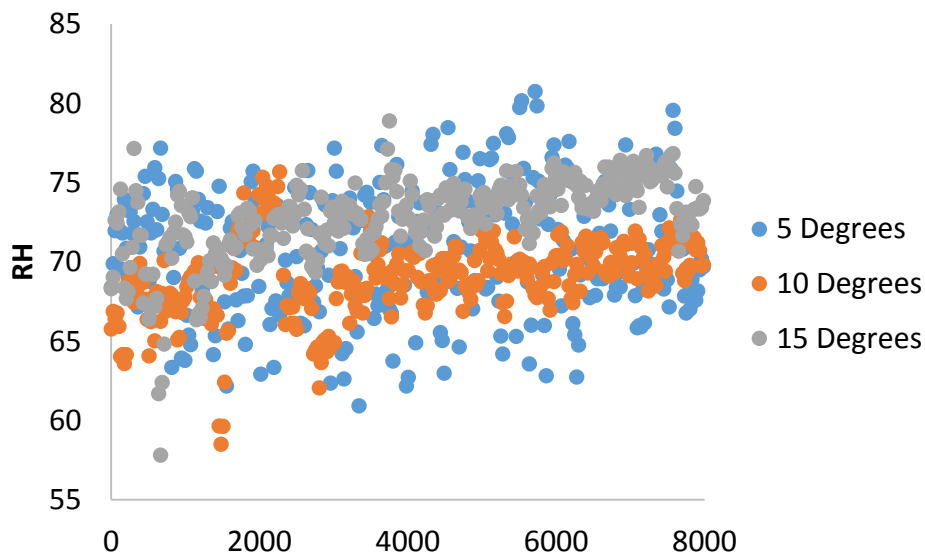


Figure 5.11 *Fluctuations in RH for critical values*

5.6 Long run performance

A long run test of the MEE over approximately 12 hours was run at 6,9, 10,3 and 14,7 degrees. The long run tests revealed a lot of condensation for the test run at the supply inlet. It is suspected that the cause of this is the long-term exposure of the steam in the boiling flask.

As seen in table 3.2 for the long run tests, the measurements for 14,7 °C were unexpectedly unstable compared to 6,9 °C and 10,3 °C. In the long run test, the middle range temperature of

10,3 °C was the most stable. The instability of the measurements concerning 14,7 °C could be caused by many factors. The manual valve could be adjusted in a way that caused great fluctuations in RH and in turn latent effectiveness, as viewed in fig (5.15). It could also be due to changing conditions made by the cap. During the experiment the cap material shrunk, hardened and caused leakages of vapour. To overcome the loss in pressure, the valve opening was adjusted further, creating greater fluctuation in RH. The effects of this vary significantly from experiment to experiment, where one cap might be used several times over and others for one time use only. The sensible and latent effectiveness for the critical temperatures can be viewed below.

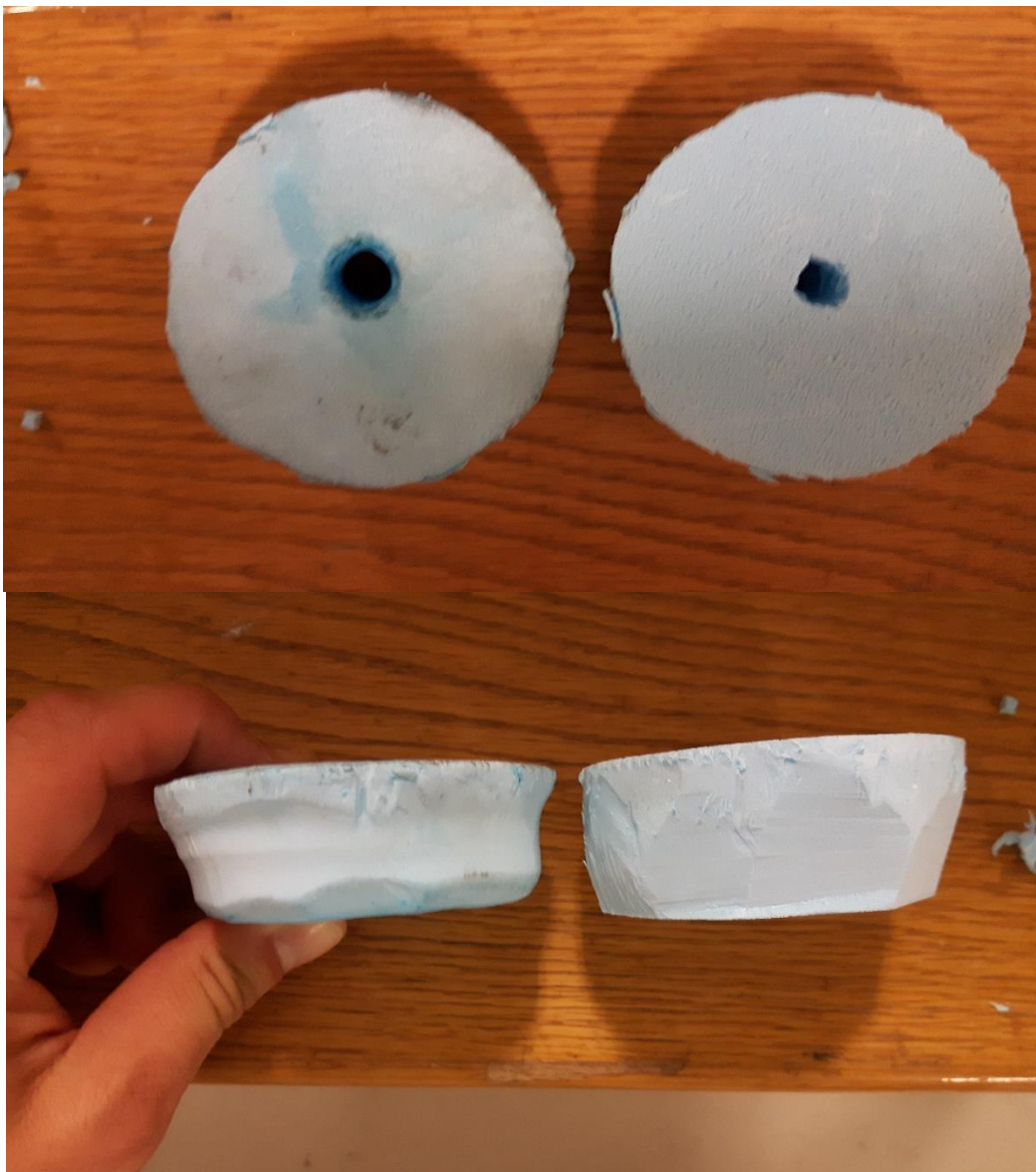


Figure 5.12 *Boiling flask cap before and after experiments. Hole has expanded due to shrinking of material.*

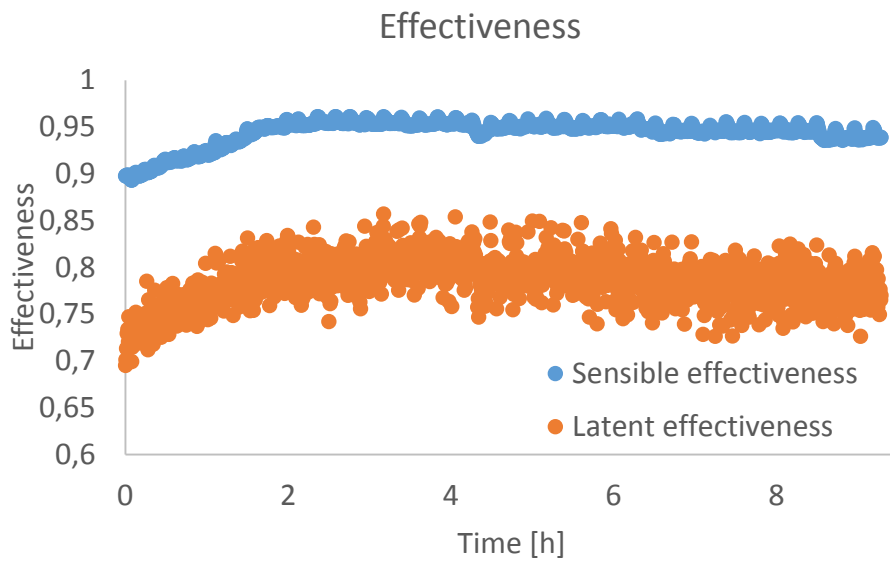


Figure 5.13 *Effectiveness for 6,9 °C supply inlet long run test*

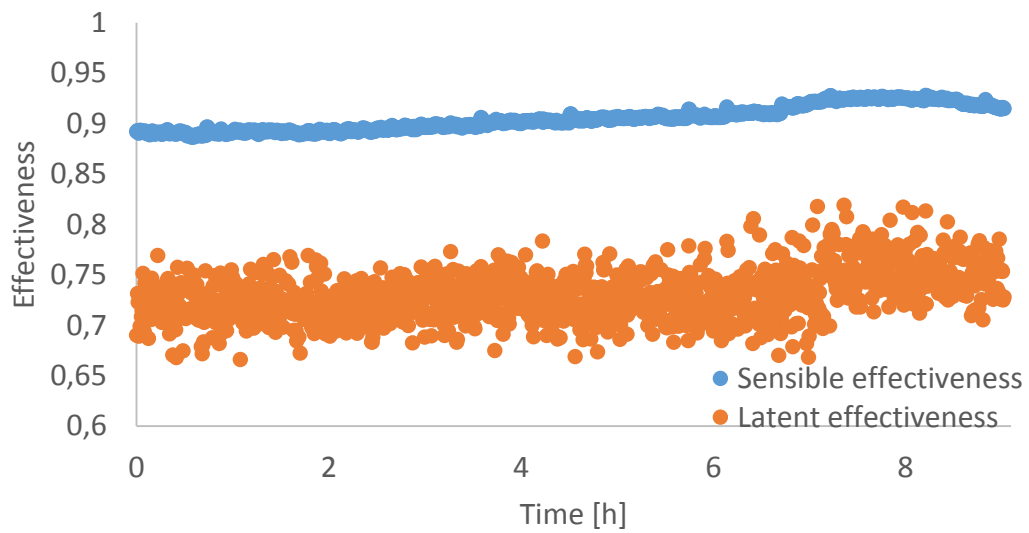


Figure 5.14 *Effectiveness for 10,3 °C supply inlet long run test*

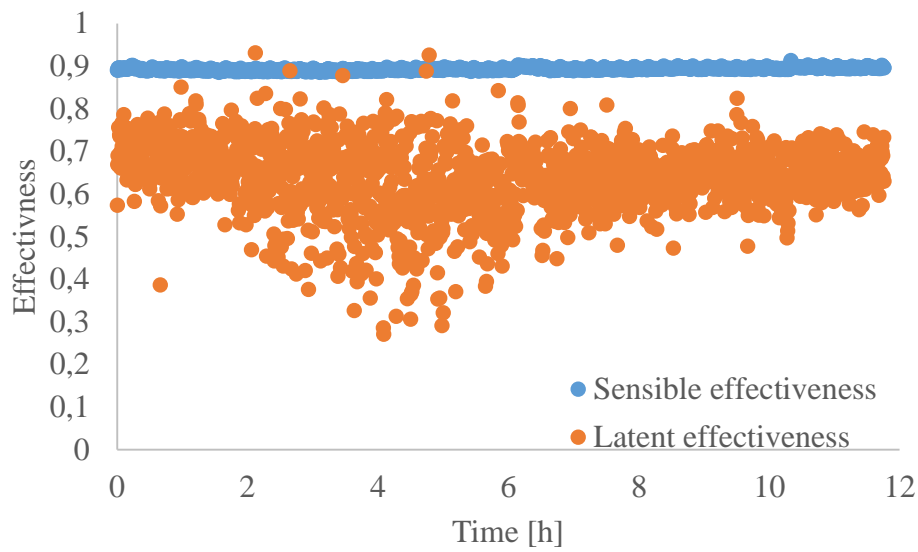


Figure 5.15 *Effectiveness for 14,7 °C supply inlet long run test*

The water trapped inside the MEE for the different temperature ranges is shown in the figures below. It is worth noting that the evaporation of water observed in figure (5.16) and (5.17) is caused by the emptying of the secondary flask connected with the orange hose as seen in fig (5.9) for condensed water. This resulted in a pressure drop in the boiling flask and no steam was able to enter the supply air for this time period. It also took a couple of minutes for the pressure inside the boiling flask to overcome the pressure inside the supply ventilation shaft.

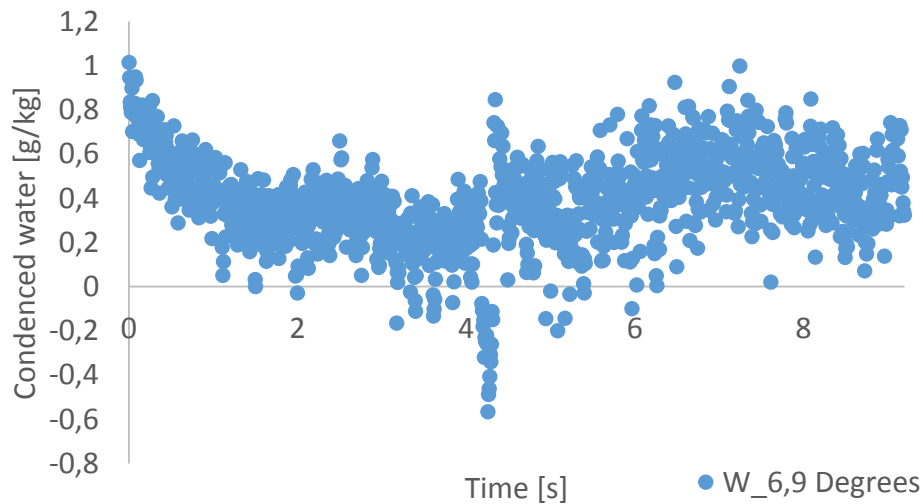


Figure 5.16 *Condensing water inside MEE for 6,9 °C supply inlet long run test*

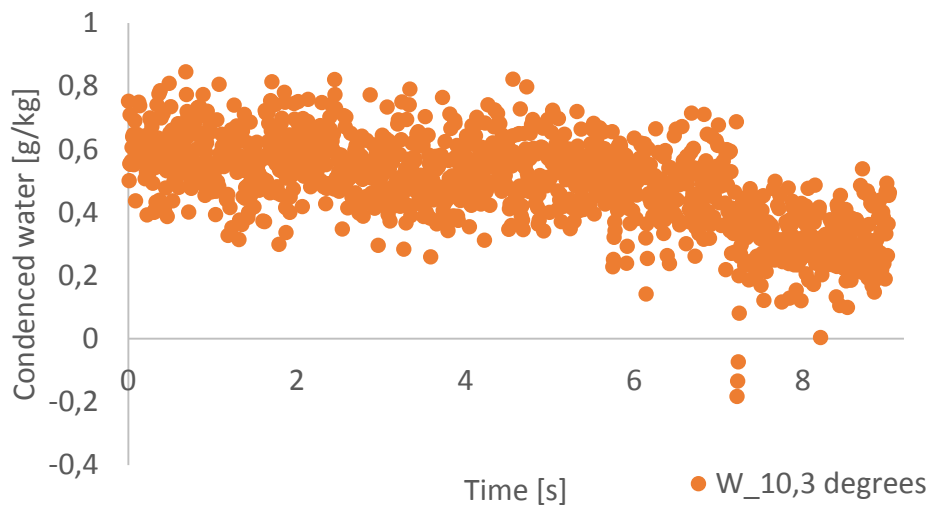


Figure 5.17 Condensing water inside MEE for 10,3 °C supply inlet long run test

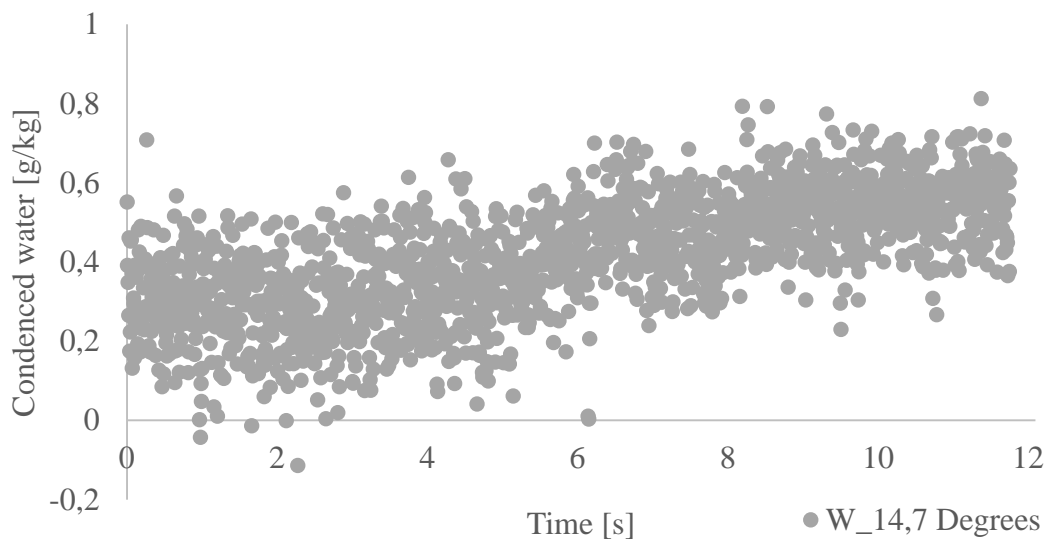


Figure 5.18 Condensing water inside MEE for 14,7 °C supply inlet long run test

In the figures below we can see the pressure drop over the MEE section for the supply side. We can see that the pressure drop remains relatively stable over the course of the experiments. The pressure drop for 6,9 °C was the most unstable. It is also possible to observe from the figures that random fluctuations occur more often with a decreasing temperature. It is in the authors view that these fluctuations probably are connected with the crumpling of the membrane as explained previously. It also fits with the change in pressure drop over the orifice plate. The decrease in pressure drop for the supply indicates a loss in flowrate through the MEE. This could be caused by the crumpling of the membrane.

	Pressure drop start		Pressure drop finish	
Temperature	Supply	Exhaust	Supply	Exhaust
14,7 °C	29	29	29	29
10,3 °C	28	28	25	30
6,9 °C	28	28	20	29

Table 5.3 Pressure drop over orifice plate at start and finish long run

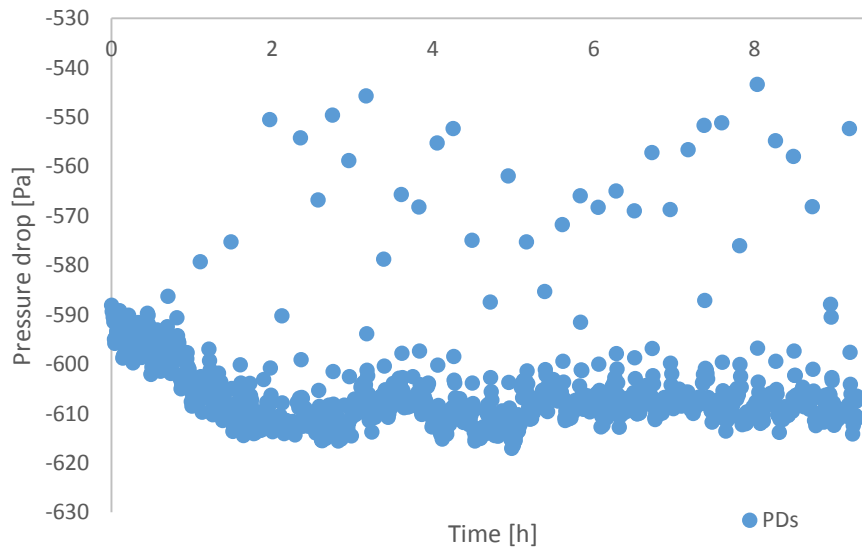


Figure 5.19 Pressure drop over MEE supply side at 6,9 °C supply inlet

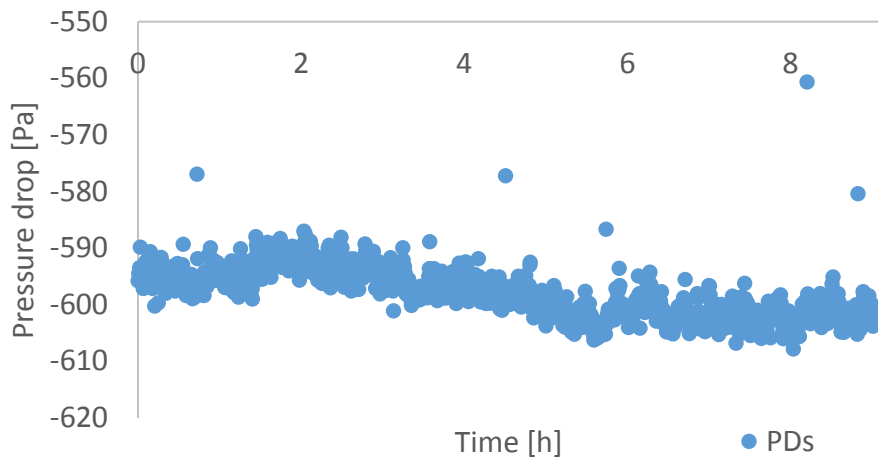


Figure 5.20 *Pressure drop over MEE supply side at 10,3 °C supply inlet*

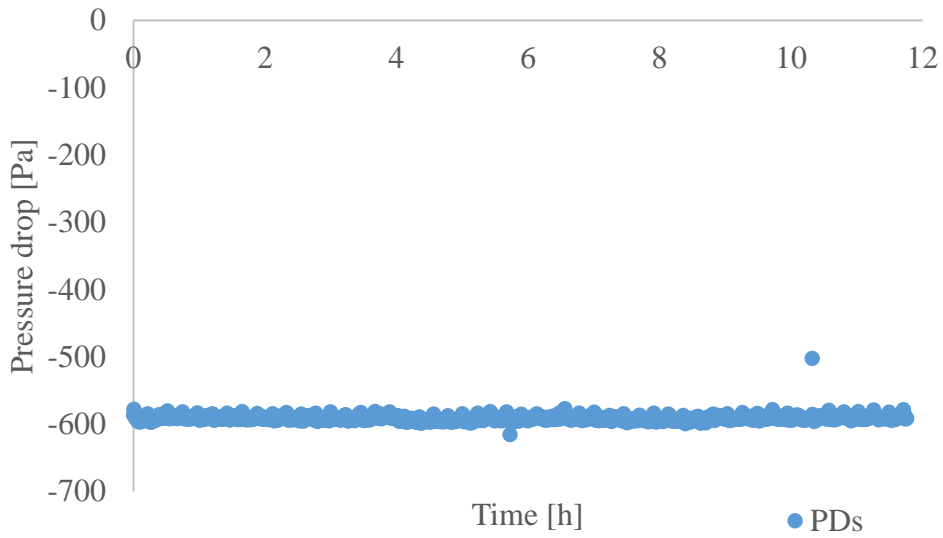


Figure 5.21 *Pressure drop over MEE supply side at 14,7 °C supply inlet*

5.7 Indoor RH

During the experiments, the exhaust inlet and supply outlet RH and temperature were noticeably similar. This raised the concern that the indoor RH humidity might get too high in the long run for a real case dwelling. In a study made in Trondheim concerning 117 houses[24] there was proposed a change of the moisture supply curve in EN ISO 13788. The following table gives the key values proposed relevant to this thesis. For temperatures lower than 5 °C, the same values for 5 °C could be used respectively.

Moisture supply[g/m³]:	Low	Medium	High
5 °C	2,5	4	6
10 °C	1,5	2,8	3,5
15 °C	0,5	1,5	3

Table 5.4 *Moisture loads in a building*

In order to determine if this would become a problem, a simple simulation of a ZEB was performed in Simien. The experimental values for the absolute moisture, latent and sensible effectiveness were combined with a finished sample house. The outdoor temperature, absolute humidity and transmissivity was considered constant. The main results for the indoor conditions gathered are summarized in the table below. The rest of the results are listed in appendix E.

Overall condition	Parameters adjusted	RH _{low}	RH _{high}	T _{low}	T _{high}
Normal	$w = w_{5,3,exp}$, $\epsilon_{s/l}=0,92/0,79$, $tr=0,74$ $t=5,3$ °C, $\dot{V} = 1,2m^3/hm^2$	34%	57,5%	21,6	29
Normal	$w = w_{10,3,exp}$, $\epsilon_{s/l}=0,90/0,76$, $tr=0,74$ $t=10,3$ °C, $\dot{V} = 1,2m^3/hm^2$	58%	92,5%	23,8	31,6
Normal	$w = w_{15,2,exp}$, $\epsilon_{s/l}=0,89/0,75$, $tr=0,74$ $t=15,2$ °C, $\dot{V} = 1,2m^3/hm^2$	100%	100%	26,1	34
Double ventilation rate	$w = w_{5,3,exp}$, $\epsilon_{s/l}=0,92/0,79$, $tr=0,74$ $t=5,3$ °C, $\dot{V} = 2,4m^3/hm^2$	23%	31%	20	24,3
Double ventilation rate	$w = w_{10,3,exp}$, $\epsilon_{s/l}=0,90/0,76$, $tr=0,74$ $t=10,3$ °C, $\dot{V} = 2,4m^3/hm^2$	28%	41%	20	26,2
Double ventilation rate	$w = w_{15,2,exp}$, $\epsilon_{s/l}=0,89/0,75$, $tr=0,74$ $t=15,2$ °C, $\dot{V} = 2,4m^3/hm^2$	33%	52%	21,7	29
Cloudy	$w = w_{5,3,exp}$, $\epsilon_{s/l}=0,92/0,79$, $tr=0,05$ $t=5,3$ °C, $\dot{V} = 1,2m^3/hm^2$	33%	40%	20	20,4
Cloudy	$w = w_{10,3,exp}$, $\epsilon_{s/l}=0,90/0,76$, $tr=0,05$ $t=10,3$ °C, $\dot{V} = 1,2m^3/hm^2$	42%	53%	20	21,4
Cloudy	$w = w_{15,2,exp}$, $\epsilon_{s/l}=0,89/0,75$, $tr=0,05$ $t=15,2$ °C, $\dot{V} = 1,2m^3/hm^2$	74,8%	91%	21,3	23,5
Rain	$w = w_{5,3,sat}$, $\epsilon_{s/l}=0,92/0,79$, $tr=0,05$ $t=5,3$ °C, $\dot{V} = 1,2m^3/hm^2$	42%	50%	20	20,4
Rain	$w = w_{10,3,sat}$, $\epsilon_{s/l}=0,90/0,76$, $tr=0,05$ $t=10,3$ °C, $\dot{V} = 1,2m^3/hm^2$	55%	68%	20	21,5
Rain	$w = w_{15,2,sat}$, $\epsilon_{s/l}=0,89/0,75$, $tr=0,05$ $t=15,2$ °C, $\dot{V} = 1,2m^3/hm^2$	90%	100%	21,5	23,6

Table 5.5 *Simulation results with different parameters*

From the results obtained in table(5.5), we can see that most of the conditions are within the recommended parameters [25]. Because the building is made according to ZEB standards, it is very well insulated. This explains the very high indoor temperature for the normal and double ventilation rate case. When the transmissivity is lowered to simulate cloudy conditions the temperature drops dramatically. We can see that the overall RH increases for higher outdoor temperatures. We see that the moisture problem could be solved with a higher infiltration rate. This could be implemented either through greater ventilation rates as shown in the table or by opening windows for cross ventilation.

6 Discussion

The first objective of this thesis was to build a flow pattern test rig to examine if the aluminium mesh influenced the airflow within the MEE. The second objective was to check the effectiveness of the MEE test rig installed during spring and autumn conditions. The parameters were chosen in affiliation with mean temperature and humidity levels for Oslo, Bergen and Trondheim. The third objective was to investigate the MEE performance and discuss its relevance for cold climates during spring and autumn conditions.

6.1 Moisture supply air

To supply the intended humidity levels of the outside air, a boiling flask was used with a resistant regulated hot plate. The steam created was fed directly into the supply airstream. The amount of steam was controlled manually by a valve. The setup of this feeding mechanism was fairly crude, which resulted in high uncertainties in regards to temperature and humidity as shown in table (3.1) and (3.2). The pressure inside the boiling flask could not be considered constant which resulted in periodical increase in temperature and relative humidity for the supply inlet, followed by a decrease in both respectively. This resulted in an increase in latent and sensible effectiveness as shown in fig (3.3) due to systematic delay in registering the change of temperature and RH at the supply outlet compared to the supply inlet.

As shown in figure (5.7) there was an excess amount of moisture left inside the MEE. Since the feeding mechanism is connected close to the supply inlet where the thermocouples and moisture sensor are located, it is suspected that the air might not be fully mixed together with the steam. This could have resulted in pockets of very humid air that condensed inside the exchanger, once fully mixed. The temperature increase of 1-2 degrees could, as mentioned earlier, also be responsible for water condensing inside the MEE.

From the results obtained through the simulations in table (5.5), most of them were within recommended parameters for RH. The simulations that fell outside this category were in humid and mild climates, typical for the south western part of Norway. Although the simulation model was fairly simple, it does give an indication that the MEE might not be the best option for mild and moist climates, typical for cities like Bergen due to health risks acquainted with a high indoor RH[25]. The extra infiltration rates would also increase energy consumption in regards of heating.

6.2 Pressure drop and flow rate

Due to technical problems with the couplings it was not possible to measure the pressure drop over the MEE and orifice plates in LabVIEW for most of the experiments. The pressure drop for the supply air over the MEE and orifice plate was measured in LabVIEW for the long running tests. The rest of the measurements were controlled manually, but were assumed to remain relatively constant throughout the experiment. As shown in table (5.5), the pressure drop over the orifice plate decreased for the supply air and increased for the exhaust air over time. This meant that the airflow rate decreased for the supply and increased for the exhaust. The decrease in supply airflow rate could be caused by crumpling of the membrane inside the

MEE blocking the airflow. The mesh, however, would protect from the crumpling to some extent. The rise in pressure drop for the exhaust outlet can be explained by the rise in temperature difference between the supply inlet and exhaust outlet. For the lower temperatures where the pressure drop over the orifice plate does not stay constant it is registered a temperature rise in the exhaust outlet air relative to the supply inlet over time. A higher temperature leads to a lower density and hence higher volume for the same mass flow. This is registered at the orifice plate as a higher volumetric flow, which causes the pressure drop to increase over time. In the two figures below, the difference is shown where there is a rise in temperature difference for 5,3 °C compared to a relative constant temperature difference for 12,6 °C

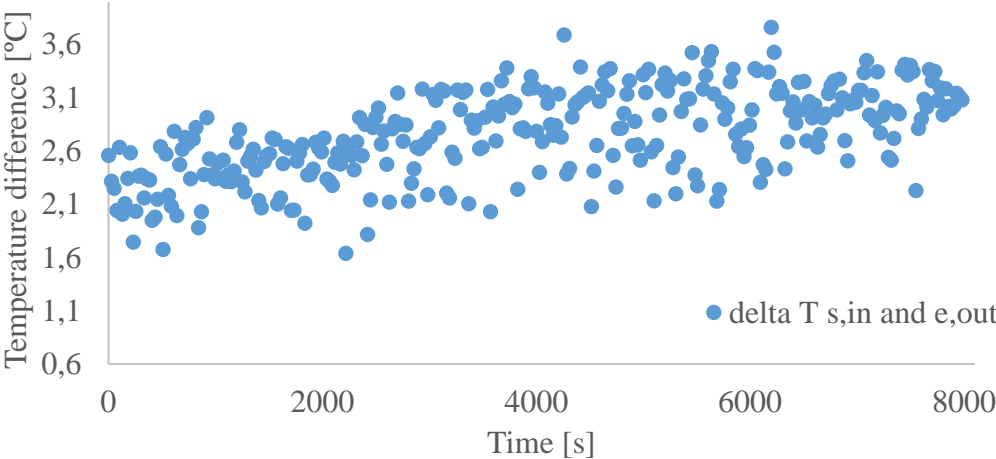


Figure 6.1 *Temperature difference over time between supply inlet and exhaust outlet for 5,3 °C.*

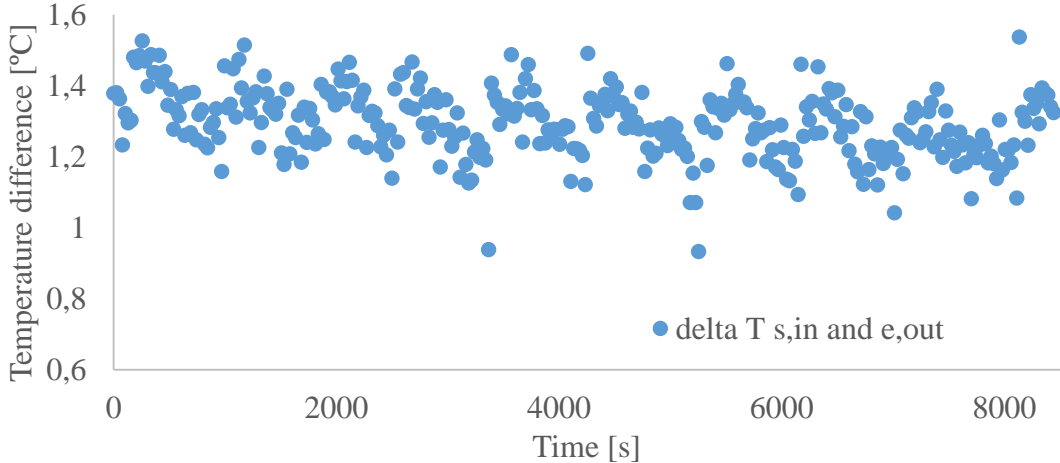


Figure 6.2 *Temperature difference over time between supply inlet and exhaust outlet for 12,6 °C.*

6.3 Moisture transfer resistance

In the theoretical modelling it was found that the moisture transfer resistance is temperature dependent. The resistance affected the moisture transfer through the membrane. This is indicated in figure (5.7), where the resistance decreases with increasing temperature, resulting in a lower condensation rate inside the MEE. Although this could be caused by a changing resistance, it could also be connected with higher condensation for the lower temperature range. This would be caused by a higher temperature difference between the steam and the cold air at 5°C compared to 15 °C. The long run test did not reveal overwhelming support for a temperature dependant moisture transfer resistant. The long run test actually showed that on average, less water condensed inside the MEE at 6,9°C compared to both 10,3°C and 14,7°C.

Parameter	6,9°C	10,3°C	14,7°C
$\frac{\bar{w}}{s}$ [g/kg*s]	0,394	0,494	0,413

Table 6.1 Average condensation rate inside MEE at the

6.4 Evaluation of the flow pattern test rig

The flow pattern test rig gave the expected laminar flow in regards to Reynolds Number calculations performed as seen from figure (5.2) and table (5.1) . The pressure drop over the mesh was relatively similar to the experimental pressure drop over the MEE test rig. The rotameters made it easy to calculate the airflow rate. There was, however, a problem with the smoke implementation method. Dräger air current tubes were used, and, because the velocity inside the channel was approximately 2,4 m/s, it was difficult to spot the smoke. The smoke was let into the channel manually, which, due to the small scale of the cross section, may have caused unwanted influence on the air stream.



Figure 6.3 Dräger air current tube

6.5 Evaluation of the MEE test rig

In order to provide the needed humidity on the supply side, a simple mechanism to increase RH was implemented. The boiling flask and the steam it provided turned out to be very difficult to regulate. This gave a very unstable RH, which was inconsistent with its variation in RH and temperature from experiment to experiment. The continuous decrease of water in the boiling flask also had its effects in the long run, sometimes causing a steady increase in the overall RH. The exhaust side, however, was regulated by an AHU providing water at 22 °C through a nozzle. It provided a relatively constant temperature and RH throughout the experiments. In the end, the MEE did yield some good results, but with a high level of uncertainty, as shown previously.

7 Conclusion

The flow pattern test rig showed that the airstream was only marginally affected by the aluminium mesh. The airflow was shown to have a laminar flow, due to its low inertial forces compared to its viscous forces.

The experimental testing showed that the MEE prototype had a very high sensible and latent effectiveness due to its counter flow properties. The sensible and latent effectiveness was 88,9 – 92,2 % and 73,6-79,8%, respectively, for supply inlet at 5°C-15°C, 70%RH and exhaust inlet at 22°C. The prototype also revealed that the effectiveness was negligibly influenced by temperature change in supply inlet air, even though there was some condensation inside the MEE. In accordance with the theory, and as indicated through experimental testing, condensation inside the MEE decreased with increasing temperature.

The high efficiency of the exchanger did, however, cause some concerns about the moisture content of the indoor environment. The simulations using a ZEB model of a simple building resulted in humidity levels within and outside the desired parameters. It was, however, in the author's opinion that small measures, like opening a window for cross ventilation or doubling the air change rate, would be sufficient in order to maintain acceptable RH levels. However, it was also argued that the MEE should not be implemented in mild and humid climates, such as in Bergen, due to health risks triggered by a high RH, as well as extra cost due to heating.

Since the water added to the supply side was controlled manually and through a very crude mechanism, there was a rather high uncertainty surrounding the RH and temperature. These were expected to affect the lower temperature range more than the higher, due to a lower capacity to hold water. This was confirmed by the temperature and RH fluctuations as shown in figure (5.10) and (5.11) in the experimental results. During the long run tests, however, it was shown that there was less condensation inside the MEE for the lower temperature range of 6,8°C than that of 10,3°C and 14,7°C. It is in the author's opinion that this might be due to the uncertainties surrounding the boiling flask and its crude implementation method.

8 Further Work

If the MEE is going to be used for further investigations, some modifications need to be made.

In order to provide a more stable RH for the supply inlet, the boiling flask should be connected further from the MEE or replaced with a more reliable and controllable device, such as the AHU for the exhaust air. It should also be possible to visualise the presence of any condensation at the supply inlet due to steam not fully mixing with the air.

Even if the preliminary simulations for the humidity level were determined to be within the parameter, this was a fairly basic simulation. In future testing of the MEE in spring and autumn conditions, a room could be connected to the supply air outlet and exhaust air inlet. With the room connected, a test with different moisture loads in accordance with table (5.) could be performed. Through this experiment it could be determined whether there is any reason for concern about mould or other hazards connected with excessive moisture. Furthermore, research could be conducted into bypass systems if it is indeed found that the moisture conditions are unsatisfactory.

References

1. Alonso, M.J., et al. *Heat and mass transfer in membrane-based total heat exchanger, membrane study*. in *7th International Cold Climate HVAC Conference*. 2012.
2. Mardiana-Idayu, A. and S.B. Riffat, *Review on heat recovery technologies for building applications*. *Renewable and Sustainable Energy Reviews*, 2012. **16**(2): p. 1241-1255.
3. Kassai, M. and C.J. Simonson, *Performance investigation of liquid-to-air membrane energy exchanger under low solution/air heat capacity rates ratio conditions*. *Building Services Engineering Research and Technology*, 2015. **36**(5): p. 535-545.
4. Aarnes, *Membrane based heat exchanger*, in *EPT*. 2012, NTNU. p. 142.
5. Liu, P., *Experimental and analytical investigation of the performance of a quasi-counter-flow air-to-air membrane energy exchanger in cold climates*. 2015.
6. Kalamees, T., et al., *The effects of ventilation systems and building fabric on the stability of indoor temperature and humidity in Finnish detached houses*. *Building and Environment*, 2009. **44**(8): p. 1643-1650.
7. Liu, P., et al. *Frosting limits for counter-flow Membrane Energy Exchanger (MEE) in cold climates*. in *Indoor Air 2014 - 13th International Conference on Indoor Air Quality and Climate*. 2014.
8. Alonso, M.J., et al., *Performance of a lab-scale membrane-based energy exchanger*. *Applied Thermal Engineering*.
9. Rafati Nasr, M., et al., *Evaluation of defrosting methods for air-to-air heat/energy exchangers on energy consumption of ventilation*. *Applied Energy*, 2015. **151**: p. 32-40.
10. Justo Alonso, M., et al., *Review of heat/energy recovery exchangers for use in ZEBs in cold climate countries*. *Building and Environment*, 2015. **84**: p. 228-237.
11. Norge, S., *Calculation of energy performance of buildings, Method and data*, in *NS 3031*. 2014.
12. Zhang, L.Z., *Heat and mass transfer in a quasi-counter flow membrane-based total heat exchanger*. *International Journal of Heat and Mass Transfer*, 2010. **53**(23-24): p. 5478-5486.
13. Woods, J., *Membrane processes for heating, ventilation, and air conditioning*. *Renewable and Sustainable Energy Reviews*, 2014. **33**: p. 290-304.
14. Gibson, P.W., *Effect of temperature on water vapor transport through polymer membrane laminates*. *Polymer Testing*, 2000. **19**(6): p. 673-691.

15. Frank P. Incropera, D.P.D., Theodore L. Bergman, Adrienne S. Lavine, *Principles of heat and mass transfer*. Vol. Seventh edition. 2013: John Wiley & Sons, Inc.
16. ISO5167-2, *Measurement of fluid flow by means of pressure differential devices inserted in circular cross-section conduits running full*, in *ISO 5167-2 | Part 2: Orifice plates*. 2003.
17. Mulder, M., *Basic Principles of Membrane Technology*. 1996.
18. Bolton, D., *The Computation of Equivalent Potential Temperature*. Monthly Weather Review, 1980. **108**(7): p. 1046-1053.
19. Jeannine Cavender-Bares, M.G., James Brendan Heffernan, Jennifer L. Morse, *Convergence of microclimate in residential landscapes across diverse cities in the United States*. 2015.
20. Kays, W.M.a.A.L.L., *Compact heat exchangers*. 1964: McGraw - Hill.
21. Min, J. and M. Su, *Performance analysis of a membrane-based enthalpy exchanger: Effects of the membrane properties on the exchanger performance*. Journal of Membrane Science, 2010. **348**(1–2): p. 376-382.
22. Nasif, M.S., G.L. Morrison, and M. Behnia. *Heat and mass transfer in air to air enthalpy heat exchangers*. 2005.
23. Bowerman/O'Connell, *Linear Statistical Models An Applied Approach*. Vol. Second edition. 1990: Thomson Information/ Publishing Group.
24. Stig Geving, J.H., Jon A. Jenssen, *Indoor air humidity in Norwegian houses*.
25. Baughman, A., Arens, Edward A, *Indoor humidity and human health part 1: Literature review of health effects of humidity-influenced indoor pollutants*. 1996.

Appendix

A	Calculation of discharge coefficient
B	Random uncertainty
C	Mean RH and temp cities
D	Results
E	Simien simulations
F	Risk assessment report

Appendix A – Calculation of discharge coefficient

$$\begin{aligned}
 C = & 0,5961 + 0,0261\beta^2 - 0,216\beta^8 + 0,000521 \left(\frac{10^6\beta}{Re_D} \right)^{0,7} \\
 & + (0,0188 + 0,0063A)\beta^{3,5} \left(\frac{10^6}{Re_D} \right)^{0,3} \\
 & + (0,043 + 0,080e^{-10L_1} - 0,123e^{-7L_1})(1 - 0,11A) \frac{\beta^4}{1 - \beta^4} \\
 & - 0,031(M'_2 - 0,8M'^{1,1}_2)\beta^{1,3}
 \end{aligned} \tag{52}$$

Where A:

$$A = \left(\frac{19000\beta}{Re_D} \right)^{0,8} \tag{53}$$

M'_2 is defined as:

$$M'_2 = \frac{2L'_2}{1 - \beta} \tag{54}$$

Since corner tapplings are used for the orifice plate, $L_1 = L'_2 = 0$. The discharge coefficient can therefore be simplified, giving:

$$\begin{aligned}
 C = & 0,5961 + 0,0261\beta^2 - 0,216\beta^8 + 0,000521 \left(\frac{10^6\beta}{Re_D} \right)^{0,7} \\
 & + (0,0188 + 0,0063A)\beta^{3,5} \left(\frac{10^6}{Re_D} \right)^{0,3} \\
 & + (0,043 + 0,080e^{-10*0} - 0,123e^{-7*0})(1 - 0,11A) \frac{\beta^4}{1 - \beta^4} \\
 & - 0,031(0 - 0,8 * 0)\beta^{1,3}
 \end{aligned} \tag{55}$$

Which gives:

$$\begin{aligned}
 C = & 0,5961 + 0,0261\beta^2 - 0,216\beta^8 + 0,000521 \left(\frac{10^6\beta}{Re_D} \right)^{0,7} \\
 & + \left(0,0188 + 0,0063 \left(\frac{19000\beta}{Re_D} \right)^{0,8} \right) \beta^{3,5} \left(\frac{10^6}{Re_D} \right)^{0,3}
 \end{aligned} \tag{56}$$

Appendix B – Random Uncertainty

70 % supply inlet, 60% exhaust inlet

71% 5,3 °C			72% 6,4 °C		
Type	Uncertainty	Tfactor	Type	Uncertainty	Tfactor
RHs,in	7,84186083	1,97	RHs,in	6,12063938	1,97
RHs,out	0,87460379	1,97	RHs,out	0,92959015	1,97
RHe,in	0,91631374	1,97	RHe,in	0,92959015	1,97
RHe,out	2,78566578	1,97	RHe,out	0,92959015	1,97
Ts,in	0,76027577	1,97	Ts,in	0,92959015	1,97
Ts,out	0,21810048	1,97	Ts,out	0,92959015	1,97
Te,in	0,04485574	1,97	Te,in	0,92959015	1,97
Te,out	0,75460245	1,97	Te,out	0,92959015	1,97
Sensible e	0,01506188	1,97	Sensible e	0,92959015	1,97
Latent e	0,03818117	1,97	Latent e	0,92959015	1,97
71% 6,8 °C			68% 7,4 °C		
Type	Uncertainty	Tfactor	Type	Uncertainty	Tfactor
RHs,in	4,7498654	1,97	RHs,in	4,51218309	1,97
RHs,out	1,19522731	1,97	RHs,out	1,03676275	1,97
RHe,in	1,16151596	1,97	RHe,in	0,92796658	1,97
RHe,out	2,14164307	1,97	RHe,out	2,10620033	1,97
Ts,in	0,47537199	1,97	Ts,in	0,46153797	1,97
Ts,out	0,44692049	1,97	Ts,out	0,11761439	1,97
Te,in	0,02460094	1,97	Te,in	0,04121168	1,97
Te,out	0,75308545	1,97	Te,out	0,50778432	1,97
Sensible e	0,02985443	1,97	Sensible e	0,0087515	1,97
Latent e	0,05196963	1,97	Latent e	0,0327386	1,97
66% 8,3 °C			72% 9,7 °C		
Type	Uncertainty	Tfactor	Type	Uncertainty	Tfactor
RHs,in	5,51799416	1,97	RHs,in	4,44318624	1,97
RHs,out	1,34522017	1,97	RHs,out	0,94410636	1,97
RHe,in	1,03166178	1,97	RHe,in	0,78626612	1,97
RHe,out	3,36637754	1,97	RHe,out	2,26896582	1,97
Ts,in	0,45556749	1,97	Ts,in	0,44505065	1,97
Ts,out	0,1109293	1,97	Ts,out	0,14514972	1,97
Te,in	0,03010638	1,97	Te,in	0,02238012	1,97
Te,out	0,39782143	1,97	Te,out	0,44353831	1,97
Sensible e	0,00765713	1,97	Sensible e	0,01022042	1,97
Latent e	0,03205339	1,97	Latent e	0,04021379	1,97

70% 10,3 °C			72% 11,5 °C		
Type	Uncertainty	Tfactor	Type	Uncertainty	Tfactor
RHs,in	4,83260008	1,97	RHs,in	5,07760275	1,97
RHs,out	0,90115983	1,97	RHs,out	0,9982857	1,97
RHe,in	0,66288493	1,97	RHe,in	0,70442085	1,97
RHe,out	2,91229339	1,97	RHe,out	4,657805	1,97
Ts,in	0,24290664	1,97	Ts,in	0,3367606	1,97
Ts,out	0,05312964	1,97	Ts,out	0,0668109	1,97
Te,in	0,03067111	1,97	Te,in	0,0224113	1,97
Te,out	0,20686965	1,97	Te,out	0,26685816	1,97
Sensible e	0,0043224	1,97	Sensible e	0,00716018	1,97
Latent e	0,03591515	1,97	Latent e	0,04994822	1,97
70% 12,6 °C			70% 13 °C		
Type	Uncertainty	Tfactor	Type	Uncertainty	Tfactor
RHs,in	5,40751651	1,97	RHs,in	3,53116104	1,97
RHs,out	1,09248959	1,97	RHs,out	1,10947784	1,97
RHe,in	0,85879951	1,97	RHe,in	1,17559649	1,97
RHe,out	3,36376176	1,97	RHe,out	2,17865525	1,97
Ts,in	0,29981177	1,97	Ts,in	0,20612705	1,97
Ts,out	0,0796642	1,97	Ts,out	0,05424014	1,97
Te,in	0,0419209	1,97	Te,in	0,04283862	1,97
Te,out	0,23714134	1,97	Te,out	0,18885591	1,97
Sensible e	0,00942721	1,97	Sensible e	0,00229464	1,97
Latent e	0,0660482	1,97	Latent e	0,04691519	1,97
70% 13,7 °C			68% 14,5 °C		
Type	Uncertainty	Tfactor	Type	Uncertainty	Tfactor
RHs,in	3,42284595	1,97	RHs,in	3,95177119	1,97
RHs,out	1,11076093	1,97	RHs,out	1,10238762	1,97
RHe,in	0,91084429	1,97	RHe,in	1,06558553	1,97
RHe,out	2,51472406	1,97	RHe,out	2,70039603	1,97
Ts,in	0,30121694	1,97	Ts,in	0,3408145	1,97
Ts,out	0,12074995	1,97	Ts,out	0,10837121	1,97
Te,in	0,10719585	1,97	Te,in	0,07067333	1,97
Te,out	0,24477303	1,97	Te,out	0,30719486	1,97
Sensible e	0,00183162	1,97	Sensible e	0,0042858	1,97
Latent e	0,04611466	1,97	Latent e	0,05216646	1,97

73% 15,1 °C

Type	Uncertainty	Tfactor
RHs,in	4,97567077	1,97
RHs,out	0,99020731	1,97
RHe,in	0,91009469	1,97
RHe,out	3,88353372	1,97
Ts,in	0,34783062	1,97
Ts,out	0,05336841	1,97
Te,in	0,04592218	1,97
Te,out	0,33446046	1,97
Sensible e	0,00619872	1,97
Latent e	0,06376595	1,97

Long run test:

69% 6,9 °C			69% 10,3 °C		
Type	Uncertainty	Tfactor	Type	Uncertainty	Tfactor
RHs,in	6,93	1,96	RHs,in	3,88	1,96
RHs,out	1,12	1,96	RHs,out	0,93	1,96
RHe,in	1,06	1,96	RHe,in	0,91	1,96
RHe,out	2,41	1,96	RHe,out	1,77	1,96
Ts,in	0,90	1,96	Ts,in	0,40	1,96
Ts,out	0,34	1,96	Ts,out	0,21	1,96
Te,in	0,11	1,96	Te,in	0,11	1,96
Te,out	0,83	1,96	Te,out	0,46	1,96
Sensible e	2,71	1,96	Sensible e	2,34	1,96
Latent e	4,89	1,96	Latent e	4,76	1,96

70% 14,7 °C		
Type	Uncertainty	Tfactor
RHs,in	5,61	1,96
RHs,out	1,65	1,96
RHe,in	1,56	1,96
RHe,out	4,77	1,96
Ts,in	0,37	1,96
Ts,out	0,23	1,96
Te,in	0,24	1,96
Te,out	0,29	1,96
Sensible e	0,58	1,96
Latent e	16,83	1,96

Appendix C – Mean RH and temp cities

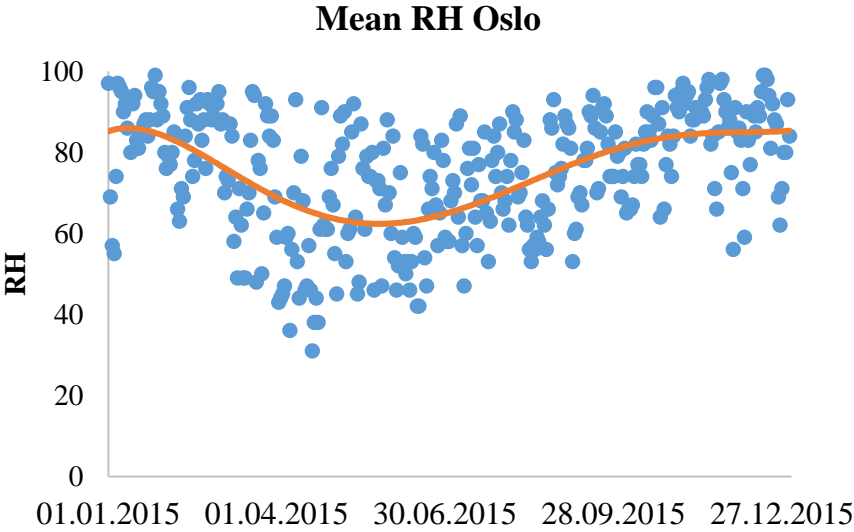


Figure C-1 Mean RH over one year in Oslo

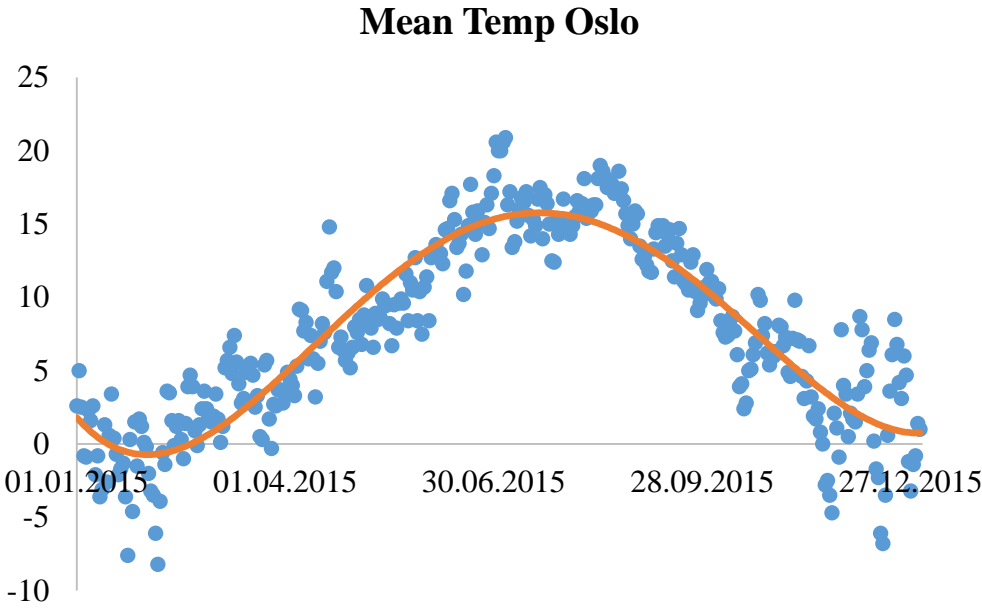


Figure C-2 Mean temperature over one year in Oslo

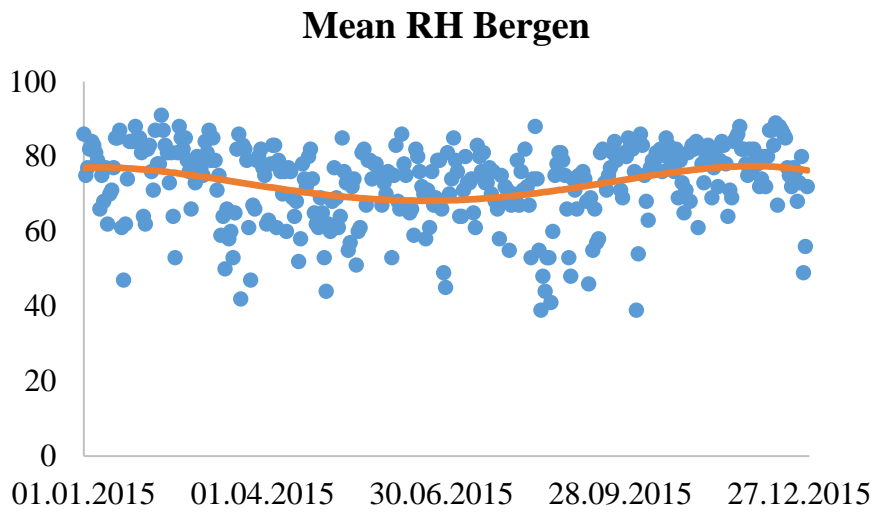


Figure C-3 *Mean RH over one year in Bergen*

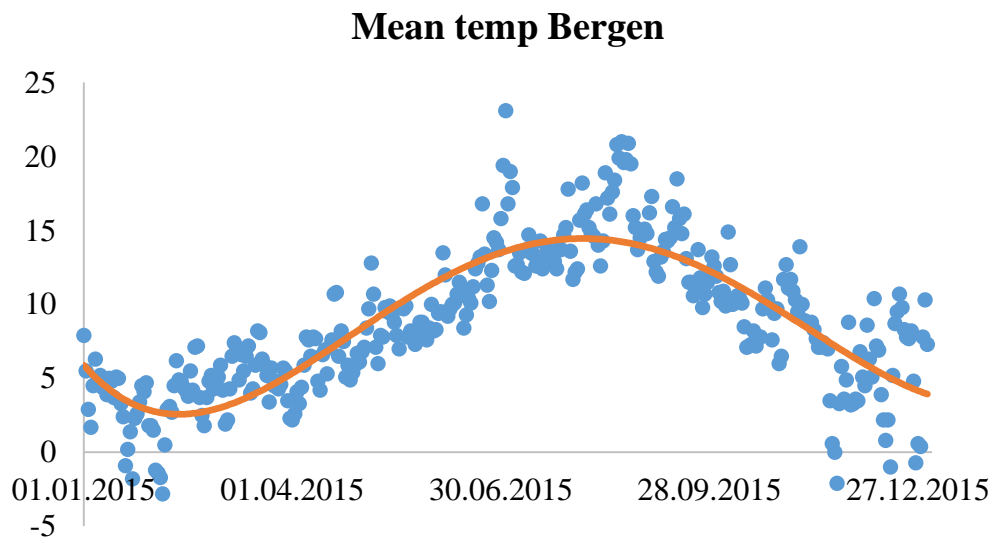


Figure C-4 *Mean temperature over one year in Bergen*

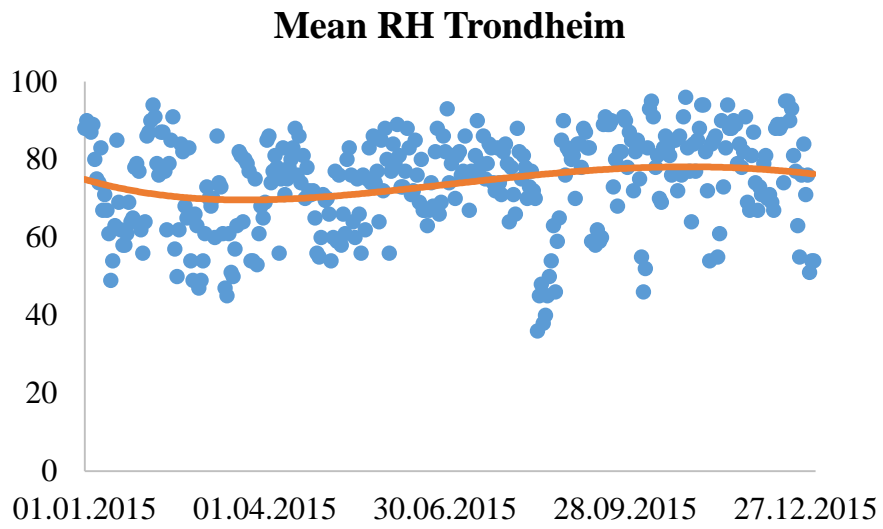


Figure C-5 *Mean RH over one year in Trondheim*

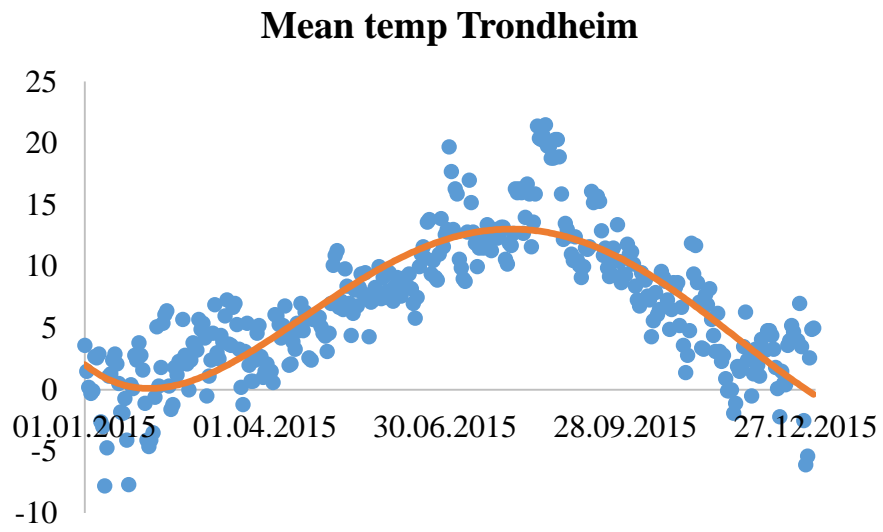
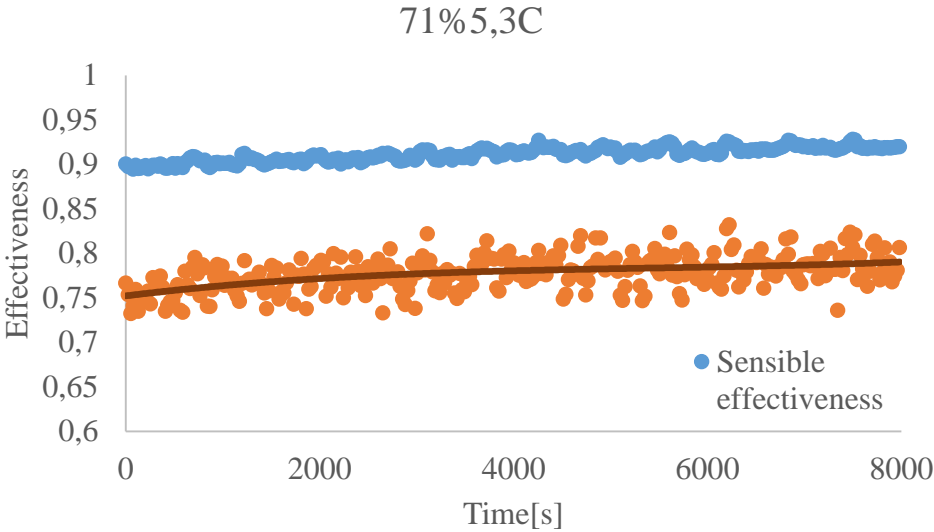
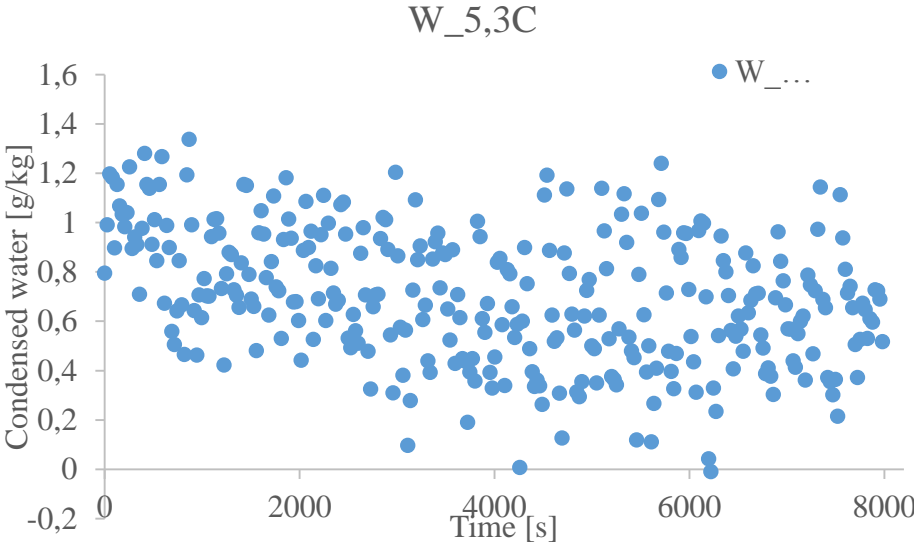


Figure C-6 *Mean temperature over one year in Trondheim*

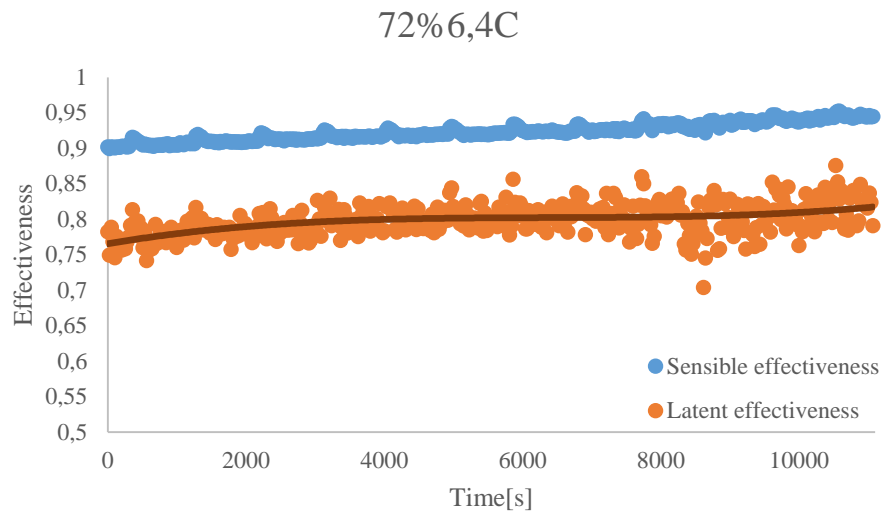
Appendix D – Results



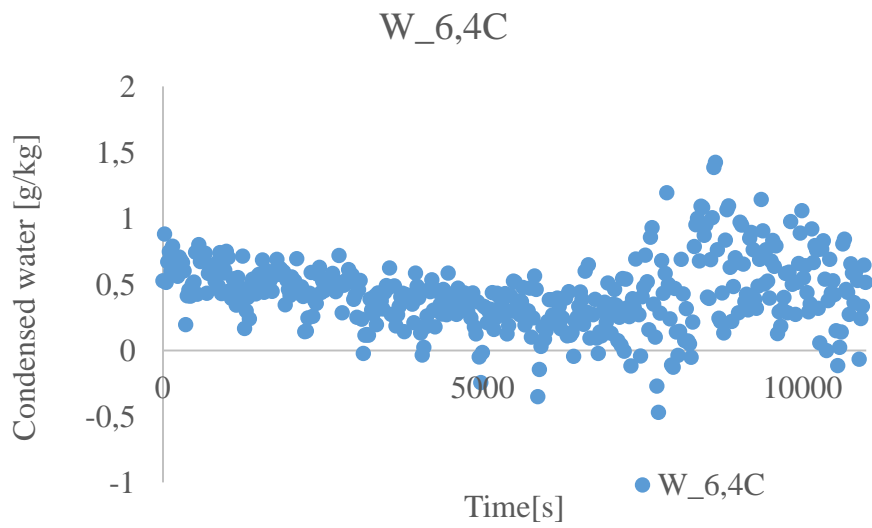
D-1 Sensible and latent effectiveness



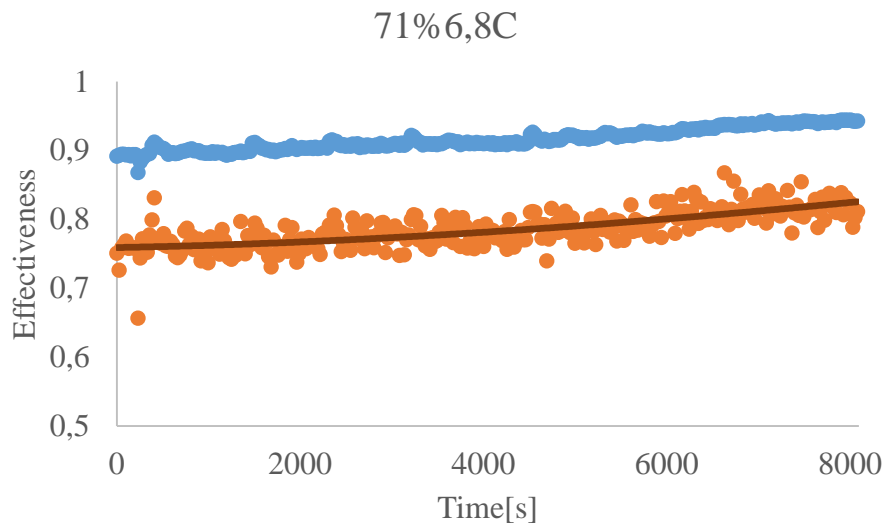
D-2 Grams of water trapped inside MEE per kg air



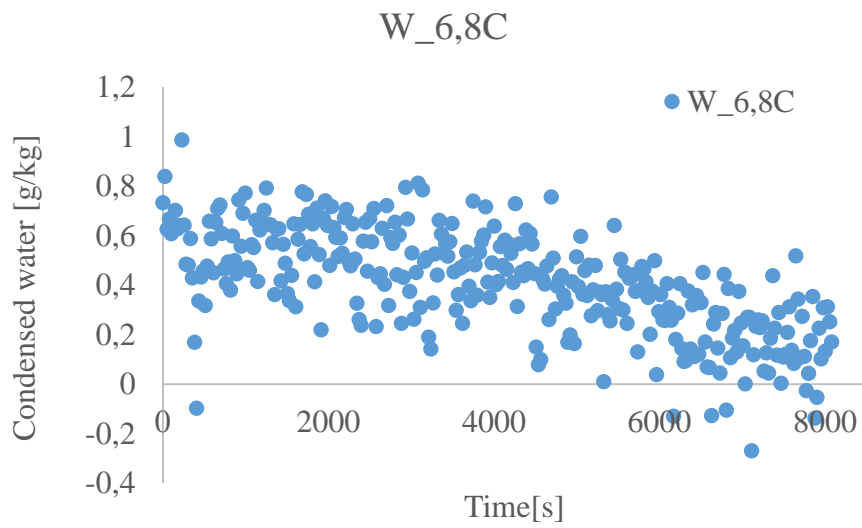
D-3 Sensible and latent effectiveness



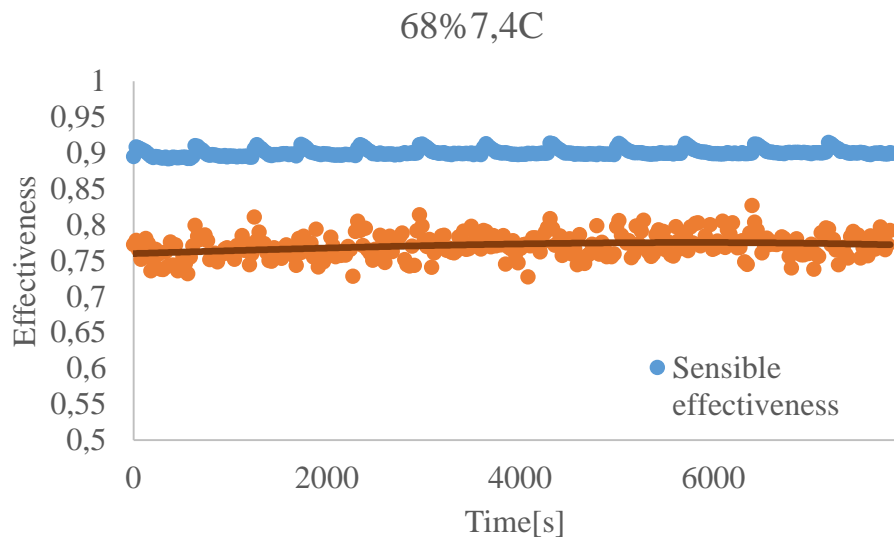
D-4 Grams of water trapped inside MEE per kg air



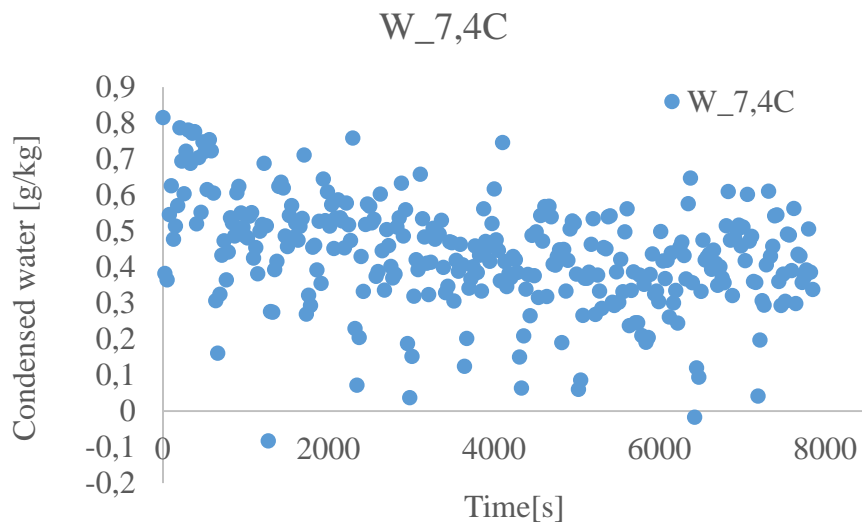
D-5 Sensible and latent effectiveness



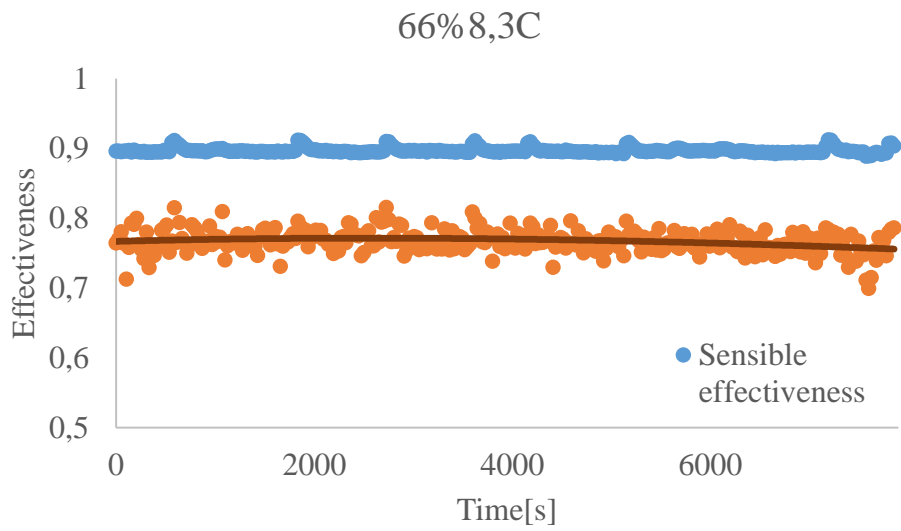
D-6 Grams of water trapped inside MEE per kg air



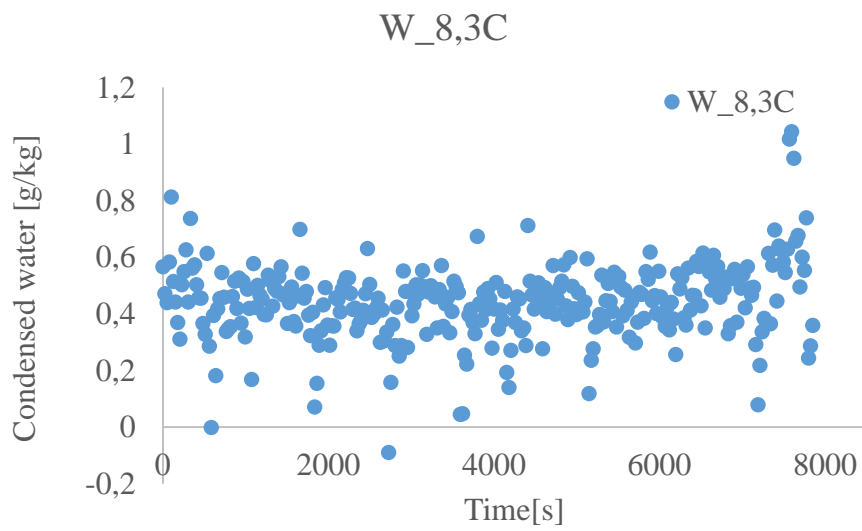
D-7 Sensible and latent effectiveness



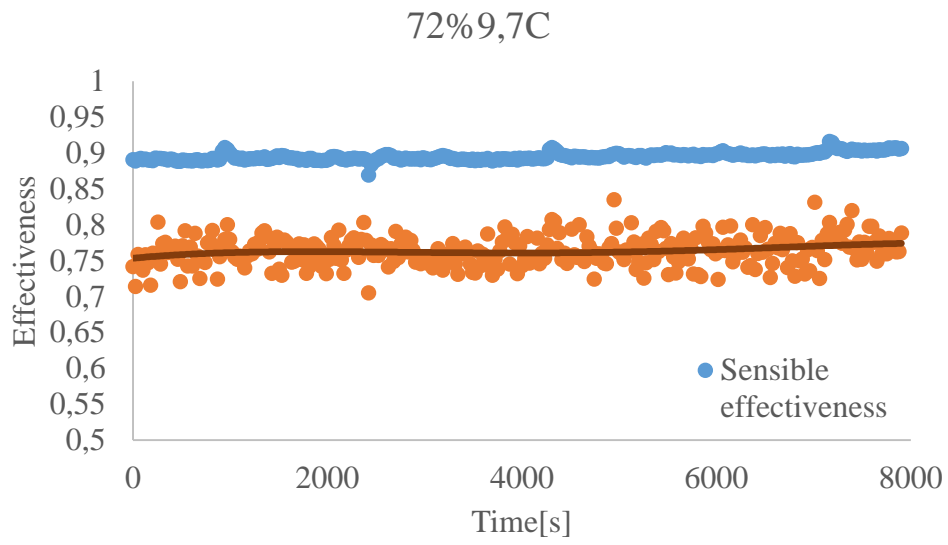
D-8 Grams of water trapped inside MEE per kg air



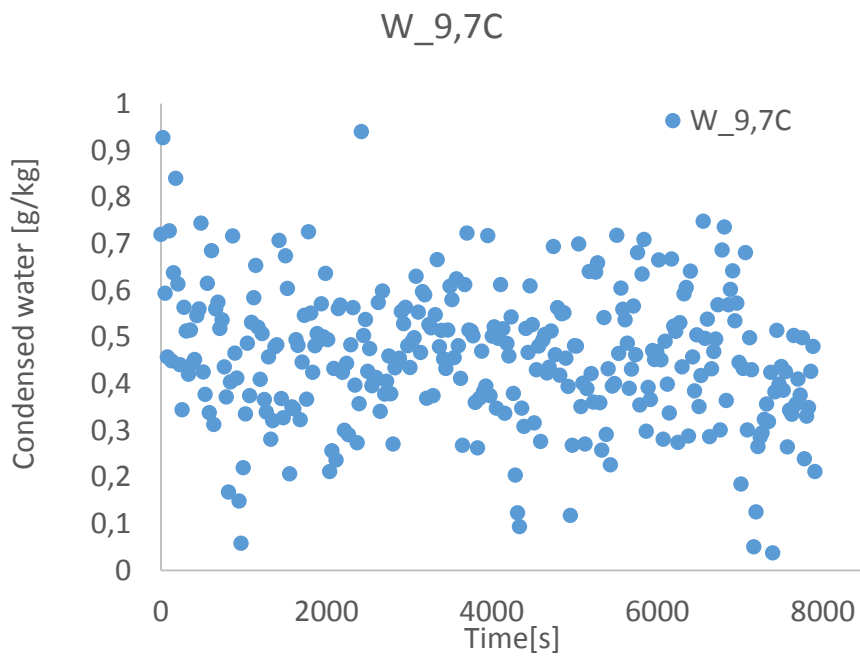
D-9 Sensible and latent effectiveness



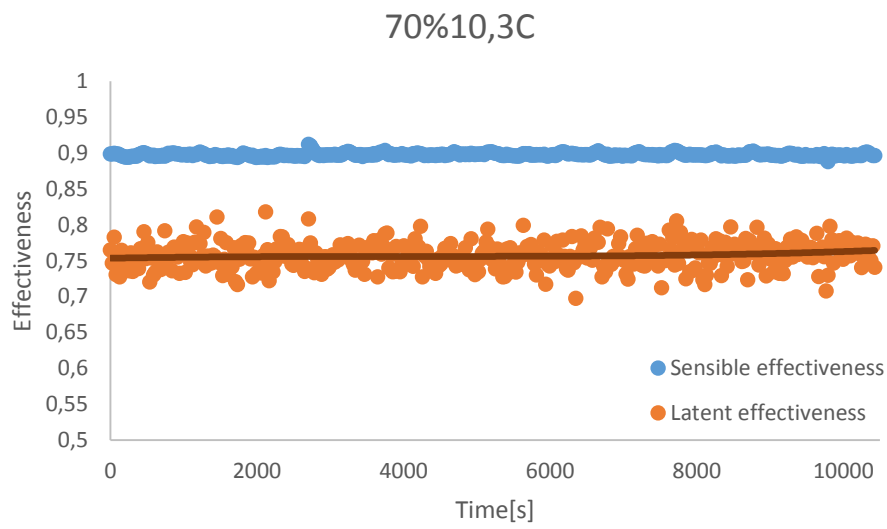
D-10 Grams of water trapped inside MEE per kg air



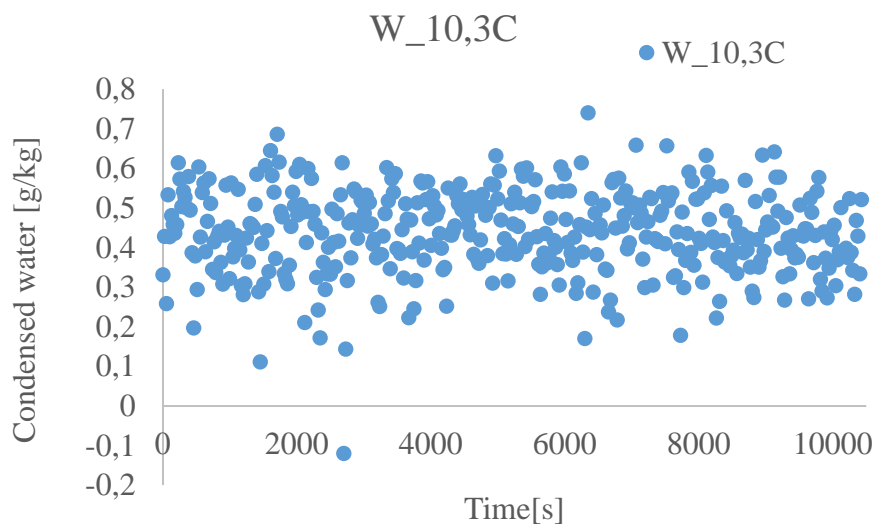
D-11 Sensible and latent effectiveness



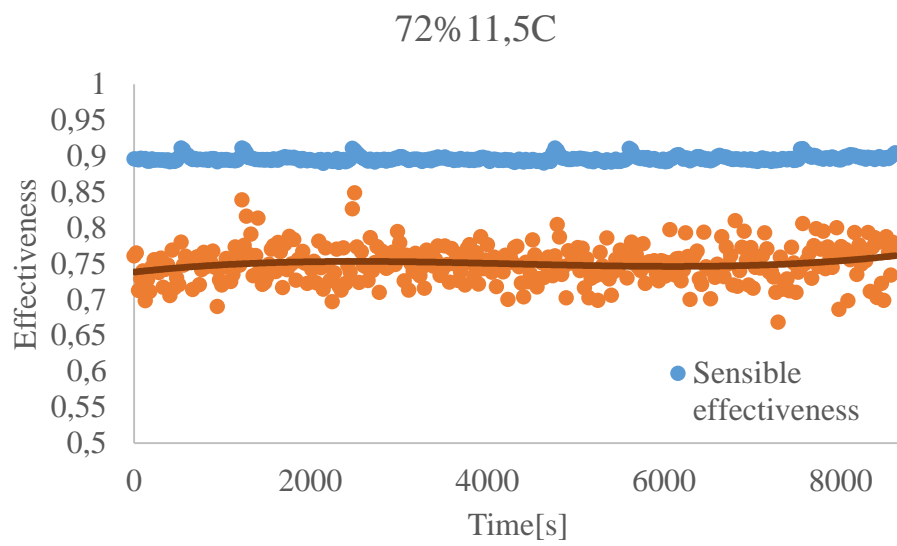
D-12 Grams of water trapped inside MEE per kg air



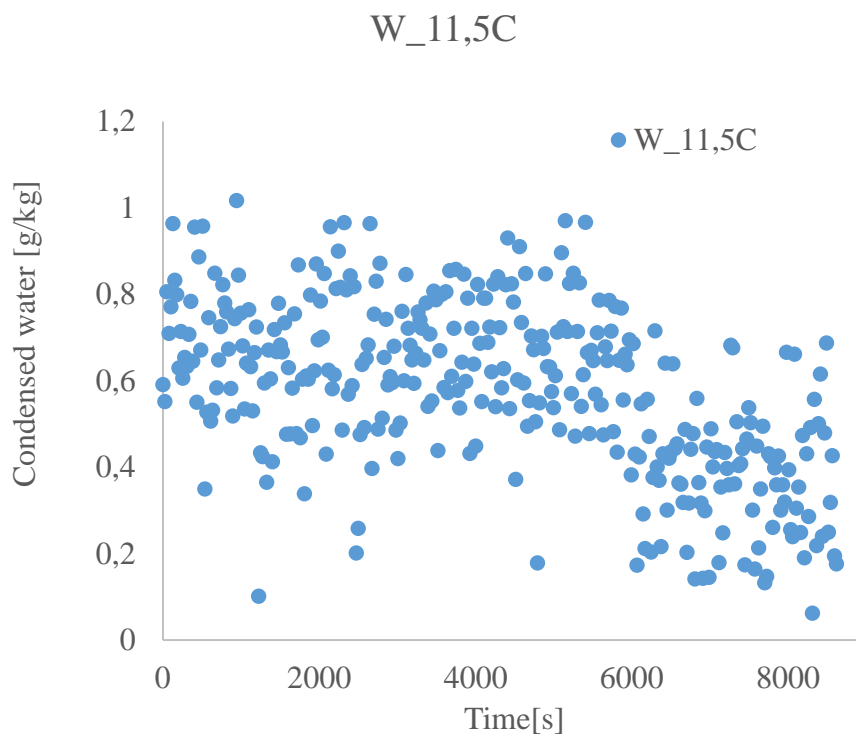
D-13 Sensible and latent effectiveness



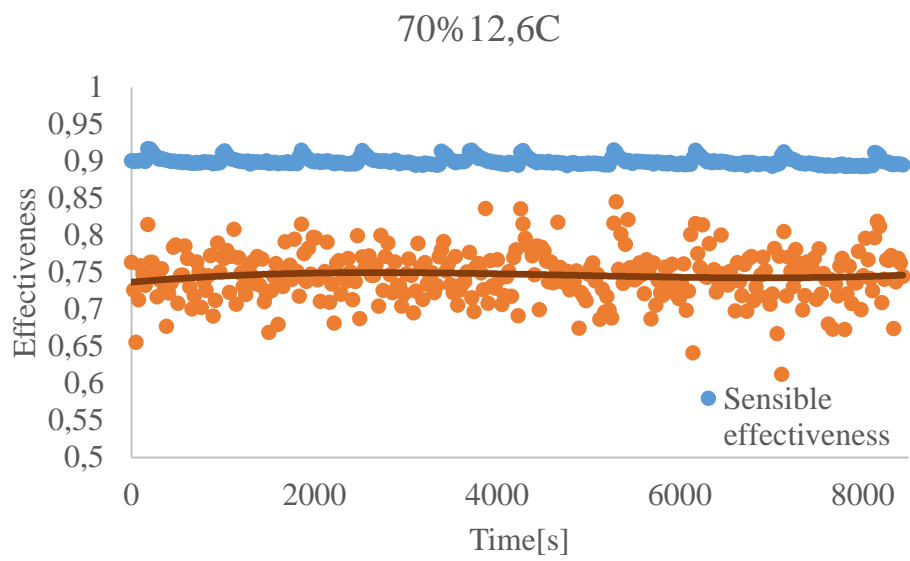
D-14 Grams of water trapped inside MEE per kg air



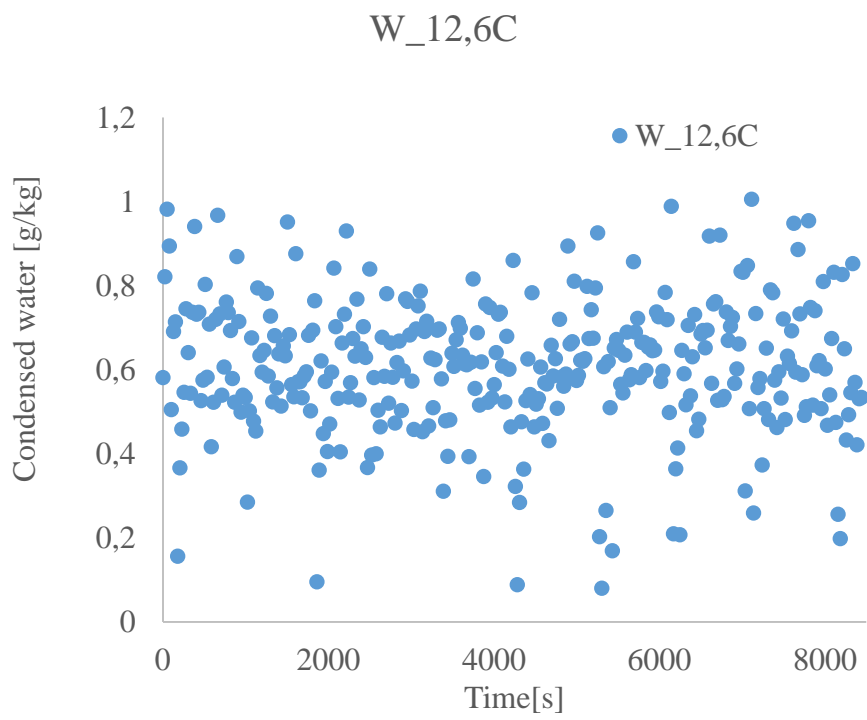
D-15 Sensible and latent effectiveness



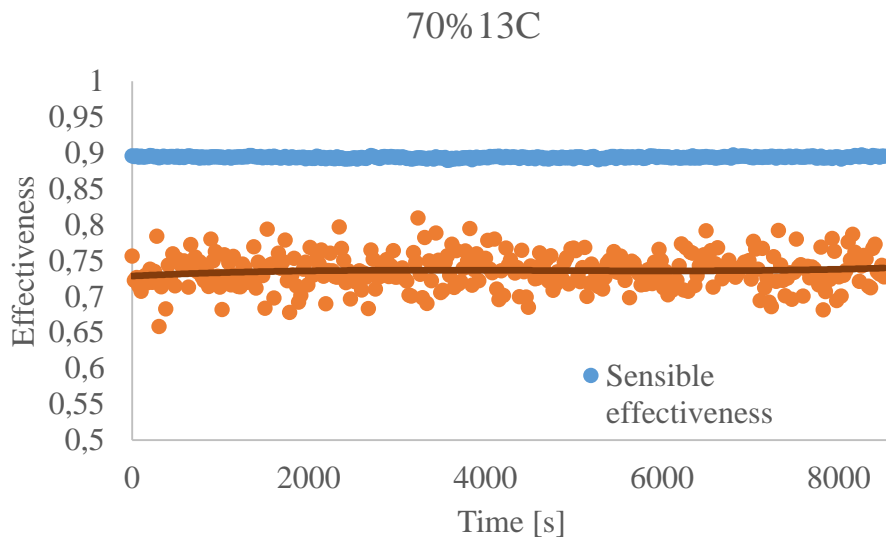
D-16 Grams of water trapped inside MEE per kg air



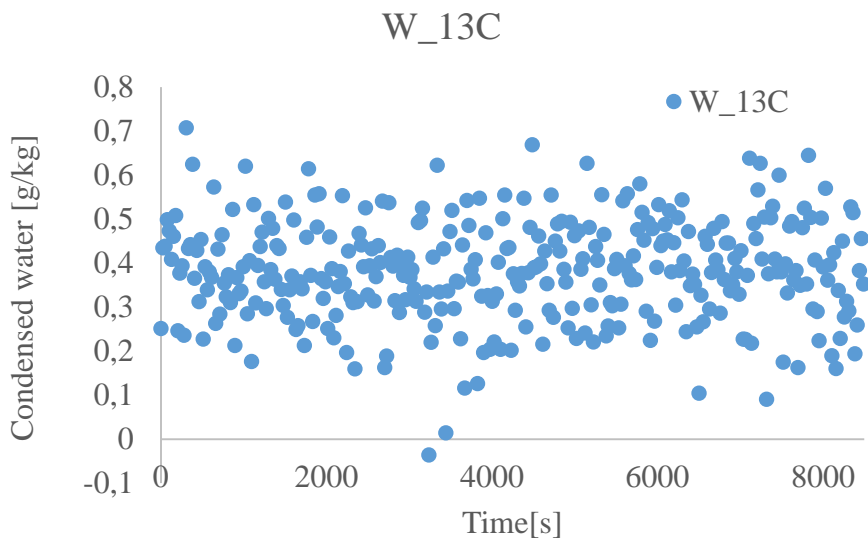
D-17 Sensible and latent effectiveness



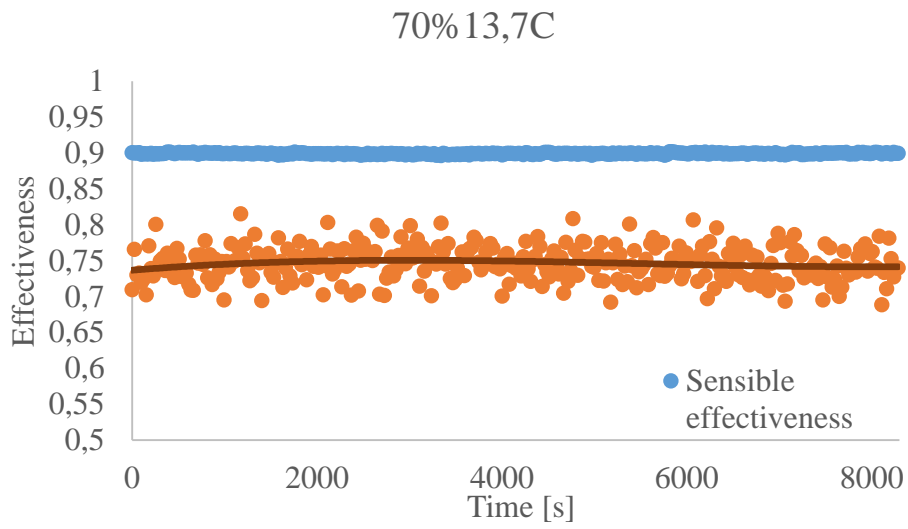
D-18 Grams of water trapped inside MEE per kg air



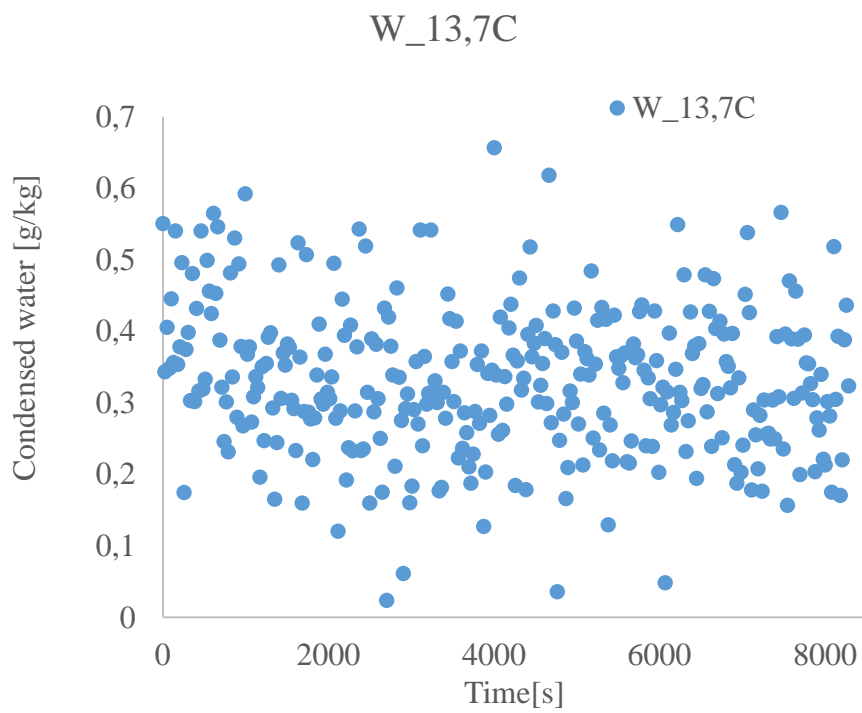
D-19 Sensible and latent effectiveness



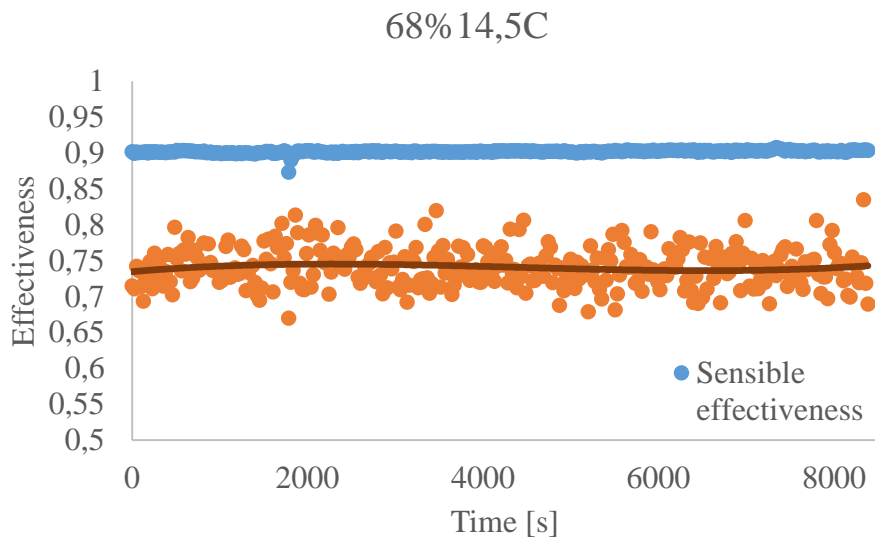
D-20 Grams of water trapped inside MEE per kg air



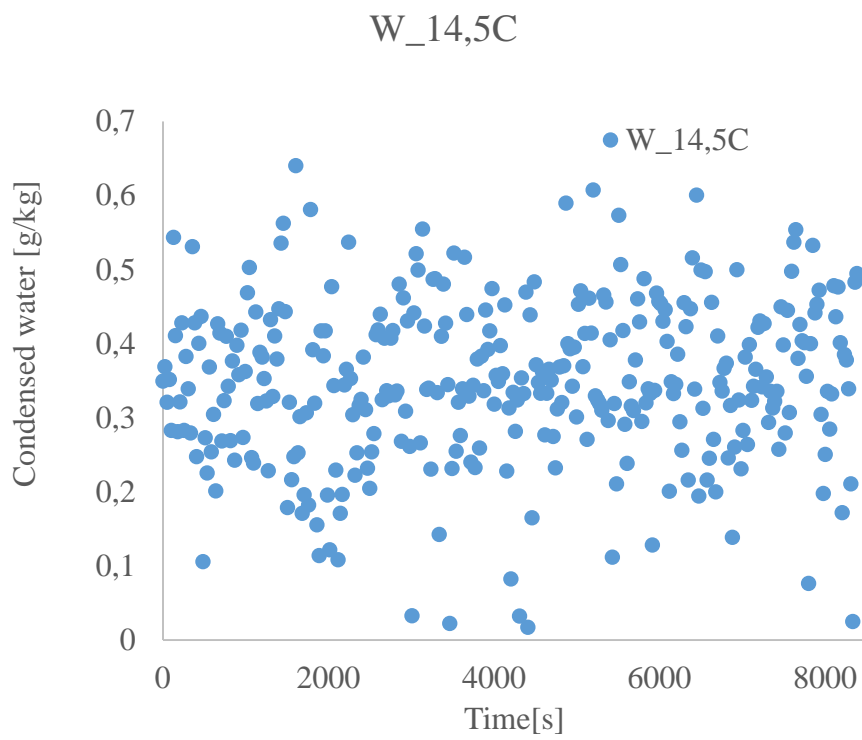
D-21 Sensible and latent effectiveness



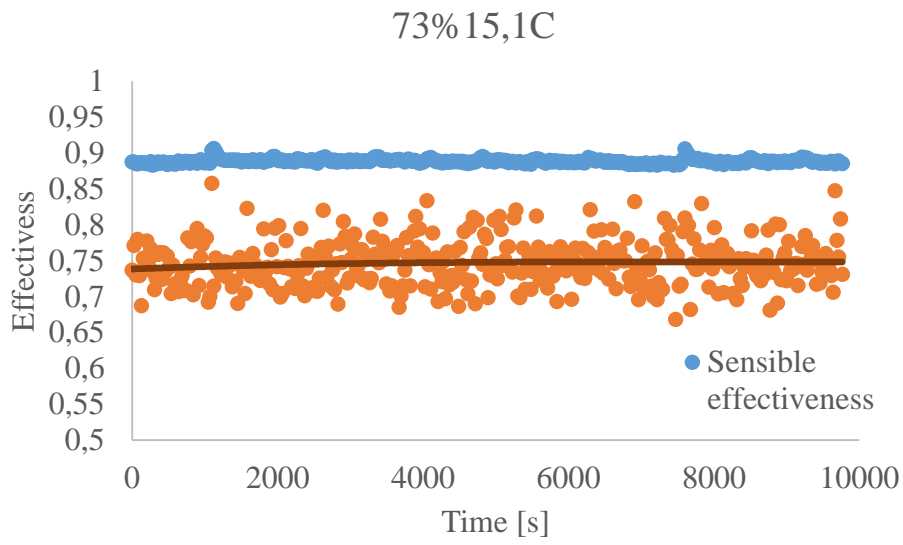
D-22 Grams of water trapped inside MEE per kg air



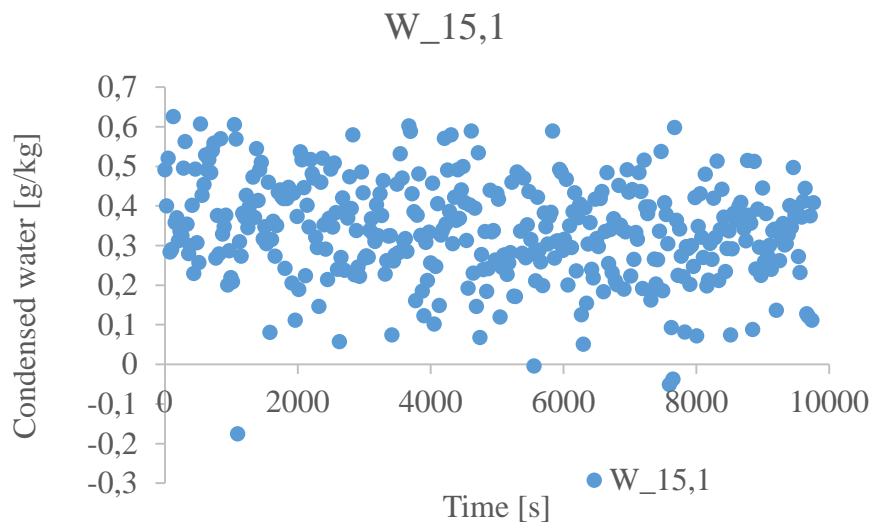
D-23 Sensible and latent effectiveness



D-24 Grams of water trapped inside MEE per kg air



D-25 Sensible and latent effectiveness



D-26 Grams of water trapped inside MEE per kg air

Appendix E –Simien simulations

CAV		
Temperature [°C]	Latent effectiveness	Sensible effectiveness
5,3	0,79	0,92
10,3	0,76	0,9
15,1	0,75	0,89

E-T-1 Input values for effectiveness in CAV

Inndata sommersimulering	
Beskrivelse	Verdi
Simuleringsdato	21/04
Simulerte døgn	5
Dagtype	Normal driftsdag
Bekledning [clo]	1,0
Aktivetsnivå personer [met]	1,0
Bruker egendefinerte klimadata	-
Transmissivitet atmosfære	0,74
Vanndampinnhold [g/kg]	4,1
Maksimaltemperatur [°C]	5,3
Mimumstematperatur [°C]	5,3
Tidspunkt maks. utetemperatur	14:30
CO2 konsentrasjon [PPM]	380
Markrefleksjonskoeffisient	0,20
Vindhastighet [m/s]	2,5

E-1 Input values in Simien 5,3C Normal conditions

Inndata klima	
Beskrivelse	Verdi
Klimasted	Oslo
Breddegrad	59° 55'
Lengdegrad	10° 45'
Tidssone	GMT + 1
Klimadata	Egendefinerte
Transmissivitet atmosfære	0,74
Absolutt luftfuktighet	4,1 g/kg
Markrefleksjonskoeffisient	0,20
Minimum utetemperatur	5,3 °C
Maksimum utetemperatur	5,3 °C
Vindhastighet	2,5 m/s

E-2 Input values in Simien 5,3C Normal conditions

Inndata sommersimulering	
Beskrivelse	Verdi
Simuleringsdato	21/04
Simulerte døgn	5
Dagtype	Normal driftsdag
Bekledning [clo]	1,0
Aktivitetsnivå personer [met]	1,0
Bruker egendefinerte klimadata	-
Transmissivitet atmosfære	0,74
Vandampinnhold [g/kg]	4,1
Maksimaltemperatur [°C]	5,3
Mimumsttemperatur [°C]	5,3
Tidspunkt maks. utetemperatur	14:30
CO2 konsentrasjon [PPM]	380
Markrefleksjonskoeffisient	0,20
Vindhastighet [m/s]	2,5

E-3 Input values in Simien 5,3C Double ventilation

Inndata klima	
Beskrivelse	Verdi
Klimasted	Oslo
Breddegrad	59° 55'
Lengdegrad	10° 45'
Tidssone	GMT + 1
Klimadata	Egendefinerte
Transmissivitet atmosfære	0,74
Absolutt luftfuktighet	4,1 g/kg
Markrefleksjonskoeffisient	0,20
Minimum utetemperatur	5,3 °C
Maksimum utetemperatur	5,3 °C
Vindhastighet	2,5 m/s

E-4 Input values in Simien 5,3C Double ventilation

Inndata sommersimulering	
Beskrivelse	Verdi
Simuleringsdato	21/04
Simulerte døgn	5
Dagtype	Normal driftsdag
Bekledning [clo]	1,0
Aktivitetsnivå personer [met]	1,0
Bruker egendefinerte klimadata	-
Transmissivitet atmosfære	0,05
Vandampinnhold [g/kg]	4,1
Maksimaltemperatur [°C]	5,3
Mimumsttemperatur [°C]	5,3
Tidspunkt maks. utetemperatur	14:30
CO2 konsentrasjon [PPM]	380
Markrefleksjonskoeffisient	0,20
Vindhastighet [m/s]	2,5

E-5 Input values in Simien 5,3C Cloudy

Inndata klima	
Beskrivelse	Verdi
Klimasted	Oslo
Breddegrad	59° 55'
Lengdegrad	10° 45'
Tidssone	GMT + 1
Klimadata	Egendefinerte
Transmissivitet atmosfære	0,05
Absolutt luftfuktighet	4,1 g/kg
Markrefleksjonskoeffisient	0,20
Minimum utetemperatur	5,3 °C
Maksimum utetemperatur	5,3 °C
Vindhastighet	2,5 m/s

E-6 Input values in Simien 5,3C Cloudy

Inndata sommersimulering	
Beskrivelse	Verdi
Simuleringsdato	21/04
Simulerte døgn	5
Dagtype	Normal driftsdag
Bekledning [clo]	1,0
Aktivitetsnivå personer [met]	1,0
Bruker egendefinerte klimadata	-
Transmissivitet atmosfære	0,05
Vanndampinnhold [g/kg]	5,5
Maksimaltemperatur [°C]	5,3
Mimumsttemperatur [°C]	5,3
Tidspunkt maks. utetemperatur	14:30
CO2 konsentrasjon [PPM]	380
Markrefleksjonskoeffisient	0,20
Vindhastighet [m/s]	2,5

E-7 Input values in Simien 5,3C Rain

Inndata klima	
Beskrivelse	Verdi
Klimasted	Oslo
Breddegrad	59° 55'
Lengdegrad	10° 45'
Tidssone	GMT + 1
Klimadata	Egendefinerte
Transmissivitet atmosfære	0,05
Absolutt luftfuktighet	5,5 g/kg
Markrefleksjonskoeffisient	0,20
Minimum utetemperatur	5,3 °C
Maksimum utetemperatur	5,3 °C
Vindhastighet	2,5 m/s

E-8 Input values in Simien 5,3C Rain

Inndata sommersimulering	
Beskrivelse	Verdi
Simuleringsdato	21/04
Simulerte døgn	5
Dagtype	Normal driftsdag
Bekledning [clo]	1,0
Aktivetsnivå personer [met]	1,0
Bruker egendefinerte klimadata	-
Transmissivitet atmosfære	0,74
Vanndampinnhold [g/kg]	5,6
Maksimaltemperatur [°C]	10,3
Mimumstperatur [°C]	10,3
Tidspunkt maks. utetemperatur	14:30
CO2 konsentrasjon [PPM]	380
Markrefleksjonskoeffisient	0,20
Vindhastighet [m/s]	2,5

E-9 Input values in Simien 10,3C Normal conditions

Inndata klima	
Beskrivelse	Verdi
Klimasted	Oslo
Breddegrad	59° 55'
Lengdegrad	10° 45'
Tidssone	GMT + 1
Klimadata	Egendefinerte
Transmissivitet atmosfære	0,74
Absolutt luftfuktighet	5,6 g/kg
Markrefleksjonskoeffisient	0,20
Minimum utetemperatur	10,3 °C
Maksimum utetemperatur	10,3 °C
Vindhastighet	2,5 m/s

E-10 Input values in Simien 10,3C Normal conditions

Inndata sommersimulering	
Beskrivelse	Verdi
Simuleringsdato	21/04
Simulerte døgn	5
Dagtype	Normal driftsdag
Bekledning [clo]	1,0
Aktivetsnivå personer [met]	1,0
Bruker egendefinerte klimadata	-
Transmissivitet atmosfære	0,74
Vanndampinnhold [g/kg]	5,6
Maksimaltemperatur [°C]	10,3
Mimumstperatur [°C]	10,3
Tidspunkt maks. utetemperatur	14:30
CO2 konsentrasjon [PPM]	380
Markrefleksjonskoeffisient	0,20
Vindhastighet [m/s]	2,5

E-11 Input values in Simien 10,3C Double ventilation

Inndata klima	
Beskrivelse	Verdi
Klimasted	Oslo
Breddegrad	59° 55'
Lengdegrad	10° 45'
Tidssone	GMT + 1
Klimadata	Egendefinerte
Transmissivitet atmosfære	0,74
Absolutt luftfuktighet	5,6 g/kg
Markrefleksjonskoeffisient	0,20
Minimum utetemperatur	10,3 °C
Maksimum utetemperatur	10,3 °C
Vindhastighet	2,5 m/s

E-12 Input values in Simien 10,3C Double ventilation

Inndata sommersimulering	
Beskrivelse	Verdi
Simuleringsdato	21/04
Simulerte døgn	5
Dagtype	Normal driftsdag
Bekledning [clo]	1,0
Aktivitetsnivå personer [met]	1,0
Bruker egendefinerte klimadata	-
Transmissivitet atmosfære	0,05
Vandampinnhold [g/kg]	5,6
Maksimaltemperatur [°C]	10,3
Mimumsttemperatur [°C]	10,3
Tidspunkt maks. utetemperatur	14:30
CO2 konsentrasjon [PPM]	380
Markrefleksjonskoeffisient	0,20
Vindhastighet [m/s]	2,5

E-13 Input values in Simien 10,3C Cloudy

Inndata klima	
Beskrivelse	Verdi
Klimasted	Oslo
Breddegrad	59° 55'
Lengdegrad	10° 45'
Tidssone	GMT + 1
Klimadata	Egendefinerte
Transmissivitet atmosfære	0,05
Absolutt luftfuktighet	5,6 g/kg
Markrefleksjonskoeffisient	0,20
Minimum utetemperatur	10,3 °C
Maksimum utetemperatur	10,3 °C
Vindhastighet	2,5 m/s

E-14 Input values in Simien 10,3C Cloudy

Inndata sommersimulering	
Beskrivelse	Verdi
Simuleringsdato	21/04
Simulerte døgn	5
Dagtype	Normal driftsdag
Bekledning [clo]	1,0
Aktivetsnivå personer [met]	1,0
Bruker egendefinerte klimadata	-
Transmissivitet atmosfære	0,05
Vanndampinnhold [g/kg]	7,8
Maksimaltemperatur [°C]	10,3
Mimumstperatur [°C]	10,3
Tidspunkt maks. utetemperatur	14:30
CO2 konsentrasjon [PPM]	380
Markrefleksjonskoeffisient	0,20
Vindhastighet [m/s]	2,5

E-15 Input values in Simien 10,3C Rain

Inndata klima	
Beskrivelse	Verdi
Klimasted	Oslo
Breddegrad	59° 55'
Lengdegrad	10° 45'
Tidssone	GMT + 1
Klimadata	Egendefinerte
Transmissivitet atmosfære	0,05
Absolutt luftfuktighet	7,8 g/kg
Markrefleksjonskoeffisient	0,20
Minimum utetemperatur	10,3 °C
Maksimum utetemperatur	10,3 °C
Vindhastighet	2,5 m/s

E-16 Input values in Simien 10,3C Rain

Inndata sommersimulering	
Beskrivelse	Verdi
Simuleringsdato	21/04
Simulerte døgn	5
Dagtype	Normal driftsdag
Bekledning [clo]	1,0
Aktivetsnivå personer [met]	1,0
Bruker egendefinerte klimadata	-
Transmissivitet atmosfære	0,74
Vanndampinnhold [g/kg]	7,9
Maksimaltemperatur [°C]	15,2
Mimumstperatur [°C]	15,2
Tidspunkt maks. utetemperatur	14:30
CO2 konsentrasjon [PPM]	380
Markrefleksjonskoeffisient	0,20
Vindhastighet [m/s]	2,5

E-17 Input values in Simien 15,1C Normal conditions

Inndata klima	
Beskrivelse	Verdi
Klimasted	Oslo
Breddegrad	59° 55'
Lengdegrad	10° 45'
Tidssone	GMT + 1
Klimadata	Egendefinerte
Transmissivitet atmosfære	0,74
Absolutt luftfuktighet	7,9 g/kg
Markrefleksjonskoeffisient	0,20
Minimum utetemperatur	15,2 °C
Maksimum utetemperatur	15,2 °C
Vindhastighet	2,5 m/s

E-18 Input values in Simien 15,1C Normal conditions

Inndata sommersimulering	
Beskrivelse	Verdi
Simuleringsdato	21/04
Simulerte døgn	5
Dagtype	Normal driftsdag
Bekledning [clo]	1,0
Aktivitetsnivå personer [met]	1,0
Bruker egendefinerte klimadata	-
Transmissivitet atmosfære	0,74
Vanndampinnhold [g/kg]	7,9
Maksimaltemperatur [°C]	15,2
Mimumsttemperatur [°C]	15,2
Tidspunkt maks. utetemperatur	14:30
CO2 konsentrasjon [PPM]	380
Markrefleksjonskoeffisient	0,20
Vindhastighet [m/s]	2,5

E-19 Input values in Simien 15,1C Double ventilation

Inndata klima	
Beskrivelse	Verdi
Klimasted	Oslo
Breddegrad	59° 55'
Lengdegrad	10° 45'
Tidssone	GMT + 1
Klimadata	Egendefinerte
Transmissivitet atmosfære	0,74
Absolutt luftfuktighet	7,9 g/kg
Markrefleksjonskoeffisient	0,20
Minimum utetemperatur	15,2 °C
Maksimum utetemperatur	15,2 °C
Vindhastighet	2,5 m/s

E-20 Input values in Simien 15,1C Double ventilation

Inndata sommersimulering	
Beskrivelse	Verdi
Simuleringsdato	21/04
Simulerte døgn	5
Dagtype	Normal driftsdag
Bekledning [clo]	1,0
Aktivitetsnivå personer [met]	1,0
Bruker egendefinerte klimadata	-
Transmissivitet atmosfære	0,05
Vanndampinnhold [g/kg]	7,9
Maksimaltemperatur [°C]	15,2
Mimumsttemperatur [°C]	15,2
Tidspunkt maks. utetemperatur	14:30
CO2 konsentrasjon [PPM]	380
Markrefleksjonskoeffisient	0,20
Vindhastighet [m/s]	2,5

E-21 Input values in Simien 15,1C Cloudy

Inndata klima	
Beskrivelse	Verdi
Klimasted	Oslo
Breddegrad	59° 55'
Lengdegrad	10° 45'
Tidssone	GMT + 1
Klimadata	Egendefinerte
Transmissivitet atmosfære	0,05
Absolutt luftfuktighet	7,9 g/kg
Markrefleksjonskoeffisient	0,20
Minimum utetemperatur	15,2 °C
Maksimum utetemperatur	15,2 °C
Vindhastighet	2,5 m/s

E-22 Input values in Simien 15,1C Cloudy

Inndata sommersimulering	
Beskrivelse	Verdi
Simuleringsdato	21/04
Simulerte døgn	5
Dagtype	Normal driftsdag
Bekledning [clo]	1,0
Aktivitetsnivå personer [met]	1,0
Bruker egendefinerte klimadata	-
Transmissivitet atmosfære	0,05
Vanndampinnhold [g/kg]	10,8
Maksimaltemperatur [°C]	15,2
Mimumsttemperatur [°C]	15,2
Tidspunkt maks. utetemperatur	14:30
CO2 konsentrasjon [PPM]	380
Markrefleksjonskoeffisient	0,20
Vindhastighet [m/s]	2,5

E-23 Input values in Simien 15,1C Rain

Inndata klima	
Beskrivelse	Verdi
Klimasted	Oslo
Breddegrad	59° 55'
Lengdegrad	10° 45'
Tidssone	GMT + 1
Klimadata	Egendefinerte
Transmissivitet atmosfære	0,05
Absolutt luftfuktighet	10,8 g/kg
Markrefleksjonskoeffisient	0,20
Minimum utetemperatur	15,2 °C
Maksimum utetemperatur	15,2 °C
Vindhastighet	2,5 m/s

E-24

Input values in Simien 15,1C Rain

Risk Assessment Report

Membrane energy exchanger test rig

Prosjektnavn	New type of energy exchanger for ventilation air
Apparatur	Membrane energy exchanger test rig
Enhet	NTNU
Apparaturansvarlig	Hans Martin Mathisen
Prosjektleder	Hans Martin Mathisen
HMS-koordinator	Morten Grønli
HMS-ansvarlig (linjeleder)	Olav Bolland
Plassering	C050 refrigeration lab
Romnummer	Room B038
Risikovurdering utført av	Martin Lundekvam

Approval:

Apparatur kort (UNIT CARD) valid for:	Martin Lundekvam
Forsøk pågår kort (EXPERIMENT IN PROGRESS) valid for:	Martin Lundekvam

Rolle	Navn	Dato	Signatur
Prosjektleder	Hans Martin Mathisen		
HMS koordinator	Morten Grønli		
HMS ansvarlig (linjeleder)	Olav Bolland		

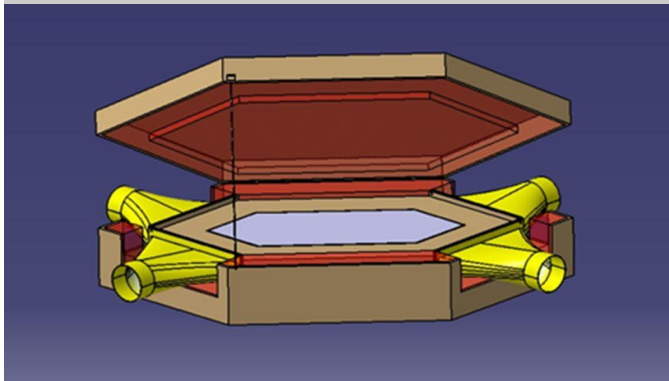
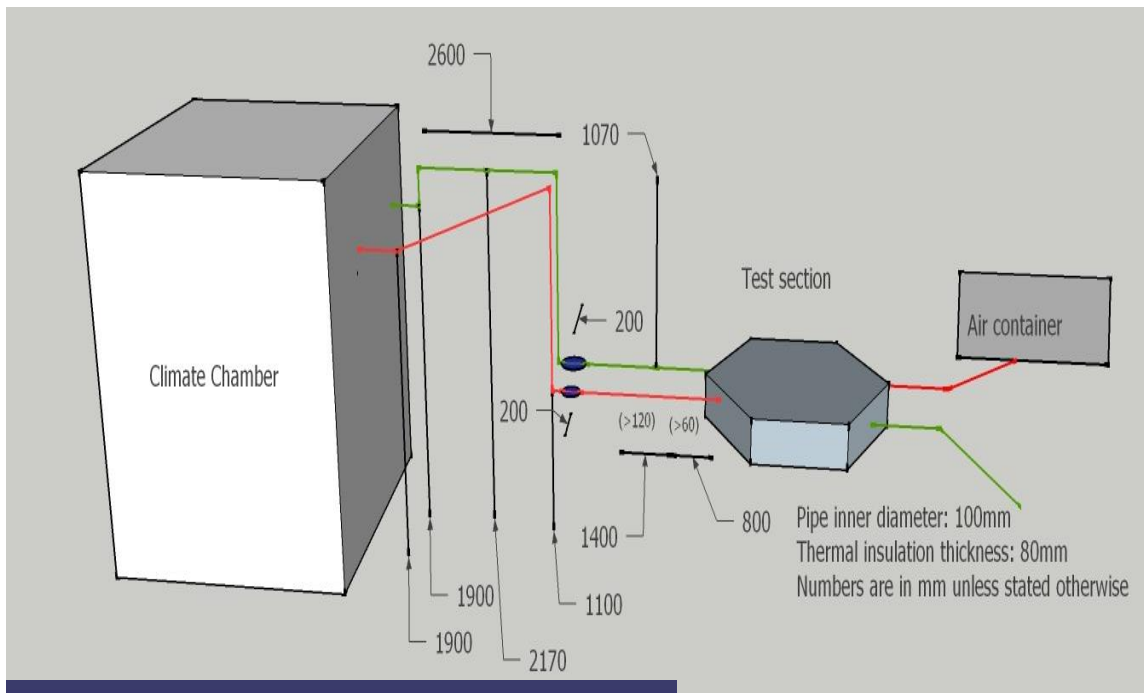
TABLE OF CONTENTS

Preface	v
Sammendrag	vii
Abstract	vii
List of Figures:	viii
List of Tables:.....	vii
Definitions:.....	viii
Nomenclature	viii
1 Introduction	1
1.1 Background.....	1
1.2 Objective.....	2
2 Literature review and state of the art.....	3
2.1 Introduction to frosting.....	3
2.2 Configurations	4
2.3 Flow patterns Quasi-counter flow MEE.....	5
2.4 Membrane properties	6
2.4.1 Dense membranes	6
2.4.2 Porous membranes	6
2.5 Test rig membrane	7
3 Theoretical modelling	9
3.1 Flow pattern test rig.....	9
3.1.1 Dimensioning entry and exit length	9
3.1.2 Volumetric flow rate	10
3.2 Membrane energy exchanger test rig	11
3.2.1 Pressure drop and airstream velocity	11

3.2.2	Moisture transfer resistance	12
3.2.3	Heat and mass transfer	14
3.2.3	Effectiveness	16
3.3	Uncertainty	17
4	Experimental setup	21
4.1	Flow pattern setup	21
4.2	Quasi-counter-flow setup	22
4.2.1	Relative humidity	23
4.2.2	HSE report.....	23
5	Results	25
5.1	Flow pattern test rig	25
5.1.1	Pressure drop	25
5.1.2	Flow pattern.....	25
5.2	Effectiveness.....	27
5.3	Moisture and condensation	30
5.4	Pressure drop	31
5.5	Temperature and RH fluctuation	32
5.6	Long run performance	34
5.7	Indoor RH	41
6	Discussion	43
6.1	Moisture supply air	43
6.2	Pressure drop and flow rate	43
6.3	Moisture transfer resistance.....	45
6.4	Evaluation of the flow pattern test rig	45
6.5	Evaluation of the MEE test rig	46

7	Conclusion.....	47
8	Further Work.....	49
	References.....	51
	Appendix.....	53
	Appendix A – Calculation of discharge coefficient.....	54
	Appendix B – Random Uncertainty.....	55
	Appendix C – Mean RH and temp cities.....	58
	Appendix D – Results.....	61
	Appendix E –Simien simulations.....	74
	Appendix F – Risk assessment report.....	83
1	introduction.....	i
2	Organisation.....	i
3	RISK MANAGEMENT in the PROJECT.....	i
4	DESCRIPTIONS OF EXPERIMENTAL SETUP.....	iii
5	Evacuation from the experimental area.....	v
6	Warning.....	v
	6.1 Before experiments.....	v
	6.2 Abnormal situation.....	vi
7	Assessment of technical safety.....	vii
	7.1 HAZOP.....	vii
	7.2 Flammable, reactive and pressurized substances and gas.....	vii
	7.3 Pressurized equipment.....	vii
	7.4 Effects on the environment (emissions, noise, temperature, vibration, smell).....	viii
	7.5 Radiation.....	viii
	7.6 Chemicals.....	viii

7.7	Electricity safety (deviations from the norms/standards)	ix
8	Assessment of operational safety	ix
8.1	Procedure HAZOP	ix
8.2	Operation procedure and emergency shutdown procedure	ix
8.3	Training of operators	ix
8.4	Technical modifications	ix
8.5	Personal protective equipment.....	x
8.6	General Safety	x
8.7	Safety equipment	x
9	Quantifying of RISK - risk matrix	x
10	Regulations and guidelines.....	xi
11	DOcUMENTAtion	xii
	Attachment A: Process and instrumentation diagram	1



.....	2
Attachment B: HAZOP template	3
Attachment E: Procedure for running experiments.....	A
Attachment f: Training of operators	C
Apparaturkort / UnitCard	E
FORSØK PÅGÅR /EXPERIMENT IN PROGRESS.....	G

1 introduction

A membrane air-to-air energy exchanger rig has been assembled. The performance of the exchanger will be tested for the air with different temperature and humidity. The working conditions of the test is listed in the table below.

Parameters	Conditions
Working media	Air with atmospheric pressure
Air temperature	0 °C – 15 °C
Air relative humidity	0 % - 60 %
Air-flow rate	30-60 m ³ /h
Pressure	± 100 Pa

The air temperature, relative humidity, flow rate and pressure drop at the inlets and outlets of the exchanger will be measured and recorded with Labview program through the data logger.

2 Organisation

Rolle	
Prosjektleder	Hans Martin Mathisen
Apparaturansvarlig	Hans Martin Mathisen
Romansvarlig	(Lars Konrad Sørensen)
HMS koordinator	Morten Grønli
HMS ansvarlig (linjeleder):	Olav Bolland

3 RISK MANAGEMENT in the PROJECT

Hovedaktiviteter risikostyring	Nødvendige tiltak, dokumentasjon	DATE
--------------------------------	----------------------------------	------

Prosjekt initiering	Prosjekt initiering mal	
Veiledningsmøte Guidance Meeting	Skjema for Veiledningsmøte med pre-risikovurdering	
Innledende risikovurdering Initial Assessment	Fareidentifikasjon – HAZID Skjema grovanalyse	
Vurdering av teknisk sikkerhet Evaluation of technical security	Prosess-HAZOP Tekniske dokumentasjoner	
Vurdering av operasjonell sikkerhet Evaluation of operational safety	Prosedyre-HAZOP Opplæringsplan for operatører	
Sluttvurdering, kvalitetssikring Final assessment, quality assurance	Uavhengig kontroll Utstedelse av apparaturkort Utstedelse av forsøk pågår kort	

The climate chamber provides the cold air needed for the experiment. The air container delivers the constant indoor air with a water-to-air tube and fin heat exchanger. The humidity level is regulated with a nozzle spraying water vapor. An on/off switch with Labview controls the nozzle. The relative humidity of the cold air is supplied by water steam generated from boiling water in flask heated by hot plate.

The air states will be monitored by the thermocouples, pitot tube, humidity meter, orifice plate and endoscope which will be described in the equipment list table.

Instrument list			
Description	Output signal	Manufacture	Model
Manometer	mV	DPM	TT470S
Orifice plate	Pa	Lab	
Pitot tube	Pa	Lab	
Thermocouple T1-T16	mV	Lab	T type
Endoscope	Graphics	MEDIT	SCVBS5.5-1
Data logger		National Instruments	NI Cdaq-9178
Hot plate	Heat	Clas ohlson	HP102-T2
Air handling unit		Covent	CEAE-035
Solenoid valve	Degrees of opening	ASCO	SC E210
Fan		OSTBERG	CK 100A

Equipment list			
Description	Manufacture	Material	Model
Membrane energy exchanger	Lab	Polypropylene membrane, aluminium mesh and plastic	Custom made
Air diffusor	Lab		Custom made

Pipe		aluminum	
------	--	----------	--

Shutdown procedure occurs by switching of the fan, air handling unit and cooling system in climate chamber. Delivering air is stopped by switching off the fan. The temperature in the climate chamber will return to normal room temperature over time after the cooling system has been switched off.

5 Evacuation from the experimental area

Evacuate at signal from the alarm system or local gas alarms with its own local alert with sound and light outside the room in question, see 6.2

Evacuation from the rigging area takes place through the marked emergency exits to the assembly point, (corner of Old Chemistry Kjelhuset or parking 1a-b.)

Action on rig before evacuation:

- Switch off the fans connected to exchanger
- Switch off the hot plate
- Switch off the cooling system in cold chamber
- Switch off the fan integrated with air handling unit
- Switch off the warm water supply

6 Warning

6.1 Before experiments

Send an e-mail with information about the planned experiment to:

iept-experiments@ivt.ntnu.no

The e-mail must include the following information:

- Name of responsible person:
- Experimental setup/rig:
- Start Experiments: (date and time)
- Stop Experiments: (date and time)

You must get the approval back from the laboratory management before start up. All running experiments are notified in the activity calendar for the lab to be sure they are coordinated with other activity.

6.2 Abnormal situation

FIRE

If you are NOT able to extinguish the fire, activate the nearest fire alarm and evacuate area. Be then available for fire brigade and building caretaker to detect fire place.

If possible, notify:

NTNU	SINTEF
Morten Grønli, Mob: 918 97 515	Harald Mæhlum, Mob: 930 14 986
Olav Bolland: Mob: 918 97 209	Petter Røkke, Mob: 901 20 221
NTNU – SINTEF Beredskapstelefon	800 80 388

GAS ALARM

If a gas alarm occurs, close gas bottles immediately and ventilate the area. If the level of the gas concentration does not decrease within a reasonable time, activate the fire alarm and evacuate the lab. Designated personnel or fire department checks the leak to determine whether it is possible to seal the leak and ventilate the area in a responsible manner.

Alert Order is in the above paragraph.

PERSONAL INJURY

- First aid kit in the fire / first aid stations
- Shout for help
- Start life-saving first aid
- **CALL 113** if there is any doubt whether there is a serious injury

OTHER ABNORMAL SITUATIONS

NTNU:

You will find the reporting form for non-conformance on:

<https://innsida.ntnu.no/wiki/-/wiki/Norsk/Melde+avvik>

SINTEF:

Synergi

7 Assessment of technical safety

7.1 HAZOP

See Chapter 13 "Guide to the report template".

The experiment set up is divided into the following nodes:

Node 1	Test section
Node 2	Cold chamber
Node 3	Air handling unit
Node 4	Humidifier with hot plate

Attachments, Form: Hazop_mal

Conclusion: (Safety taken care of by filling enough water into flask and checking it frequently)

7.2 Flammable, reactive and pressurized substances and gas

Are any flammable, reactive and pressurized substances and gases in use?

NO	
----	--

Attachments: EX zones?

Conclusion: Not any flammable, reactive and pressurized substances and gases in use

7.3 Pressurized equipment

Is any pressurized equipment in use?

NO	
----	--

Attachments: Certificate for pressurized equipment (see Attachment to Risk Assessment)

Conclusion: No pressurized equipment in use

7.4 Effects on the environment (emissions, noise, temperature, vibration, smell)

Will the experiments generate emission of smoke, gas, odour or unusual waste?

Is there a need for a discharge permit, extraordinary measures?

NO	
----	--

Attachments:

Conclusion: No effects on the environment

7.5 Radiation

See Chapter 13 "Guide to the report template".

NO	
----	--

Attachments:

Conclusion: No radiation

7.6 Chemicals

Will any chemicals or other harmful substances be used in the experiments? Describe how the chemicals should be handled (stored, disposed, etc.) Evaluate the risk according to safety datasheets, MSDS. Is there a need for protective actions given in the operational procedure?

NO	
----	--

Attachments: MSDS

Conclusion: No harmful substances will be used in the experiments.

7.7 Electricity safety (deviations from the norms/standards)

NO	
----	--

8 Assessment of operational safety

Ensure that the procedures cover all identified risk factors that must be taken care of. Ensure that the operators and technical performance have sufficient expertise.

8.1 Procedure HAZOP

The method is a procedure to identify causes and sources of danger to operational problems.

Attachments:: HAZOP_MAL_Prosegyre

8.2 Operation procedure and emergency shutdown procedure

The operating procedure is a checklist that must be filled out for each experiment.

Emergency procedure should attempt to set the experiment set up in a harmless state by unforeseen events.

Attachments: Procedure for running experiments

Emergency shutdown procedure:

8.3 Training of operators

A Document showing training plan for operators

- *What are the requirements for the training of operators?*
- *What it takes to be an independent operator*
- *Job Description for operators*

Attachments: Training program for operators

8.4 Technical modifications

- *Technical modifications that must be made by Technical staff*

8.5 Personal protective equipment

- Use gloves when there is opportunity for contact with hot/cold surfaces.

Conclusion:

8.6 General Safety

- The area around the staging attempts shielded.
- Gantry crane and truck driving should not take place close to the experiment.
- Gas cylinders shall be placed in an approved carrier with shut-off valve within easy reach.

8.7 Safety equipment

- Warning signs, see the Regulations on Safety signs and signaling in the workplace

9 Quantifying of RISK - risk matrix




The risk matrix will provide visualization and an overview of activity risks so that management and users get the most complete picture of risk factors.

IDnr	Aktivitet-hendelse	Frekv-Sans	Kons	RV
1	High temperature of the hot plate	1	B	B1

CONSEQUENCES	Catastrophic	E1	E2	E3	E4	E5
	Major	D1	D2	D3	D4	D5
	Moderate	C1	C2	C3	C4	C5
	Minor	B1	B2	B3	B4	B5
	Insignificant	A1	A2	A3	A4	A5
		Rare	Unlikely	Possible	Likely	Almost
		PROBABILITY				

Table 8. Risk Matrix

Table 9. The principle of the acceptance criterion. Explanation of the colors used in the matrix

COLOUR		DESCRIPTION
Red		Unacceptable risk Action has to be taken to reduce risk
Yellow		Assessment area. Actions has to be considered
Green		Acceptable risk. Action can be taken based on other criteria

10 Regulations and guidelines

Se <http://www.arbeidstilsynet.no/regelverk/index.html>

- Lov om tilsyn med elektriske anlegg og elektrisk utstyr (1929)
- Arbeidsmiljøloven
- Forskrift om systematisk helse-, miljø- og sikkerhetsarbeid (HMS Internkontrollforskrift)
- Forskrift om sikkerhet ved arbeid og drift av elektriske anlegg (FSE 2006)
- Forskrift om elektriske forsyningsanlegg (FEF 2006)
- Forskrift om utstyr og sikkerhetssystem til bruk i eksplosjonsfarlig område NEK 420
- Forskrift om håndtering av brannfarlig, reaksjonsfarlig og trykksatt stoff samt utstyr og anlegg som benyttes ved håndteringen
- Forskrift om Håndtering av eksplosjonsfarlig stoff
- Forskrift om bruk av arbeidsutstyr.
- Forskrift om Arbeidsplasser og arbeidslokaler
- Forskrift om Bruk av personlig verneutstyr på arbeidsplassen
- Forskrift om Helse og sikkerhet i eksplosjonsfarlige atmosfærer
- Forskrift om Høytrykksspyling
- Forskrift om Maskiner
- Forskrift om Sikkerhetsskiltning og signalgivning på arbeidsplassen
- Forskrift om Stillaser, stiger og arbeid på tak m.m.
- Forskrift om Sveising, termisk skjæring, termisk sprøyting, kullbuemeisling, lodding og sliping (varmt arbeid)
- Forskrift om Tekniske innretninger
- Forskrift om Tungt og ensformig arbeid
- Forskrift om Vern mot eksponering for kjemikalier på arbeidsplassen (Kjemikalieforskriften)
- Forskrift om Vern mot kunstig optisk stråling på arbeidsplassen
- Forskrift om Vern mot mekaniske vibrasjoner
- Forskrift om Vern mot støy på arbeidsplassen

Veiledninger fra arbeidstilsynet

se: <http://www.arbeidstilsynet.no/regelverk/veiledninger.html>

11 DOcUMENTATion

- Tegninger, foto, beskrivelser av forsøksoppsetningen
- Hazop_mal
- Sertifikat for trykkpåkjent utstyr
- Håndtering avfall i NTNU
- Sikker bruk av LASERE, retningslinje
- HAZOP_MAL_Prosedeyre
- Forsøksprosedeyre
- Opplæringsplan for operatører
- Skjema for sikker jobb analyse, (SJA)
- Apparatorkortet
- Forsøk pågår kort

Attachment to Risk Assessment report

Membrane energy exchanger test rig

Prosjektnavn	New type of energy exchanger for ventilation air
Apparatur	Membrane energy exchanger test rig
Enhet	NTNU
Apparaturansvarlig	Hans Martin Mathisen
Prosjektleder	Hans Martin Mathisen
HMS-koordinator	Morten Grønli
HMS-ansvarlig (linjeleder)	Olav Bolland
Plassering	C050 refrigeration lab
Romnummer	Room B038
Risikovurdering utført av	Martin Lundekvam

TABLE OF CONTENTS

Attachment A: Process and instrumentation diagram	1
Attachment B: HAZOP template	3
Attachment E: Procedure for running experiments	A

Attachment f: Training of operators C

Apparaturkort / UnitCard E

FORSØK PÅGÅR /EXPERIMENT IN PROGRESS G

Attachment A: Process and instrumentation diagram

Attachment B: HAZOP template

Project:							Page
Node: 1. Test section 2. Cold chamber 3. Air handling unit							
Ref	Guideword	Causes	Consequences	Safeguards	Recommendations	Action	Date/Sign
	N/A	N/A	N/A	N/A	N/A	N/A	

Project:							Page
Node: 4. Humidifier with hot plate							
Ref	Guideword	Causes	Consequences	Safeguards	Recommendations	Action	Date/Sign
	No flow	Out of water	High temperature of flask	Pour enough water at the beginning of the experiment and close the hot plate when the tests finish			

Attachment E: Procedure for running experiments

Prosjekt New type of energy exchanger for ventilation air	Dato	Signatur
Apparatur Membrane energy exchanger test rig		
Prosjektleder Hans Martin Mathisen		

	Conditions for the experiment:	Completed
	Experiments should be run in normal working hours, 08:00-16:00 during winter time and 08.00-15.00 during summer time. Experiments outside normal working hours shall be approved.	
	One person must always be present while running experiments, and should be approved as an experimental leader.	
	An early warning is given according to the lab rules, and accepted by authorized personnel.	
	Be sure that everyone taking part of the experiment is wearing the necessary protecting equipment and is aware of the shut down procedure and escape routes.	
	Preparations	Carried out
	Post the “Experiment in progress” sign.	
	<i>Start up procedure</i>	

	<i>The start-up is implemented by switching on the cooling system mounted in cold chamber(climate chamber), fans, air handling unit and Labview system</i>	
	During the experiment	
	<i>Control of temperature, pressure e.g.</i>	
	End of experiment	
	<i>Shut down procedure</i>	
	<i>Shutting down the cooling system in cold chamber(climate chamber), fans in the test pipes, air handling unit and Labview system can end the experiment</i>	
	Remove all obstructions/barriers/signs around the experiment.	
	Tidy up and return all tools and equipment.	
	Tidy and cleanup work areas.	
	Return equipment and systems back to their normal operation settings (fire alarm)	
	To reflect on before the next experiment and experience useful for others	
	Was the experiment completed as planned and on scheduled in professional terms?	
	Was the competence which was needed for security and completion of the experiment available to you?	
	Do you have any information/ knowledge from the experiment that you should document and share with fellow colleagues?	

Operator(s):

Navn	Dato	Signatur
Martin Lundekvam		

Attachment f: Training of operators

Prosjekt		
New type of energy exchanger for ventilation air	Dato	Signatur
Apparatur		
Membrane energy exchanger test rig		
Prosjektleder		
Hans Martin Mathisen		

	Knowledge about EPT LAB in general	
	Lab <ul style="list-style-type: none"> • Access • routines and rules • working hour 	
	Knowledge about the evacuation procedures.	
	Activity calendar for the Lab	
	Early warning, iept-experiments@ivt.ntnu.no	
	Knowledge about the experiments	
	Procedures for the experiments	
	Emergency shutdown.	
	Nearest fire and first aid station.	

I hereby declare that I have read and understood the regulatory requirements has received appropriate training to run this experiment and are aware of my personal responsibility by working in EPT laboratories.

Operator(s):

Navn	Dato	Signatur
Martin Lundekvam		

Apparaturkort / UnitCard

Dette kortet SKAL henges godt synlig på apparaturen!

This card MUST be posted on a visible place on the unit!

Apparatur (Unit)	
Membrane energy exchanger test rig	
Prosjektleder (Project Leader)	Telefon mobil/privat (Phone no. mobile/private)
Hans Martin Mathisen	93059175
Apparaturansvarlig (Unit Responsible)	Telefon mobil/privat (Phone no. mobile/private)
Martin Lundekvam	99323065
Sikkerhetsrisikoer (Safety hazards)	
Low air temperature (-15 °C) leakage might occur	
Sikkerhetsregler (Safety rules)	
Use gloves when disconnecting the cold air pipe with exchanger header	
Nødstopprosedyre (Emergency shutdown)	
Emergency stop switches are located behind the computer which will cut power to all fans and instrumentations.	

Her finner du (Here you will find):

Prosedyrer (Procedures)	At the test rig
Bruksanvisning (Users manual)	At the test rig

Nærmeste (Nearest)

Brannslukningsapparat (fire extinguisher)	KuldeLab
Førstehjelpsskap (first aid cabinet)	KuldeLab

NTNU

SINTEF Energi

Institutt for energi og prosessteknikk

Avdeling energiprosesser

Dato

Dato

Signert

Signert

FORSØK PÅGÅR / EXPERIMENT IN PROGRESS

Dette kortet SKAL henges opp før forsøk kan starte!

This card MUST be posted on the unit before the experiment startup!

Apparatur (Unit)	
Membrane energy exchanger	
Prosjektleder (Project Leader)	Telefon mobil/privat (Phone no. mobile/private)
Hans Martin Mathisen	93059175
Apparaturansvarlig (Unit Responsible)	Telefon mobil/privat (Phone no. mobile/private)
Hans Martin Mathisen	93059175
Godkjente operatører (Approved Operators)	Telefon mobil/privat (Phone no. mobile/private)
Martin Lundekvam	99323065
Prosjekt (Project)	
New type of energy exchanger for ventilation air	
Forsøksstid / Experimental time (start - stop)	
28/02/2016 – 15/06	
Kort beskrivelse av forsøket og relaterte farer (Short description of the experiment and related hazards)	
Will test the exchanger for temperatures 0-15 °C with different humidity levels. The test rig consists of two environmental chambers, four fans, a test section, and connecting pipes.	

NTNU

Institutt for energi og prosessteknikk

Dato

Signert

SINTEF Energi

Avdeling energiprosesser

Dato

Signert
